Aus der Sektion für Rheumatologie und Klinische Immunologie
der Medizinischen Klinik und Poliklinik IV
Klinik der Ludwig-Maximilians-Universität München
Direktor: Prof. Dr. med. Martin Reincke

GARP derived TGFβ promotes acetylation-mediated Foxp3 protein stabilization and Treg functionality

Dissertation
zum Erwerb des Doktorgrades der Naturwissenschaften (Dr. rer. nat.)
an der Medizinischen Fakultät der
Ludwig-Maximilians-Universität zu München

vorgelegt von
Peter Lehmkuhl
aus
Recklinghausen

Jahr
2022

Mit Genehmigung der Medizinischen Fakultät
der Universität München

Betreuer:	Prof. Dr. rer. nat. Ludger Klein
Zweitgutachterin:	Prof. Dr. rer. nat. Elfriede Nößner
Dekan:	Prof. Dr. med. Thomas Gudermann
Tag der mündlichen Prüfung:	18.10.2022

Table of Contents

Abbreviations

A	Alexa Fluor
Ab	Antibody
AC	Allele count
AcK	Acetylated lysine
ACTB	Actin beta
AD	Autosomal dominant
AF	Allele frequency
AIRE	Autoimmune regulator
AN	Allele number
APC	Antigen presenting cell
APC	Allophycocyanin
APS	Ammonium persulfate
Arg	Arginine
ATCC	American Type Culture Collection
bp	Base pair
BMT	Bonemarrow transplant
BSA	Bovine serum albumin
cDNA	Complementary DNA
CD	Cluster of differentiation
cds	Coding sequence
CFSE	Carboxyluorescein succinimidyl ester
CGD	Chronic granulomatous disease
ChIP	Chromatin immunoprecipitation
CID	Combined immunodeficiencies
Chr	Chromosome
CHX	Cycloheximide
CIA	Collagen-induced arthritis
CNS	Conserved non-coding sequence

Cre	Cyclization recombination
C-Ter	C-terminus
CTLA4	Cytotoxic T lymphocyte-associated antigen 4
CVID	Common variable immunodeficiency
Cys	Cysteine
DC	Dendritic cell
DMEM	Dulbecco's Modified Eagle Medium
DMSO	Dimethyl sulfoxide
DNA	Deoxyribonucleic acid
dNTP	Deoxyribonucleotide triphosphate
ds	Double-stranded
DTT	Dithiothreitol
EAE	Experimental autoimmune encephalomyelistis
ec	Extracellular
ECM	Extracellular matrix
EDTA	Ethylendinitrotetraacetic acid
E	Exon
FACS	Fluorescence activated cell sorting
FAM	Fluorescein amidite
FCS	Fetal calf serum
FITC	Fluorescein isothiocyanate
Flp	Flippase
Foxp3	Forkhead box P3
FRET	Fluorescence resonance energy transfer
FRT	Flippase recognition target
GARP	Glycoprotein A repetitions predominant
gDNA	Genomic DNA
Gln	Glutamine
HANKS	Hank's Balanced Salt Solution

hc	Healthy control
HDAC	Histone deacetylase
HEK	Human embryonic kidney
hi	High
HRP	Horseradish peroxidase
HSTC	Hematopoietic stem cell transplantation
ic	Intracellular
IFN	Interferon
Ig	Immunoglobulin
IL	Interleukin
IPEX	Immunodeficiency, polyendocrinopathy, and enteropathy, Xlinked syndrome
I-TASSER	Iterative Threading ASSEmbly Refinement
iTreg	Induced regulatory T cell
kb	Kilobase
kDa	Kilo Dalton
LAP	Latency associated protein
LRR	Leucine rich repeat
LTBP	Latent TGF-β binding protein
MACS	Magnetic activated cell sorting
MFI	Mean fluorescence intensity
MGB	Minor groove binder
mo	Moderate
mRNA	Messenger RNA
NAM	Nicotinamide
NK cells	Natural killer cells
NP	Nonyl phenoxypolyethoxylethanol
nt	Nucleotide
N-Ter	N-terminus
NRP	Neuropilin

P1	Upstream promoter 1
P2	Downstream promoter 2
PAGE	Polyacrylamide gel electrophoresis
PBMC	Peripheral blood mononuclear cells
PBS	Phosphate buffered saline
PCR	Polymerase chain reaction
PE	Phycoerythrin
PE-Cy7	Phycoerythrin-Cyanine7
PFA	Paraformaldehyde
PID	Primary immunodeficiency
PMA	Phorbol myristate acetate
pt	Patient
RA	Rheumatoid arthritis
RCF	Relative centrifugal force
RIPA	Radioimmunoprecipitation assay
RNA	Ribonucleic acid
RPMI	Roswell Park Memorial Institute
RSBE	Repressive Smad binding element
SBE	Smad binding element
SCID	Severe combined B cell and T cell immunodeficiency disorder
SD	Standard deviation
SDS	Sodium dodecyl sulfate
SEM	Standard error of the mean
SLE	Systemic lupus erythematodes
siRNA	Small interfering RNA
SNP	Single nucleotide polymorphism
STAT3	Signal transducer and activator of transcription 3
SQL	Structured Query Language
T1D	Type-1 diabetes

TAE	Tris-Acetate-EDTA
Taq	*Thermus aquaticus*
TBS	Tris-buffered saline
TBST	Tris-buffered saline with 0.1% Tween
Tconvs	Conventional T cells
TCR	T cell receptor
Teff	Effector T cell
TEMED	Tetramethylethylenediamine
TGF	Transforming growth factor
Th cell	T helper cell
Treg	Regulatory T cell
TSA	Trichostatin A
TSDR	Treg specific demethylated region
TSS	Transcription start site
UTR	Untranslated region
VCF	Variant Call Format
VIC	Victoria
WES	Whole-exome sequencing
wt	Wild-type
XLA	X-linked agammaglobulinemia
XLAAD	X-linked autoimmunity and allergic dysregulation

Summary

Diseases of immune dysregulation are frequently caused by single gene mutations in central pathways of immune tolerance. They are characterised by heterogeneous clinical manifestations with autoimmune symptoms based on defects in mechanisms regulating self-tolerance. Identification of the genetic cause of such diseases has critical implications for the treatment of patients. To identify underlying molecular etiologies, patients suffering from immune dysregulation were subjected to whole-exome sequencing. Two patients bearing previously undescribed mutations of *LRRC32* encoding glycoprotein A repetitions predominant (GARP) were identified. GARP has been recently described to be specifically expressed on regulatory T cells (Tregs) and is important for their suppressive capacity. GARP is involved in TGFβ1 activation by binding latent TGFβ1 in the cytoplasm and translocating it to the cell surface. The importance of fully functional Tregs is well described for maintaining immunological self-tolerance and homeostasis of the immune system. Tregs control destructive immune responses against pathogens and limit reactions towards self antigens. However, the function of this TGFβ1 source and the underlying mechanisms are not yet completely understood.

My PhD thesis presents data that reinforces the importance of GARP as a regulator of Treg function and stability. It describes two patients with *LRRC32* mutations, characterises the function of GARP in cellular and molecular detail and demonstrates the importance of functional Tregs for physiological immune homeostasis in men and mice. The study identifies a novel link between GARP dependent TGFβ signalling in Tregs and expression of the Treg specific histone deacetylase (HDAC)9 that promotes Foxp3 deacetylation, which contributes to an instable dysfunctional Treg phenotype.

The research shows that Tregs from patients with *LRRC32* mutations have only minimal GARP expression on the cell surface and reduced TGFβ signalling. Tregs from these patients further show a strongly diminished Treg suppressor function and significant reduction in Treg numbers and frequency. GARP functions are characterised in a novel molecular detail using a model of conditional Garp-deficiency in mice. Here the study confirms increased susceptibility to inflammatory diseases once GARP expression is decreased on Tregs. Consistent with the effects observed in patients, Garp-deficiency in mice leads to absence of latent TGFβ on the cell surface of Tregs, reduced TGFβ signalling and diminished suppressor function. Further, Treg from Garp-deficient mice exhibit an unstable phenotype due to diminished Foxp3 protein acetylation and stability. In sum, the PhD thesis reinforces the understanding of immunological mechanisms of

immune dysregulation and expands the knowledge of immunological function of GARP as an important regulator of Treg stability.

Zusammenfassung

Erkrankungen mit Immundysregulation werden häufig durch Mutationen einzelner Gene verursacht, die wichtige Funktionen für die zentrale immun Toleranz tragen. Sie zeichnen sich durch heterologe klinische Manifestationen aus, die auf Defekten in Mechanismen zur Regulation der Selbsttoleranz beruhen. Die Identifizierung der genetischen Ursache solcher Krankheiten hat entscheidende Auswirkungen auf die Behandlung der betroffenen Patienten. Um die zugrundeliegende molekulare Ätiologie bei Patienten zu erkennen die an Immundysregulation leiden, wurden diese mittels whole exom sequencing untersucht. Dabei wurden zwei Patienten identifiziert, die bisher unbeschriebene Mutationen in *LRRC32* aufweisen. *LRRC32* kodiert glycoprotein A repetions predominant (GARP). Erst kürzlich wurde beschrieben, dass GARP spezifisch auf der Oberfläche von regulatorischen T-Zellen (Tregs) exprimiert wird und wichtig für deren suppressive Kapazität ist. GARP ist zudem in die Aktivierung von TGFβ1 involviert. Es bindet latentes TGFβ1 im Zytoplasma und bewirkt die Translokation an die Zelloberfläche. Die Bedeutung von voll funktionstüchtigen Tregs für die Aufrechterhaltung der immunologischen Selbsttoleranz und Homöostase des Immunsystems durch die Kontrolle von destruktiven Immunantworten gegen Pathogene und durch Limitierung von Reaktionen gegen körpereigene Antigene, ist gut beschrieben. Ihre Funktion als Quelle für TGFβ1 und die damit verbundenen Mechanismen sind allerdings noch nicht vollständig aufgeklärt.

In meiner Dissertation präsentiere ich Daten, die die Bedeutung von GARP als Regulator der Treg-Funktion und Treg-Stabilität unterstreicht. Die Arbeit beschreibt zwei Patienten mit *LRRC32*-Mutationen, charakterisiert detailliert die zellulären und molekularen Funktionen von GARP in Tregs und demonstriert die Bedeutung von GARP für die Funktionalität von Tregs zur Aufrechterhaltung der Immunhomöostase in Mensch und Maus. Die Doktorarbeit präsentiert eine neue Verbindung zwischen GARP-abhängigem TGFβ-Signalling und der Expression der Treg-spezifischen Histone-Deacetylase HDAC9, welche die Deacetylierung von Foxp3 bewirkt und zu einem instabilen dysfunktionalen Treg-Phänotyp beiträgt.

Die Forschungsarbeit zeigt, dass Tregs von Patienten mit *LRRC32*-Mutationen nur eine minimale GARP-Expression auf der Zelloberfläche und ein reduziertes TGFβ-Signalling aufweisen. Tregs dieser Patienten zeigen außerdem eine stark verminderte Treg-Suppressorfunktion und eine signifikante Reduktion der Treg-Anzahl und -Frequenz. Die Funktionen von GARP wurden mit Hilfe eines Mausmodells mit konditionaler Garp-Defizienz

in einem neuartigen molekularen Detail charakterisiert. Maus-Experimente bestätigten eine erhöhte Anfälligkeit für entzündliche Erkrankungen, bei einer Verminderung der GARP-expression auf Tregs. In Übereinstimmung mit den Ergebnissen, die bei Patienten beobachtet wurden, führte der Garp-Mangel auch bei Mäusen zu einer Abwesenheit von latentem TGFβ auf der Zelloberfläche von Tregs, reduziertem TGFβ-Signalling und verminderter Treg-Suppressorfunktion. Außerdem zeigten Tregs von Garp-defizienten Mäusen einen instabilen Phänotyp aufgrund von verminderter Foxp3 Protein-Acetylierung und -Stabilität. Die Ergebnisse der vorliegenden Dissertation ergänzen und verbessern unser Verständnis der immunologischen Mechanismen der Immundysregulation und erweitern das Wissen über die immunologischen Funktionen von GARP als wichtigem Regulator der Treg-Stabilität.

1 Introduction

1.1 The immune system

The human body is constantly exposed to infectious viral, bacterial, fungal or parasitic organisms and thus has evolved the immune system to offer protection. Immunity is divided into two types - the innate and adaptive immune responses that interact cooperatively. Innate responses are the first instance of defence, carried out by granulocytes and macrophages, acting within minutes to hours but nonspecific to the pathogens. Adaptive immunity is based on lymphocytes and antibodies, providing highly specific defence against pathogens later during infection and offer an additional long-lasting resistance to re-infection known as immunological memory (Alberts et al., 2002; Janeway et al., 2001).

Lymphocytes are divided into two main groups: B lymphocytes (B cells) that can develop into plasma cells and provide antibody-mediated immunity and T lymphocytes (T cells). T cells can be further divided into two types: cluster of differentiation (CD)4^+ T cells that act as coordinators and regulators of the adaptive immune response and CD8 T cells that can develop into cytotoxic T cells capable of killing infected cells. Lymphocytes in a resting state with no previous specific antigen contact are inactive “naïve” precursor cells that require antigen stimulation and co-signals by antigen-presenting cells (APCs) to become fully activated and to proliferate and differentiate into antigen-specific effector cells (Murphy et al., 2012).

1.2 $CD4^+$ T cells

$CD4^+$ T helper (Th) cells interact through their T cell receptors (TCRs) with major histocompatibility complex (MHC) class II molecules, presenting antigen peptide captured by APCs. Additionally to TCR recognition a co-stimulatory signal from binding of CD28 to surface molecules on APCs such as CD80 or CD86 is needed for sufficient activation (Schwartz, 1990; Schwartz, 1992). The surrounding cytokine milieu, properties of the antigen and the MHC-antigen-TRC interaction including co-stimulation define the expression of lineage specific signal transduction molecules and transcription factors in course of the $CD4^+$ T cell activation. This allows directed differentiation of naïve $CD4^+$ T lymphocytes towards specific effector $CD4^+$ T cell subsets that secrete their lineage specific cytokines (Smith et al., 1986). Initial cytokines originate from APCs and innate immune cells. Differentiated T cells are then capable to produce specific cytokines in an autocrine or paracrine manner.

Th1 and Th2 effector cells were the first described $CD4^+$ T cell subtype, discovered by Coffman and Mosmann in 1986 (Mosmann et al., 1986). Th1 cells differentiate in the presence of interleukin (IL)-12 and IL-18. Th1 cells are important for the defence against infections by bacteria or protozoa and are characterized by the cytokine production of interferon (IFN)-γ, interleukin IL-2, lymphotoxin-α (LTA), and tumor necrosis factor (TNF) (Annunziato and Romagnani, 2009; Romagnani, 2006). Th2 cell develop under the influence of IL-4. They are essential for parasitic clearance by enabling B cells to perform humoral immune responses. Th2 signature cytokines are IL-4, IL-5 and IL-13 (Annunziato and Romagnani, 2009; Mosmann et al., 1986).

Th17 cells are a distinct T helper cell subset that is induced by the pro inflammatory cytokines IL-1β, IL-6, IL-21, IL-23A and the transforming growth factor beta (TGFβ) (Acosta-Rodriguez et al., 2007; Bettelli et al., 2006; Volpe et al., 2009; Yang et al., 2008). Originally, they were identified as mediators of autoimmunity. Th17 cells are involved in recruitment and activation of neutrophils and may therefore be important for host defence against bacteria and fungi. They produce their signature cytokines IL-17A and IL-17F as well as IL-22, IL-26 and chemokine ligand 20 (CCL20) (Korn et al., 2009; Wilson et al., 2007).

The immune system offers powerful mechanisms to destroy agents of infection, however, this destructive potential bears risks when it is deregulated and can lead to detrimental tissue and cell damage in the course of autoimmune diseases. Despite of mechanisms that ensure immunological tolerance towards endogenous tissue and harmless antigens, autoimmune diseases occur as a result of unwanted, aberrant and defective immune responses (MacPherson and Austyn, 2012).

1.3 Primary immunodeficiency (PID)

PIDs, also referred to as inborn errors of immunity, is a heterogeneous group of disorders characterized by impaired development and function of one or multiple components of the immune system. PIDs manifest as increased susceptibility to infectious diseases, malignancy, autoimmunity, autoinflammatory diseases, and allergy (Bousfiha et al., 2018). These conditions result from monogenic germline mutations leading to loss of expression, loss of function or gain of function of the affected protein (Picard et al., 2018). PIDs are distinct from secondary immunodeficiencies that can be caused by viral or bacterial infections, immunoglobulin (Ig) loss, and treatment with medication for immunosuppression as well as malignancy (Duraisingham et al., 2014; Duraisingham et al., 2014; Srivastava and Wood, 2016). Primary immunodeficiencies were traditionally considered to be rare diseases with occurrence of 1 in 10,000 to 50,000. In 1952 X-linked agammaglobulinemia (XLA) was the first PID to be described (Bruton, 1952; Bucciol et al., 2019; Meyts et al., 2016). However, with ongoing discovery of novel primary immunodeficiencies fueled by technological advances in gene identification and application of next-generation sequencing the prevalence of these conditions is now considered to be at least 1 in 1,000 to 5,000. Meanwhile 430 genetic defects have been identified to cause these conditions (Tangye et al., 2020). 1,800 to 2,000 genes of the human genome have been described to be involved in immune responses, the discovery and study of PIDs has demonstrated that more than 20% of these immune related genes play non-redundant roles in immune regulation and host defense (Fischer and Rausell, 2016; Tangye et al., 2020).

The clinical manifestation of PIDs is highly variable. Clinical heterogeneity exists also within groups of patients with mutations in the same gene, but most disorders are characterized by predisposition of individuals to recurrent, chronic, atypical or severe infections (Boyle and Buckley, 2007). Primary immune deficiencies are also often associated with autoimmune diseases with mutations resulting in defects in the regulation of self-tolerance. Disease penetrance, variability in expression and interactions between genetic and environmental factors can also contribute to the phenotypic diversity of patients suffering from PIDs (McCusker and Warrington, 2011). PIDs can be broadly classified according to the component of the immune system that is primarily disrupted. Diseases are associated with defects in innate and adaptive immunity with patients prone to pathological infections. PIDs also include syndromes with autoimmunity and immune dysregulation as a defining feature (Seidel, 2014).

Disorders of adaptive immunity are primarily characterized by T cell and B cell immunodeficiency. T cells carry out cell-mediated immune responses. Defects occurring in T cell development, differentiation or maturation result in T cell (cellular) immunodeficiency disorders. Patients suffering from T cell defects may be lymphopenic, evident by abnormally low levels of lymphocytes. However, normal T cell numbers are not indicative of their function and further investigations are needed in patients with clinical symptoms consistent with immunodeficiency (Bonilla et al., 2015; Notarangelo, 2010).

B cells play a major role in humoral immunity by production of antibodies. Disruptions in B cell development or maturation lead to B cell (antibody-deficiency) disorders. B cell antibody-deficiency disorders are the most frequent type of PIDs (Bonilla et al., 2015). They are a heterogeneous group of disorders defined by increased susceptibility to bacterial respiratory tract infections. Patients may display recurrent and often severe sinopulmonary infections after 6 months of age. Diarrhea, fatigue, sensorineural hearing loss and autoimmune manifestations are also common. More than 50% of cases of humoral immunodeficiency are patients diagnosed in adulthood (Bonilla et al., 2016). Humoral deficiency is often apparent in absent or reduced serum Ig or is defined by normal or increased serum Ig levels with abnormal function (Conley et al., 2009; Fischer et al., 2017; Oliveira and Fleisher, 2010). Common disorders of this category are XLA, selective IgA deficiency and common variable immunodeficiency (CVID). CVID is a heterogeneous disorder that usually has a later age of onset compared to other PIDs and occurs in patients that are above the age of 10 years. It is defined by poor or absent response to immunization, reduced serum concentrations of IgG and low levels of IgA or IgM. Patients suffer from recurrent sinopulmonary infections, autoimmune and granulomatous disease, enhanced risk of malignancy like lymphoma and gastric carcinoma as well as gastrointestinal complications (Conley et al., 2009). Milder forms of antibody-deficiency disorders, such as selective IgA deficiency that is characterized by low or absent serum levels of IgA with normal IgG and IgM levels, only cause a particular susceptibility to infections in one-third of patients (Bonilla et al., 2005).

Since antibody production is mediated by B cells that require functional T cells, most T cell impairments result in severe combined B cell and T cell immunodeficiency disorders (SCIDs) (Boyle and Buckley, 2007; Notarangelo, 2010). Less profound disorders resulting from low CD4, CD8 T cell numbers, B cell numbers or low Ig are classified as combined immunodeficiencies (CID).

Patients with SCID usually show symptoms within the first year of life with chronic diarrhea, failure to thrive, skin rashes and severe recurrent infections (Bonilla et al., 2005). Infections in SCID patients often lead to early mortality. Less severe CIDs include Wiskott-Aldrich syndrome, DiGeorge syndrome and X-linked lymphoproliferative disease that are not characteristically lethal and often present later in childhood with recurrent infections and clinical symptoms varying on the specific syndrome (McCusker et al., 2018; Notarangelo, 2010).

Disorders of innate immunity can be divided into phagocyte (neutrophils, macrophages and dendritic cells) and complement defects. Innate immune responses are the first line of defense against bacteria, fungi and small parasites. It relies on recognition of conserved features of pathogens and rapid activation to help eliminate the threats. The induction of the inflammatory cascade is essential in the removal of invading organisms from the system. Inability of the innate immunity to identify pathogens delays the induction of an appropriate immune response and can lead to more severe infection (Murphy et al., 2012). Phagocytes eliminate invading pathogens by phagocytosis. Complement proteins enable phagocytosis by identification and opsonization of foreign antigens (Janeway et al., 2001). Deficiency in the function or development of any of these mechanisms of the innate immunity can lead to PIDs. Patients with innate immunodeficiency disorders may present symptoms at any age with unusual infections or difficulties to resolve infections. Patients with phagocyte disorders affecting cell number, function or both can experience pyogenic (puss-like) bacterial and fungal infections of the skin, internal organs and the respiratory tract. Painful sores around the mouth are also common. Chronic granulomatous disease (CGD) and hyper-IgE syndrome are common diseases caused by phagocyte defects. Hyper-IgE syndrome results from a mutation in the signal transducer and activator of transcription 3 (STAT3), affecting phagocytic cell recognition and osteoclast function involved in bone remodeling. It is characterized by high IgE levels, staphylococcal infections of the skin, lungs and bone as well as abnormalities in bone structure (Freeman and Holland, 2010; Notarangelo, 2010).

PIDs with complement deficiencies are rare and account for less than 1% of identified cases. Deficiencies in the complement pathway have clinical manifestations as systemic autoimmune disease similar to lupus erythematosus (SLE-like syndrome) or show recurring infections with encapsulated organisms (Bonilla et al., 2005; Notarangelo et al., 2006).

Furthermore, some forms of immunodeficiency are defined by autoimmune manifestations, resulting from defects in the regulation of self-tolerance (Coutinho and Carneiro-Sampaio, 2008;

Notarangelo et al., 2006). In many cases lymphocytes might be present but dysfunctional. They are unable to prevent the development of autoreactivity and thus cause autoimmune diseases (Lehman, 2015). Mutations in the autoimmune regulator (*AIRE*) disrupt central immune tolerance by insufficient deletion of T cell clones that recognize self antigens with high affinity. Mutations in *AIRE* cause autoimmune polyendocrinopathy-candidiasis-ectodermal dystrophy syndrome. Mutations affecting regulatory T cells (Tregs) are one of the main factors that lead to immune dysregulation. Mutations in Forkhead box P3 (*FOXP3*) for example cause polyendocrinopathy, enteropathy, X-linked (IPEX) syndrome (Bennett et al., 2001). Mutations in cytotoxic T lymphocyte-associated antigen 4 (*CTLA4*) result in CTLA4 haploinsufficiency (Kuehn et al., 2014; Schubert et al., 2014).

Clinical presentation of PID patients is highly variable. Most disorders have, however, increased susceptibility to infection as a common nominator. An early diagnosis of PID can be critical for successful treatment and to prevent mortality. PIDs should be suspected in children and adults that suffer from recurrent pneumonias and/or sinus, ear and cutaneous infections. Warning signs are also failure of infants to grow normally or to gain weight, chronic diarrhea with weight loss, recurrent organ or skin abscesses, persistent thrush, a need for intravenous antibiotics to clear infections and a family history of PID (Modell et al., 2011). With a growing catalog of identified mutations resulting in PIDs screening of patients that fall in these categories, the use of next generation sequencing applications like WES can be a potent diagnostic tool.

The treatment of PID patients is complex and generally includes both definitive and supportive strategies. CID and SCID can be treated with immunoglobulin replacement therapy or antibiotic and antifungal prophylaxis to reduce the severity and frequency of infections. Definitive therapy with bone marrow transplants (BMT) or hematopoietic stem cell transplantation (HSCT) can prevent the fatality of SCID. The common therapy approach for B cell disorders is Ig replacement therapy, which many patients will require indefinitely. Additionally, antibiotic and antifungal therapy may be necessary depending on the etiology of the specific B cell disorder (Shehata et al., 2010).

The treatment to manage innate disorders depends on the type of defect. Patients with phagocyte disorders receive primarily supportive therapy including antibiotic and anti-fungal prophylaxis. Cytokine replacement therapy and BMT are also options that have been shown to be effective in patients with CGD (Bonilla et al., 2005). In cases of complement deficiencies patients are treated with antibiotic prophylaxis to prevent recurring infections. Due to increased risk of infection,

multivalent meningococcal vaccinations, pneumococcal and Haemophilus influenza vaccines may be administered (McCusker and Warrington, 2011).

PID with autoimmunity can be challenging in patients, due to increasing risk for infections resulting from medication to control autoimmunity. Treatments can include steroids, Cyclosporine and cell depleting monoclonal antibodies (Amaya-Uribe et al., 2019). The prognosis of patients with PIDs depends on the etiology of the disorder. In general, patient outcomes and long-term survival have improved in the recent decades on the basis of advances in BMT and HSCT techniques and routine vaccination that provide herd immunity and thereby decrease the circulation of infectious disease.

1.4 Autoimmunity

The immune system evolved various mechanisms to control and prevent self-reactivity. An irregularity in one or multiple of these mechanisms can result in a breakdown of tolerance. The most common defects that are associated with autoimmune disease development affect peripheral tolerance rather than central tolerance (Theofilopoulos et al., 2017). Initial triggers for autoimmunity mostly involve recognition of self or foreign molecules by innate sensors. Recognition leads to inflammatory responses and can engage latent autoreactive T cells and B cells. Abnormal responses to self antigens have been connected to over 80 autoimmune diseases. Autoreactive T cells that escape thymic deletion are found in most healthy individuals. But even intermediate level of autoimmunity apparent as circulating autoantibodies and lesser tissue infiltrates do not necessarily lead to clinical consequences, since they can be kept in check by regulatory mechanisms. In other cases, even low level autoreactivity can lead to pathogenic autoimmunity. Autoimmune diseases have high prevalence in the population (7-9%) and especially occur in females. These are divided into organ-specific diseases, for example, Type-1 diabetes (T1D), inflammatory bowel disease (IBD), and multiple sclerosis and systemic diseases, for example, rheumatoid arthritis (RA) systemic lupus erythematosus (SLE) and Sjögren's syndrome. Autoimmune diseases are mainly driven by helper T cells and can be mediated by autoantibodies or cytotoxic T cells (Theofilopoulos et al., 2017).

Most autoimmune reactions arise from a combination of genetic and environmental factors (Kono and Theofilopoulos, 2017). Genetic susceptibility is mostly described as a sum of common risk variants that on their own would only have small effects and be insufficient to trigger autoimmunity (Gutierrez-Arcelus et al., 2016; Hunt et al., 2013). Genetic polymorphisms

in immune-related genes can lead to defective regulation or reduced threshold for lymphocyte activation. In autoimmune diseases both the adaptive and innate immune response are involved. However, there exist also monogenic mutations that associate with so-called autoinflammatory diseases, which arise from over-activation of the innate immune system alone (Park et al., 2012).

Among the several hundred loci connected to autoimmunity that often affect immune-system-related genes, major histocompatibility complex (MHC) haplotypes have the broadest association with autoimmune diseases. Genes including CTLA4, IL23R, PTPN22 and TYK2 have also been frequently described. Mutations in Foxp3, AIRE, IFIH1, DNASE1, TREX1, C1Q or C4A are found in rare monogenic autoimmune diseases. Mutations like these have provided insights to understand the pathogenesis of autoimmunity. However, these predisposing genetic risk factors only account for a portion of the overall disease (Theofilopoulos et al., 2017).

It has been shown that autoimmunity displays a sex dimorphism with a higher incidence of autoimmune diseases in females (Rubtsova et al., 2015). X-chromosome effects and gonadal hormones contribute to the sex bias, which is more pronounced after puberty. Estrogen interferes with B cell tolerance and enhances immune responses by regulating the expression of key immunity factors such as AIRE, IFN-γ and TLR trafficking protein UNC93B1 (Grimaldi et al., 2006; Markle and Fish, 2014; Ter Horst et al., 2016). The gut microbiota, which is influenced by sex hormones, also exhibits a sex dimorphism that may contribute to the differences in autoimmunity observed in male and female (Markle et al., 2013; Yurkovetskiy et al., 2013).

Environmental factors can initiate or augment the activation of self-reactive lymphocytes. Infections, diet, stress, microbiota, smoking as well as UV light irradiation have been described as factors for autoimmune reactions (Marrie, 2004; Mills, 2011; Root-Bernstein and Fairweather, 2014). On the one hand infections have been described as triggers by epitope spreading and strong innate pattern recognition receptor activation. On the other hand infections have been reported to protect against experimental autoimmune encephalomyelitis and MS in mice (Ochoa-Reparaz et al., 2010). Furthermore, the decrease of infections in industrialized countries resulting from higher hygiene standards correlates with the increase of autoimmune diseases (Belkaid and Hand, 2014; Fleming and Fabry, 2007), and a western diet defined by high salt, saturated fat, protein and high sugar intake has been shown to associate with increased disease incidence (Odegaard et al., 2012; Thorburn et al., 2014). Diet influences the gut microbiota, which is strongly linked to the immune system (Kuhn and Stappenbeck, 2013). UV irradiation is known as an environmental trigger for cutaneous lupus by causing apoptotic cell death. Apoptosis

increases the stress of nuclear antigens, especially when dead cells cannot be cleared efficiently (Kuhn et al., 2014). However, the mechanisms and interplay of environmental factors and genetic predisposition that impact on autoimmunity are still little understood.

The human gut microbiota is an ecosystem of 500-1000 bacteria species beneficial for physiological processes such as food digestion, competition for pathogens, metabolism and for the proper function of the immune system. Therefore, the gut microbiota has strong implications on human's health (Kamada et al., 2013; Louis and O'Byrne, 2010; Neish, 2009). Disturbances in the microbiota, called dysbiosis, have been observed in several autoimmune diseases like inflammatory bowel disease (IBD), asthma and allergies (Thorburn et al., 2015; Trompette et al., 2014; Wang et al., 2015). Dysbiosis commonly results in gut inflammation and alterations of intestinal immunity (Chassaing and Gewirtz, 2014). Furthermore, it was shown that disturbed microbiota could lead to Treg deficiency and activation of proinflammatory Th17 cells (Cani et al., 2008; Veldhoen et al., 2008). Fermentation of dietary fibers and production of short-chain fatty acids, particularly butyrate, are of special importance as they exert anti-inflammatory effects and promote the generation of peripheral Tregs (Arpaia et al., 2013; Furusawa et al., 2013; Smith et al., 2013). The bacterial product polysaccharide A offers immunological protection by induction of IL-10 producing Tregs (Mazmanian et al., 2008; Neff et al., 2016). Dysbiosis of oral microbiota has also been reported in humans with RA (Scher et al., 2016). Porphyromonas gingivalis is an oral bacteria that has the ability to citrullinate host peptides, generating citrullinated self antigens that promote autoimmune reactions in RA (Wegner et al., 2010). Aggregatibacter actinomycetemcomitans has been shown to contribute to the production of antibodies against citrullinated peptides in RA by activating citrullinating enzymes in neutrophils and releasing citrullinated antigens (Konig et al., 2016). These findings suggest to target dysbiosis as a new therapeutic approach for several autoimmune disorders.

Another central factor for autoimmunity is the escape of auto-reactive immune cells from the thymus (T cells) and fetal liver or bone marrow (B cells) that can elicit destructive anti-self responses. Autoreactivity occurs in the adaptive immune system due to the fact that lymphocyte antigen receptor specificity is generated randomly (MacPherson and Austyn, 2012). While negative selection eliminates the vast majority of autoreactive T cell through induction of apoptosis (clonal deletion), rendered unresponsiveness (anergy) or Treg differentiation, it is prone to substantial leakage (Kalekar et al., 2016; Legoux et al., 2015; Malhotra et al., 2016; Yu et al., 2015). The APECED syndrome (autoimmune polyendocrinopathy-candidiasis-ectodermal dystrophy) also known as APS-1 is an example for an autoimmune disease defined by inadequate

central deletion of autoreactive T cells. This rare disease is caused by mutations in the *AIRE* gene, a transcription factor expressed in the medulla of the thymus mediating the expression of peripheral-tissue-restricted self molecules that are essential for the elimination of self-reactive T cells (Bansal et al., 2017). APECED is defined by the destruction of endocrine organs as a result of inadequate T cell activity. Autoreactive B cells also escape central tolerance, ~55-75% of early immature B cells display autoreactivity. The autoreactive fraction reduces to ~40% for bone-marrow immature B cells and peripheral transitional B cells, and further to ~20% for mature naive B cells (Meffre, 2011; Nemazee, 2017; Wardemann et al., 2003). This progressive reduction of self-reactive B cells is achieved by apoptosis, anergy and changed non-autoreactive receptor specificity (receptor editing) (Nemazee, 2017). Patients with SLE, RA, T1D, Sjögren's syndrome or multiple sclerosis are often associated with polyspecific B cell clones that produce IgG pathogenic autoantibodies (Avrameas, 1991; Meffre, 2011; Nemazee, 2017).

In the context of a fully functional immune system escaped autoreactive T cells and B cells are controlled by peripheral tolerance mechanisms in the form of inhibitory molecules, anergy, ignorance and suppression by Treg cells (Theofilopoulos et al., 2017). Inhibitory molecules like CTLA4, PD1, LAG3, TIM3, VISTA, TIGIT and FcγRIIb are expressed on the surface of T cells and B cells to limit excessive immune responses against foreign and self antigens. Deficiency in some of these molecules result in autoimmune diseases driven by autoreactive lymphocytes, which are commonly present in the peripheral, but kept in check in healthy individuals (Ceeraz et al., 2017; Macauley et al., 2014; Okazaki et al., 2013; Paterson and Sharpe, 2010; Pincetic et al., 2014; Schmitt et al., 2016). Lymphocytes acquire unresponsiveness known as anergy, when T cells recognize antigens in absence of costimulatory molecules or when B cells lack T cell help for activation (Fathman and Lineberry, 2007; Zikherman et al., 2012). However, T cell anergy is a transient state mediated by molecules that limit proximal TCR signalling in combination with transcriptional silencing and induction of regulatory factors. This state can be reversed under inflammatory conditions. Anergic B cells have a half-life of ~5 days. To maintain unresponsiveness, they are controlled by continuous low-level interactions with antigen and inhibitory signalling by tyrosine kinase Lyn, tyrosine phosphatase SHP-1 and inositol phosphatase SHIP-1. A conditional knockout in any of these molecules in B cells leads to systemic autoimmunity in mice (Getahun et al., 2016; Lamagna et al., 2014). Autoreactive T cells and B cells can also remain dormant in the periphery due to ignorance, in the case that tissue-specific antigens are unattainable behind anatomical barriers or located in immunologically privileged sites such as the brain, eye and testis. This sequestration can be

impaired by infections and other causes of tissue damage and enable the activation of former ignorant autoreactive cells, leading to disease development (Prasad et al., 2016).

$CD4^+$ $CD25^+$ $Foxp3^+$ Tregs exert the most relevant suppressive effect on innate and adaptive immune responses (Li and Rudensky, 2016; Morikawa and Sakaguchi, 2014). Treg suppression requires cell-to-cell contact and is mediated by inhibitory molecules (CTLA4, IL-10, TGFβ and IL35), cytolysis, modulation of maturation and DC function, as well as interference with metabolic processes (Liu et al., 2015; Procaccini et al., 2016). Functional and numerical abnormalities in Treg cells associate with human autoimmune diseases. The propagation of autoimmunity is often related to a progressive increase of the effector T cell to regulatory T cell ratio. An exception are patients with psoriasis, who have increased Treg numbers in their inflamed skin; but these Tregs show abnormal behaviour and are capable of producing increased amounts of the pro-inflammatory cytokine IL-17 (Bovenschen et al., 2011). In autoimmune diseases, these IL-17 producing Tregs are likely to contribute to inflammation and to tissue injury (Zhou et al., 2009).

The innate immune system possesses sensors for foreign and self antigens that often precede and ignite adaptive responses. When misguided their responses can contribute to autoimmunity (Blasius and Beutler, 2010; Iwasaki and Medzhitov, 2015; Takeuchi and Akira, 2010). Endosomal and cytosolic sensors that differentiate foreign and self nucleic acids have been linked to multiple autoimmune diseases (Theofilopoulos et al., 2011). Important endosomal sensors are TLR3 (double-stranded RNA), TLR7, TLR8 (single stranded RNA), TLR9 deoxyribonucleic acid (DNA); cytosolic sensors include RIG-I ribonucleic acid (RNA), MDA5 (long double stranded RNA) and multiple DNA sensors (Barber, 2014; Chen et al., 2016). Activation of these sensors induces production of type I interferons and pro-inflammatory cytokines like IL-1, IL-6, IL-12 and TNF, which promote inflammatory responses (Crow, 2014).

As discussed, there are various triggers and pathways that can contribute to the initiation and propagation of autoimmune diseases. It is believed that autoimmunity arises from disruptions in multiple processes that act individually or in combination.

1.5 Regulatory T cells

Tregs are a subtype of $CD4^+$ T cells that can suppress inflammation and play a critical role in maintaining immunological self-tolerance and homeostasis (Sakaguchi et al., 2001; Shevach,

2002). Tregs terminate immune responses when an infectious agent has been eliminated. They can limit destructive responses directed against harmless or endogenous agents. While it is important to inhibit autoimmunity and chronic inflammation, the negative aspect of Treg activity needs to be taken into account. Increased numbers or activity of Tregs can, for example, obstruct anti-tumor immunity (Liu et al., 2013).

Tregs are either thymus derived natural Tregs (nTregs) or induced Tregs (iTregs). iTregs are formed in the periphery during adaptive immune responses; they can also be generated *in vitro* (Curotto de Lafaille and Lafaille, 2009). Tregs constitute approximately 5-10% of the peripheral $CD4^+$ T cell population. They are characterized by constitutive expression of the transcription factor Forkhead box P3 (Foxp3) and high levels of IL-2 receptor α-chain (CD25). Foxp3 is the key regulator of Treg function, development and maintenance of Tregs. The effectiveness of the regulatory function of Tregs is, however, critically dependent on stable Foxp3 expression (Brunkow et al., 2001; Fontenot et al., 2003; Hori et al., 2003). Transient Foxp3 expression can be induce in $CD4^+$ T cells by TGFβ1 and IL-2 stimulation, known as induced Tregs (iTregs). In contrast to Tregs their Foxp3 expression is transient. In absence of TGFβ1 iTregs lose Foxp3 as well as their suppressive capacities (Tone et al., 2008). Stable expression of Foxp3 is primarily ensured through Treg-specific demethylation of the *FOXP3* gene (Polansky et al., 2008).

Tregs suppress immune responses against infections, tumor cells, and allergens by regulating the activity of various immune cells including T cells, B cells, NK cells as well as monocytes and dendritic cells (DC) (Belkaid, 2008; Knutson et al., 2007). Tregs act, however, primarily on $CD4^+$ and $CD8^+$ T cells (Schmidt et al., 2012). Treg mediated suppression functions by cell-cell contact and soluble factors. Four major mechanisms have been described: suppression by inhibitory cytokines (TGFβ, IL-10, and IL-35), suppression by metabolic disruption (IL-2 deprivation), suppression by cytolysis (secretion of granzyme A) and suppression by modulating DC function and maturation by the co-inhibitory molecule CTLA4 (Asseman et al., 1999; Li et al., 2006; Thornton and Shevach, 1998).

Treg derived TGFβ can suppress NK cell and $CD4^+$ T cell activity in tumor microenvironments (Strauss et al., 2007). Furthermore, TGFβ is important for the inhibition of $CD8^+$ T cells in T1D (Green et al., 2003). IL-10 was shown to be critical in Treg-mediated suppression of intestinal and pulmonary inflammation (Asseman et al., 1999). IL-35 is an anti-inflammatory cytokine produced by Tregs that limits early T cell proliferation, thus preventing Th1 and Th17 development (Collison et al., 2007). Tregs disrupt metabolic pathways through expression of

ectoenzymes CD39 and CD73 on their surface. Production and transport of cyclic adenosine monophosphate (cAMP) into target T effector cells through gap junctions leads to the upregulation of inducible cAMP early repressor (ICER). ICER inhibits NFAT and IL-2 transcription resulting in apoptosis by IL-2 deprivation (Kobie et al., 2006; Safinia et al., 2015). The significance of IL-2 deprivation through Tregs by capturing available IL-2 facilitated by their high CD25 expression remains disputed (Fontenot et al., 2003; Pandiyan et al., 2007). Tregs are able to induce apoptosis in target cells through a cell-cell contact dependent mechanism. It has been described that activated Tregs kill target cells through the perforin/granzyme pathway by inducing serine protease granzyme A or B (Grossman et al., 2004). Furthermore, it has been observed that CTLA4 leads to downregulation of CD80/CD86 on APCs, which limits their ability to provide a co-stimulatory signal and to activate T cells (Takahashi et al., 2000; Vignali et al., 2008).

CD25 is upregulated in murine and human $CD4^+$ T cells upon activation. For mice Foxp3 has been shown to be a valuable Treg marker. In humans Foxp3 is less reliable for the identification of Treg cells, as it can be transiently upregulated at low levels in activated effector T cells and does not always correlate with suppressive capacity (Sakaguchi et al., 2010). GARP is a Treg-specific surface molecule, which is expressed upon Treg activation that binds latent TGFβ and facilitates its surface localization. The GARP/latent TGFβ1 complex regulates the bioavailability and activation of TGFβ by enabling the interaction with integrin αVβ8 and release of active TGFβ1 (Edwards et al., 2014; Wang et al., 2012).

1.6 GARP

GARP, also known as leucine rich repeat containing protein 32 (LRRC32), is a latent TGFβ binding protein (LTBP) distinctly expressed in activated Foxp3$^+$ Tregs, megakaryocytes and platelets (Macaulay et al., 2007; Tran et al., 2009). The 80kDa, 662 amino acid transmembrane protein shares over 80% identity between human and mouse. GARP consists of an extracellular region containing 20 leucine rich repeats (LRRs) that build an alpha/beta horseshoe fold, a hydrophobic transmembrane domain and a 15-residue C-terminal cytoplasmic domain (Lienart et al., 2018; Ollendorff et al., 1994). The N-terminus of GARP contains a 17-residue signal peptide, which is cleaved for the translocation of mature GARP to the cell surface (Chan et al., 2011).

GARP binds latent TGFβ1 by disulfide bonds (Cys192, Cys-331) in the cytoplasm and facilitates its surface localization, thereby regulating the bioavailability and activation of TGFβ (Wang et al., 2012). TGFβ is a pleiotropic cytokine with potent immunoregulatory properties. The TGFβ1, - β2 and -β3 isoforms are expressed as latent, inactive cytokines that require several tightly regulated steps for maturation (Robertson and Rifkin, 2013). TGFβ1 is the predominant isoform expressed by regulatory T cells. Newly synthesized homodimeric precursor pro-TGFβ is processed by intracellular cleavage by furin, producing still inactive latent TGFβ, non-covalently bound to latency associated protein (LAP) that prevents receptor binding by masking the interaction sites (Kehrl et al., 1986; Shi et al., 2011; Stockis et al., 2009). The mechanism how Tregs process this complex to release mature TGFβ from LAP is not fully understood yet. But it has been shown that metalloproteases and interactions with integrins $\alpha_v\beta_6$ and $\alpha_v\beta_8$ on the cell surface release active TGFβ1 and TGFβ3 (Edwards et al., 2014; Munger et al., 1999; Taylor, 2009). Integrin $\alpha_v\beta_8$ is expressed in stimulated Tregs and associates with the GARP/latent-TGFβ complex. It was further demonstrated that antibodies against β_8 can block TGFβ1 activation in human Tregs (Stockis et al., 2017). LAP contains an RGD motif that facilitates the interaction with α_v integrins, when the RGD motif is disrupted by mutation; mice resemble the phenotype of TGFβ1 deficiency (Rifkin, 2005; Yang et al., 2007). In contrast to other LTBPs the GARP-LAP complex is not secrete to the extracellular matrix (ECM) but instead tethers to the cell membrane (Miyazono et al., 1991; Tran et al., 2009). Soluble GARP that lacks the transmembrane domain is not able to activate TGFβ1 in the presence of α_v integrins (Wang et al., 2012). Induced expression of GARP in human embryonic kidney (HEK)293 cells facilitates surface localization of latent TGFβ1 but is also not sufficient to release mature TGFβ1 (Brown and Marshall, 2019). GARP regulates the bioavailability of mature TGFβ by providing an

interaction platform on the cell surface of Tregs for α_v integrin dependent activation (Stockis et al., 2017).

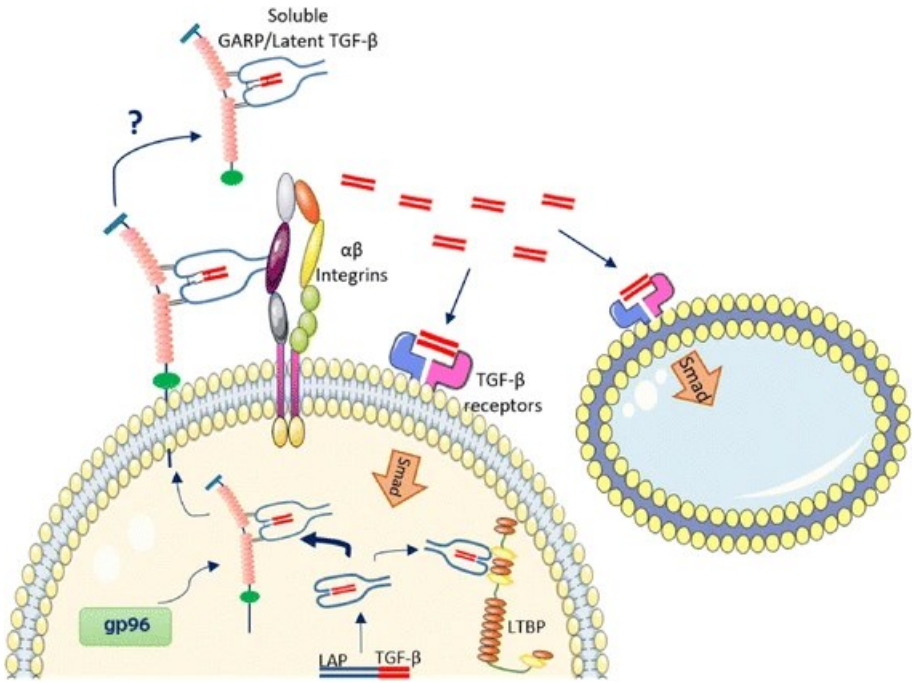

Figure 1 GARP functions in TGFβ maturation and activation
TGFβ is synthesized as inactive homodimeric precursor pro-TGFβ that is intracellular cleaved by furin, yielding still inactive latent TGFβ. GARP associates with latent TGFβ. The GARP/latent TGFβ complex associates with alpha-beta integrins (αVβ6 and αVβ8) on the cell surface to release mature TGFβ. Mature TGFβ interacts with TGFβ receptors on the cell surface activating Smad signalling in both an autocrine and paracrine fashion. The GARP/latent TGFβ complex can also be released from the cell surface as soluble GARP, but how TGFβ is activated from the soluble complex is not clear. Adapted from (Metelli et al., 2018).

It has been shown that GARP as a mediator of TGFβ maturation is important for enhancing the suppressive phenotype of Tregs, it is also involved in the maintenance of Treg-mediated peripheral tolerance (Cuende et al., 2015; Hahn et al., 2013; Meyer-Martin et al., 2016). Antibody inhibition (Cuende et al., 2015) and genetic suppression of GARP (Tran et al., 2009) confirm that GARP is necessary for the activation of TGFβ1 in Tregs and results in impaired Treg suppression (Probst-Kepper et al., 2010; Stockis et al., 2009). GARP-deficient mice have no detectable LAP on the surface of activated Tregs and patients with mutations in GARP show markedly decreased levels of LAP upon activation, indicating that GARP is solely responsible for the surface localization of the latent-TGFβ complex in Tregs (Edwards et al., 2013; Lehmkuhl et al., 2021).

Studies have shown that GARP is a specific marker for activated Treg and thus important for their suppressive function. GARP expression on Tregs is upregulated after TCR stimulation. IL-2 and IL-4 can induce GARP expression in murine Tregs. It is, however, not dependent on TGFβ

since TGFβ-deficient Tregs retain GARP expression. Foxp3 expression is required for GARP expression, but not sufficient to induce GARP expression on its own (Edwards et al., 2013; Tran et al., 2009; Wang et al., 2009). Gene expression of *LRRC32* in human T cells is defined by the methylation of two alternative promoters: upstream promoter 1 (P1) and downstream promoter 2 (P2). P2 is almost completely demethylated in both Tregs and Th cells, but several methylated CpG islands within the downstream P1 promoter block the transcription of GARP in Th cells. In Tregs this methylation in P1 is less significant and allows the binding of Foxp3 and subsequently the binding of nuclear factor of activated T cells (NFAT) as well as nuclear factor κB (NF-κB) to induce GARP transcription (Haupt et al., 2016). Additionally, GARP expression can be regulated at the post-transcriptional level by microRNAs (miRNAs) (Zhou et al., 2013).

The abundance and activity of GARP can fine-tune the release of active TGFβ1. TGFβ1 released by Treg has been mainly described to act in a paracrine manner for development of other Tregs or Th17 cells (Edwards et al., 2013) and in mediating contact-dependent Treg inhibition (Cuende et al., 2015). Reduced GARP levels were found to be associated with rheumatoid arthritis (RA) (Haupt et al., 2016); patients with GARP mutations also showed severe autoimmune phenomena (Lehmkuhl et al., 2021). In addition, GARP mutations were described to be prevalent in atopic dermatitis (AD) and to increase the risk of food allergy, asthma and inflammatory bowel disease (Manz et al., 2016; Weidinger and Novak, 2016). A407T is the most frequent mutation variant of GARP in AD, the mutations result in an impairment of surface localization of GARP and lower expression of LAP on Tregs (Manz et al., 2016).

1.7 Foxp3

The forkhead/winged-helix transcription factor Foxp3 is selectively expressed in Tregs and is the key regulator of Treg function and development (Fontenot et al., 2003). Mutations in Foxp3 lead to the loss of Treg suppressor function resulting in severe autoimmune diseases in humans such as Immune dysregulation, Polyendocrinopathy, Enteropathy X-linked (IPEX) syndrome or X-linked autoimmunity and allergic dysregulation (XLAAD) syndrome (Gambineri et al., 2003; Khattri et al., 2003; Wildin et al., 2001). A frameshift mutation in the Foxp3 gene in mice, known as scurfy mice, results in defective T cell tolerance and lymphoproliferative disease that is fatal within three to four weeks of age (Brunkow et al., 2001; Godfrey et al., 1991).

Human and murine Foxp3 protein share a high degree of homology. The 431 (human) and 429 (mouse) amino acid long proteins contain a zinc finger domain, leucine zipper for

oligomerisation, a repressor domain, a C-terminal DNA binding forkhead domain and a N-terminal proline-rich domain (Hancock and Ozkaynak, 2009).

Foxp3 interacts with a variety of transcriptional factors acting as a repressor as well as activator of gene transcription (Chen et al., 2006). Most notably Foxp3 associates with NF-κB (Bettelli et al., 2005) and NFAT (Wu et al., 2006) blocking their ability to induce endogenous expression of IL-2, IL-4 and IFN-γ (Hori et al., 2003). A stable expression of Foxp3 is indispensable for the maintenance of suppressive properties in human and murine Tregs. Moreover, Foxp3 is also essential for the maintenance of immune homeostasis. Foxp3 activity is highly and specifically regulated. On a transcriptional level stable Foxp3 expression relies on epigenetic modifications in the *Foxp3* gene. In natural occurring Tregs the highly conserved CpC-rich intronic region, called Treg specific demethylated region (TSDR) or CNS2 is fully demethylated. In conventional T cells (Tconvs) this region is methylated. Foxp3 expression can still be transiently induced by TCR stimulations in combination with IL-2 and TGFβ in Tconvs, although the TSDR region remains methylated. However, iTregs lose their Foxp3 expression and suppressive identity in absence of TGFβ stimulus and no stable expression can be imprinted in this manner (Baron et al., 2007; Hori et al., 2003; Li et al., 2014; Zheng et al., 2010).

On a posttranslational level the activity and stability of Foxp3 is regulated by acetylation. It has been shown that Foxp3 protein has a short half-life and that ubiquitin-mediated proteasomal degradation can be prevented by acetylation of Foxp3 (van Loosdregt et al., 2010). Polyubiquitination initiates at lysine residues, which are unavailable when acetylated. It was shown that mutating all lysine residues into arginine in Foxp3 prevents polyubiquitination and drastically increase Foxp3 protein levels (van Loosdregt et al., 2010). Foxp3 acetylation also enhances Treg function by promoting DNA binding capabilities of Foxp3(Tao et al., 2007). The acetylation state of Foxp3 is defined by the interplay of multiple histone acetyltransferases (HAT) and histone deacetylases (HDAC) that exist in a Foxp3-associated super molecular complex (Li et al., 2007; Samanta et al., 2008; van Loosdregt et al., 2010). The HATs p300 and TIP60 have been defined as acetylation mediators of Foxp3, while Sirtuin 1, HDAC6, 7 and HDAC9 act as their counterpart that deacetylate Foxp3 (Tao et al., 2007; Xiao et al., 2010). Inhibition or knockout of histone deacetylases (HDACs) augments the suppressive function of Tregs (Tao et al., 2007; van Loosdregt et al., 2010), while genetic deletion of acetyltransferases (HATs) strongly attenuates Treg function and leads to fatal autoimmunity (Liu et al., 2014). By fine tuning the expression and activity of HATs and HDACs the acetylation of Foxp3 can be

promoted or reduced to modulate its protein stability. By defining the proteasomal turnover of Foxp3, Treg function can be regulated on a posttranslational level.

1.8 Foxp3 protein acetylation

Post-translational lysine acetylation is a reversible process governed by the antagonistic functions of HATs and HDACs (Carrozza et al., 2003). Acetylation of histone proteins was discovered in the 1960s, when core histones were described to be acetylated at the ε-amino group of lysine residues (Allfrey et al., 1964; Phillips, 1963). Acetylation of lysine residues neutralizes their positive charge that is necessary for a compact chromatin structure (Roth et al., 2001). Broad acetylation of Histone H3 and H4 results in decondensation of chromatin domains and renders them more accessible for transcription (Eberharter and Becker, 2002). HATs and HDACs also regulate the acetylation of several non-histone proteins, such as p53, NF-κB, c-Myc and Foxp3 (Zhang et al., 2012).

HDAC9 is a class II HDAC (HDAC4, HDAC5, HDAC6, HDAC7, HDAC9 and HDAC10) with a catalytic domain at the N-terminus. Class II HDACs shuttle between the nucleus and the cytoplasm; their deacetylase activity is Zn^{2+} dependent and sensitive to inhibition by Trichostatin A (TSA) (Dokmanovic et al., 2007). While the expression of most HDACs is similar in Treg and CD4+ non Treg cells, the expression of HDAC9 is significantly higher in regulatory T cells and up to 30 times greater in activated Tregs compared to Tconvs (Tao et al., 2007). HDAC9 associates with Foxp3 and promotes its deacetylation. This interaction can be antagonized by TCR and CD28 co-stimulation (Li et al., 2007). The importance of HDAC9 in controlling Treg function is especially apparent in $HDAC9^{-/-}$ mice. In these mice Foxp3 acetylation is enhanced, the frequency of $CD4^{+}$ Foxp3 T cells increased by ~50% and the suppressive capacity of Tregs is three- to fourfold higher compared to wild-type controls (Beier et al., 2012; Tao et al., 2007). Furthermore, HDAC9 is described as a negative regulator of Tregs. Zoeten et al. observed an increased local HDAC9 expression in mice with colitis, while $HDAC9^{-/-}$ mice were resistant to development of colitis (de Zoeten et al., 2010). The use of HDAC inhibitors TSA and Nicotinamid (NAM) was shown to increase Foxp3 acetylation, and to improve Foxp3 stability and Treg function. NAM is a specific inhibitor for Sirtuin-1 (Sirt1), of the HDAC III family(van Loosdregt et al., 2010).

1.9 Objectives of the thesis

Autoimmune diseases are frequently caused by single gene mutations in central pathways of immune tolerance. GARP is a protein that is specifically expressed on regulatory T cells and is important for their suppressive capacity. By binding latent TGFβ1 and enabling interactions on the cell surface GARP is involved in TGFβ1 activation. However, the function of this TGFβ1 source and the underlying mechanisms are not yet completely understood. This thesis presents research results that highlight the importance of GARP as a regulator of Treg function and the maintenance of peripheral tolerance. It reports one female and one male PID patient with previously undescribed mutations in *LRRC32*, who suffer from severe immune dysregulation and exhibit low GARP expression and Treg defects. By use of Garp-deficient mice the increased susceptibility to inflammatory diseases in the absence of GARP was confirmed and the underlying molecular mechanism deciphered. The study addresses the function of GARP in a novel molecular detail and demonstrates the relevance of functional Tregs for physiological immune homeostasis in men and mice.

The aims of my PhD thesis were:

1. to analyse patients with low GARP expression on Tregs due to mutations in *LRRC32*, resulting in dysregulated immunity;

2. to characterise the underlying molecular mechanisms in cells of conditional GARP knockout mice and patients, that culminate in functional Treg-defects;

3. to define the role of GARP in Tregs and its function as a source for TGFβ1;

4. to analyse the effect of exogenous TGFβ1 on the identified deregulations observed in Garp-deficient Tregs.

2 Materials and Methods

2.1 Materials

2.1.1 Reagents

Reagent / Cytokine	Origin
Acrylamid/bis-acrylamid 30% (37.5:1)	Merck, Darmstadt, Germany
Agarose	Merck
Albumin fraction V from bovine serum (BSA)	Merck
Ammonium chloride (NH_4Cl)	Sigma-Aldrich, St. Louis, MO
Ammonium persulfate (APS)	Sigma-Aldrich
Bromophenol blue	Merck
Carboxyfluorescein succinimidyl ester (CFSE)	Life Technologies Invitrogen, Carlsbad, CA
Complete protease inhibitor cocktail	Roche, Penzberg, Germany
Chicken type II collagen	Chondrex, MD Biosciences, Oakdale, MN
Cycloheximide (CHX)	Sigma-Aldrich
Dimethylsulfoxid (DMSO)	Merck
Dithiothreitol (DTT)	Sigma-Aldrich
DNA Gel Loading dye (6x)	Life technologies Invitrogen
Dulbecco's Modified Eagle Medium (DMEM)	Life technologies Invitrogen
Deoxyribonucleotide triphosphate (dNTP) set (100 mM solutions)	Life technologies Invitrogen
Dextran sulphate sodium (DSS)	MP Biomedicals, Solon, OH
Dynabeads™ Protein G	Thermo Fisher Scientific, San Diego, CA
ECL Western Blotting Detection Reagent	GE Healthcare, Munich, Germany
Ethanol (C_2H_5OH)	Merck
Ethylendinitrotetraacetic acid (EDTA)	Sigma-Aldrich
EX-527	Sigma-Aldrich

Ficoll lymphoflot	Biotest, Dreieich, Germany
Formaldehyde 37%	AppliChem GmbH, Darmstadt, Germany
L-glutamine ($C_5H_{10}N_2O_3$)	Life technologies Invitrogen
Glycerol ($C_3H_5(OH)_3$)	Merck
Glycine (NH_2CH_2COOH)	Merck
Hank's Balanced Salt Solution (HBSS)	Life technologies Invitrogen
Hydrochloric acid 37% (HCl)	Merck
IL-2 (Proleukin, recombinant human)	Novartis, Basel, Switzerland
IL-2 (Proleukin, recombinant mouse)	R&D Systems, Minneapolis, MN
Ionomycin	Merk
Isopropanol (C_3H_7OH)	Merck
Lipofectamin^{TM} LTX	Life technologies Invitrogen
Magnesium chloride ($MgCl_2$)	Merck
Methanol (CH_3OH)	Sigma-Aldrich
Monensin	Sigma-Aldrich
Nonyl phenoxypolyethoxylethanol-40 (NP-40)	Millipore, Billerica, MA
Non-fat dry milk powder	Real
Opti-MEM	Life technologies Invitrogen
Paraformaldehyde (PFA)	Merck
Penicillin G / streptomycin	Life technologies Invitrogen
Phorbol myristate acetate (PMA)	Sigma-Aldrich
Phosphate buffered saline (PBS)	Life technologies Invitrogen
Potassium chloride (KCl)	Merck
Protan nitrocellulose menbranes	Whatman, Dassel, Germany
RediLoad Loading buffer (10x)	Life technologies Invitrogen
Roswell Park Memorial Institute (RPMI) 1640	Life technologies Invitrogen
Saponin	Sigma-Aldrich

Sodium azide (NaN_3)	Merck
Sodium chloride (NaCl)	Merck
Sodium dihydrogen phosphate (NaH_2PO_4)	Merck
Sodium dodecyl sulfate (SDS)	Merck
Sodium hydroxide (NaOH)	Merck
SYBR safe DNA gel stain (10,000x)	Life technologies Invitrogen
TaqMan Universal PCR mastermix 2x	Life technologies Invitrogen
Tetramethylethylenediamine (TEMED)	Merck
TGFβ1 (recombinant human)	R&D Systems
TGFβ1 (recombinant mouse)	R&D Systems
Triton X-100	Sigma-Aldrich
Trichostatin A (TSA)	Sigma-Aldrich
Trypsin	Sigma-Aldrich
Tween 20	Sigma-Aldrich
Vorinostat	Sigma-Aldrich
Nicotinamide (NAM)	Sigma-Aldrich

2.1.2 Antibodies

2.1.2.1 Antibodies for cell culture

Specificity	Conjugate	Clone	Provider
Anti-human CD3	non	OKT3	From our lab, Munich, Germany
Anti-human CD28	non	CD28.2	BD Biosciences, San Diego, CA
Anti-mouse CD3	non	145-2C11	BD Biosciences
Anti-mouse CD28	non	37.51	BD Biosciences

2.1.2.2 Antibodies for flow cytometry

Specificity	Conjugate	Clone	Provider
Anti-human CD3	Fluorescein isothiocyanate (FITC)	UCHT1	Sigma-Aldrich
Anti-human CD4	Allophycocyanin (APC)	RPA-T4	Biolegend, San Diego, CA
Anti-human CD8	FITC	SK1	BD Biosciences
Anti-human CD14	FITC	UCHM-1	Sigma-Aldrich
Anti-human CD16	Phycoerythrin (PE)	3G8	Biolegend
Anti-human CD19	PE	J3-119	Beckman Coulter, Brea, CA
Anti-human CD20	FITC	2H7	BD Biosciences
Anti-human CD25	FITC	M-A251	BD Biosciences
Anti-human CD25	PE	M-A251	BD Biosciences
Anti-human CD45RA	FITC	HI100	BD Biosciences
Anti-human CD45RO	PE	UCHL1	BD Biosciences
Anti-human CD56	PE	MY31	BD Biosciences
Anti-human CD69	FITC	FN50	BD Biosciences
Anti-human Foxp3	PE	PCH101	ebioscience, San Diego, CA
Anti-human Foxp3	APC	PCH101	ebioscience
Anti-human GARP	PE	G14D9	ebioscience
Anti-human LAP	PE/cyanine 7 (Cy7)	TW7-16B4	Biolegend
Anti-mouse CD3	FITC	17A2	ebioscience
Anti-mouse CD4	PE/Cy7	GK1.5	ebioscience
Anti-mouse CD19	PE	1D3	ebioscience
Anti-mouse CD25	PE	PC61.5	ebioscience
Anti-mouse CD45.1	APC	A20	Biolegend

Anti-mouse CD45.2	PE	104	Biolegend
Anti-mouse CD304 / Neuropilin-1 (NRP1)	PE/Cy7	3DS304M	Biolegend
Anti-mouse CTLA4	APC	UC10-4B9	Biolegend
Anti-mouse Foxp3	APC	FJK-16s	ebioscience
Anti-mouse Foxp3	non	FJK-16s	ebioscience
Anti-mouse GARP	APC	YGIC86	ebioscience
Anti-mouse IL-10	APC	JES3-16E3	Biolegend
Anti-mouse LAP	APC	TW7-16B4	ebioscience
Armenian hamster IgG	APC	eBio299Arm	ebioscience
Goat anti-rabbit IgG	PE	Polyclonal	R&D Systems
Goat anti-rabbit IgG	Alexa Fluor (A)488	Polyclonal	Thermo Fisher Scientific
Goat anti-rat IgG	A488	Polyclonal	Thermo Fisher Scientific
Goat anti-rat IgG	A594	Polyclonal	Thermo Fisher Scientific
Mouse IgG1	PE	RMG1-1	Biolegend
Mouse IgG1, κ	PE/Cy7	MOPC-21	Biolegend
Mouse IgG1, κ	PE	MOPC-21	BD Biosciences
Rabbit anti-acetyl-lysine	non	RM101	Abcam
Rabbit anti-acetyl-lysine	PE/Cy7	15G10	Biolegend
Rabbit anti-SMAD3	non	Polyclonal	Thermo Fisher Scientific
Rabbit anti-phospho-SMAD2 Ser465/467)/SMAD3 (Ser423/425)	non	D27F4	Cell Signalling, Danvers, MA
Rabbit IgG XP®	non	DA1E	Cell Signalling
Rat IgG2a, κ	non	eBR2a	BD Biosciences
Rat IgG2a, κ	PE	eBR2a	BD Biosciences
Rat IgG2a, κ	PE/Cy7	eBR2a	BD Biosciences

Rat IgM, κ	PE	R4-22	BD Biosciences

2.1.2.3 Antibodies for immunoprecipitation / western blot

Specificity	Conjugate	Clone	Provider
Anti-mouse beta-actin	Horseradish peroxidase (HRP)	C4	Santa Cruz
Anti-mouse Foxp3	non	FJK-16s	ebioscience
Anti-rabbit IgG	HRP	Polyclonal	Santa Cruz
Anti-rat IgG	HRP	Polyclonal	Santa Cruz
Rabbit anti-acetyl-lysine	non	Polyclonal	Millipore, Billerica, MA
Rabbit anti-acetyl-lysine	non	RM101	Abcam

2.1.3 Ladders / Markers

Name	Provider
Biotinylated protein ladder (9-200 kilo Dalton (kDa))	Cell Signalling
GeneRuler DNA ladder (100 base pair (bp))	Fermentas, St. Leon-Rot, Germany
Prestained protein marker (11-245 kDa)	New Enland Biolabs, Ipswich

2.1.4 Serum

Name	Provider
Fetal calf serum (FCS)	Life technologies
Mouse serum	Sigma-Aldrich
Normal human serum (NHS)	From our lab, Munich, Germany
Rat serum	Sigma-Aldrich

2.1.5 Enzymes

Enzyme	Supplied Reaction Buffer	Provider
AmpliTaq DNA polymerase	10x PCR Buffer II	Life technologies
GeneAmp High Fidelity PCR Enzyme Mix	10x GeneAmp High Fidelity PCR buffer	Life technologies
Proteinase K	non	Roche

2.1.6 Single nucleotide polymorphism (SNP) genotyping assays

SNP location	SNP ID	Probe	Sequence
LRRC32 intergenic region	1750909A3	G= victoria (VIC), A= fluorescein amidite (FAM)	CCAGGCTGAGTTCCAGCTCAC CTG[G/A]CTTGACCTGCGGGA GAACAAACTG
LRRC32 intergenic region	1750909A4	G=VIC, A=FAM	AGCGGCTCAACCTGCAGGGG AACC[G/A]AGTCAGCCCCTGT GGGGGGCCAGA

2.1.7 Primers for mice genotyping

Primers were synthesized by Eurofins Genomics, Ebersberg, Germany.

Name	Primer	Sequence (5’ to 3’)
10774cre	forward primer	CTGGAAAATGCTTCTGTCCGTTTGC
10775cre	reverse primer	AATCCATCGCTCGACCAGTTTAGTTACC
24200flp	forward primer	ATGGCTTAGTTTCCCATAGAAGATACT
24201flp	reverse primer	ATCTGGTTGTCACTTAAATCCAGGTGACG

2.1.8 TaqMan gene expression assays

Gene	Assay ID	Probe	Interrogated Sequence
Human *ACTB*	Hs99999903_m1	VIC-probe	NM_001101.2
Human *LRRC32* transcript variant 2	Hs00973758_m1	FAM-probe	NM_001128922.1, XM_005273902.3
Human *HDAC9*	Hs00206843_m1	FAM-probe	NM_001204144.2, NM_001204145.2, NM_001204146.2
Mouse Actb	Mm00607939_s1	VIC-probe	NM_007393.5
Mouse Foxp3	Mm00475162_m1	FAM-probe	NM_001199347.1, NM_001199348.1, NM_054039.2
Mouse Hdac1	Mm02391771_g1	FAM-probe	NM_008228.2
Mouse Hdac2	Mm00515108_m1	FAM-probe	NM_008229.2
Mouse Hdac3	Mm00515916_m1	FAM-probe	NM_010411.2
Mouse Hdac4	Mm01299557_m1	FAM-probe	NM_207225.1
Mouse Hdac6	Mm01341125_m1	FAM-probe	NM_001130416.1, NM_010413.3
Mouse Hdac9	Mm01293999_m1	FAM-probe	NM_001271386.1, NM_024124.3

2.1.9 Vector list

Vector name	Inserted sequence
pcDNA3.1-GARP_wild-type (wt)	GARP coding sequence (cds), +139-+2127 bp of NM_001128922.1
pcDNA3.1-GARP_c.741G>A	GARP cds, +139-+2127 bp of NM_001128922.1 c.741G>A
pcDNA3.1-GARP_c.934C>T	GARP cds, +139-+2127 bp of NM_001128922.1 c.934C>T
pcDNA3.1-GARP_c.1262G>A	GARP cds, +139-+2127 bp of NM_001128922.1 c.1262G>A
pcDNA3.1-empty	none

2.1.10 Kits

Name	Origin
Acid Phosphatase, Leukocyte (TRAP) Kit	Sigma-Aldrich
Affinity Script QPCR cDNA Synthesis kit	Agilent technologies, Santa Clara, CA
Amaxa Mouse T cell Nucleofector Kit	Lonza, Cologne, Germany
Amaxa Mouse T cell Nucleofector Kit V	Lonza
$CD4^+$ T cell Isolation kit, human	Miltenyi Biotec, Bergisch Gladbach, Germany
CD25 MicroBeads II, human	Miltenyi Biotec
CD45RA MicroBeads, human	Miltenyi Biotec
$CD4^+$ T cell Isolation kit, mouse	Miltenyi Biotec
$CD25^+$ T cell Isolation kit, mouse	Miltenyi Biotec
Cytofix/Cytoperm™ Fixation and Permeabilization Solution	BD Bioscienes
Dako REAL™ Detection System	DAKO, Hamburg, Germany
FOXP3 Fix/Perm buffer set	Biolegend
High Pure PCR Template Preparation Kit	Roche
Human Foxp3 Buffer set	BD Bioscienes
Mouse Foxp3 Buffer set	BD Bioscienes
Phosflow™ Perm Buffer III	BD Bioscienes
True-Nuclear™ Transcription factor buffer set	Biolegend
RNeasy Plus Mini kit	Qiagen

2.1.11 Devices

Name	Origin
Bio-Rad PowerPac 1000	Bio-Rad, Hercules, CA
Biophotometer®D30	Eppendorf
Biosafety Cabinet (NU-437-600)	NuAire, Plymouth, MN

BZ-8100 Fluorescence Microscope	Keyence, Osaka, Japan
EC-140 Mini Blot Module	E-C Apparatus
Fluorescence activated cell sorting (FACS) Cytomics FC500	Beckman Coulter
FUJIFILM LAS-3000	Fujifilm, Tokyo, Japan
gentleMACS Dissociator	Miltenyi Biotec
Heracell 240 CO_2 incubator	Thermo Fisher Scientific
MACSmix Tube rotator	Miltenyi Biotec
Microcentrifuge 5415R	Eppendorf
Microm HM 340E	Thermo Fisher Scientific
MP225 pH Meter	Mettler Toledo, Columbus, Ohio
Nucleofector™ II	Lonza
PURELAB® Ultra	Elga, Celle, Germany
Rotixa 50 RS centrifuge	Hettich AG, Bäch, Switzerland
Unimax 1010 Orbital Shaker	Heidolph GmbH, Schwabach, Germany
UVT-28 MP transilluminator	Herolab GmbH, Wiesloch, Germany
Z2 COULTER COUNTER	Beckman Coulter
5427 R Centrifuge	Eppendorf
9800 Fast Thermal Cycler	Applied Biosystems, Foster City, CA
7500 Fast Real-time PCR System	Applied Biosystems

2.1.12 Software

Name	Origin
Excel 2011	Microsoft, Redmond, WA
I-TASSER	Zhanglab, Ann Arbor, MI
MatInspector	Genomatix, Munich, Germany
Mayday 2.30	University Tübingen
Prism 5.0a	GraphPad, La Jolla, CA
PyMOL 2.0	Schrödinger, New York

STRUM	Zhanglab, Ann Arbor, MI

2.1.13 Buffers and solutions

Buffers and solutions	Composition
Radioimmunoprecipitation assay (RIPA) Cell Lysis buffer	50 mM Tris-HCl, pH 7.6 150 mM NaCl 10 mM EDTA 0.1% SDS 0.5% NP-40 1x cOmplete™, EDTA-free Protease Inhibitor Cocktail
DNA Loading buffer (6x)	50 mM EDTA 26.1% Glycerol 0.25% Bromphenol blue
FACS buffer	PBS 2% FCS 0.01% NaN_3
Magnetic activated cell sorting (MACS) buffer	PBS 0.5% BSA 2 mM EDTA
Resolving gel (12.5%)	380 mM Tris-HCl, pH 8.8 12.5% Acrylamide/bis-acrylamide 0.2% SDS 0.2% APS 10 µl TEMED H_2O ad 10 ml
Stacking gel (4%)	126.6 mM Tris-HCl, pH 6.8 4% Acrylamide/bis-acrylamide 0.1% SDS 0.1% APS 5 µl TEMED H_2O ad 5 ml
SDS Blot buffer	20 mM Tris-HCl, pH 7.6 140 mM NaCl 0.1% Tween20
SDS Running buffer	12.5 mM Tris-HCl, pH 6.8 96 mM Glycine 0.05% SDS

SDS Sample buffer	62.5 mM Tris-HCl, pH 6.8 2% SDS 10% Glycerol 50 mM DTT 0.01% Bromophenol blue
SDS Transfer buffer	12.5 mM Tris-HCl, pH 8.3 86 mM Glycine 0.05% SDS 20% Methanol
Tris-Acetate-EDTA (TAE) buffer (50x)	242 g Tris-HCl 57.2 ml acetic acid 50 mM EDTA (pH7.6) H_2O ad 1 l
Tris-buffered saline (TBS) buffer	20 mM Tris-HCl (pH7.6) 140 mM NaCl
Tris-buffered saline with 0.1% Tween (TBST) buffer	20 mM Tris-HCl (pH7.6) 140 mM NaCl 0.1% Tween-20
Cytokine Fix buffer	PBS (pH 7.4) 4% PFA
Cytokine Perm buffer	PBS 2% FCS 0.01% NaN_3 0.1% Saponin

2.2 Methods

2.2.1 Ethics

All patients and healthy individuals provided written informed consent. The study was approved by the Ethics Committee of the Universities of Munich and Freiburg.

2.2.2 Whole-exome sequencing (WES)

All WES work was performed by members of AG Grimbacher from Albert-Ludwigs-University of Freiburg. Genomic DNA was extracted from human peripheral blood mononuclear cells (PBMCs) using QIAamp Kits (Qiagen, Hilden, Germany) following the manufacturer's instructions. WES was accomplished by following the Agilent (Santa Clara, CA) custom Sure Select exome sequencing protocol. SureSelect exome v5 probes were used to enrich the Exomes. Libraries were sequenced twice (2 flow cells) on the HiSeq 2500 v4 with a 2X76bp protocol generating 4 raw FASTQ files (sequence data files) per sample. Data pre-processing was performed according to the GATK best practices (DePristo et al., 2011; McKenna et al., 2010; Van der Auwera et al., 2013). The Data pre-processing included the following: 1) FASTQ files were converted into a unmapped BAM file (PICARD tool FastqToSam), (2) tags were added to the Illumina adapter sequences of the unmapped BAM file (PICARD tool MarkIlluminaAdapters), (3) the unmapped tagged BAM file was converted to a FASTQ file (PICARD tool SamToFastq), (4) alignment to reference genome build UCSC hg38 (BWA MEM) was performed, (5) duplicated reads were identified (MarkDuplicates PICARD), (6) BAM was recalibrated and (7) indel realigned. Variant calling was achieved with three different variant callers, GATK Haplotype caller, FreeBayes and SAMtools. BASH and R scripts were subsequently applied for (1) merging of the VCFs files, (2) identifying and unifying of dinucleotide changes and (3) formatting of the data sets for the import into an in-house specialized SQL database (GemmaDB) at the Centre of Chronic Immunodeficiency in Freiburg. Annotation of variants was performed by the Ensembl's Variant Effect Predictor (VEP) tool (https://www.ensembl.org/info/docs/tools/vep/index.html). The allele frequency (AF) data was extracted from the gnomAD exomes (v2.1.1) and genomes (v3) data sets (https://gnomad.broadinstitute.org/downloads). The individual frequency was obtained by transformation of the gnomAD AF data. Filtering of the variants was conducted by the selection of variants with (1) an individual frequency below 1% either in the internal cohort and in gnomAD (exomes or genomes) populations, which includes control cohorts such us the NHLBI-GO Exome Sequencing Project or the 1000 Genomes project, (2) a "high" or "moderate" impact

prediction, (3) an alternative allele frequency (AF1) bigger than 0.3 and read depth (DP) bigger than 20, (4) matching of zygosity of an autosomal recessive or X-linked recessive mode of inheritance, for the lack of family disease history it was no possible to identify *de novo* variants without the parents of the patients (analysis of variants was performed in regards to association with autosomal dominant conditions, results were limited to one transcript per variant (the one with the highest score)), (5) resulting candidate variants were individually analysed considering gene function and role in disease.

2.2.3 Genomic DNA isolation form mouse ear punches

Total DNA was extracted from mouse ear punches using the High Pure PCR Template Preparation Kit (Roche) according to the manufacturer's instructions. Ear punches were lysed with 200 µl Tissue Lysis Buffer and 40 µl Proteinase K in 1.5 ml Eppendorf tubes and incubated for 3 hours at 55°C. 200 µl Binding Buffer was added, mixed and incubated for 10 minutes at 70°C. 100 µl isopropanol (Merk) was added, mixed and Eppendorf tubes centrifuged at 13000 relative centrifugal force (rcf) for 5 minutes. The sample was transferred to a High Pure Filter Tube placed in a 2 ml Collection Tube and centrifuged at 8000 rcf for 1 minute. The Filter Tube was removed from the Collection Tube and assembled with a new Collection Tube. 500 µl Inhibitor Removal Buffer were added to the Filter Tube and the assembly was centrifuged at 8000 rcf for 1 minute. The Filter Tube was removed from the Collection Tube and assembled with a new Collection Tube followed by two washing steps with 500 µl Wash Buffer and centrifugation at 8000 rcf for 1 minute. While washing the flow-through was discarded and the Filter Tube placed in a fresh Collection Tube. After the last washing step, the Filter Tube was transferred to a fresh Collection Tube and centrifuged for 10 seconds at full speed. For DNA elution, the Filter Tube was transferred to a 1.5 ml Eppendorf tube, 200 µl prewarmed Elution Buffer water was applied to the Filter Tube and the tube assembly was centrifuged at 8000 rcf for 1 minute. All centrifugation steps were carried out in a 5415R microcentrifuge (Eppendorf) with a fixed angle rotor. DNA concentration and quality was assessed by analysing the absorbance ratio of 260 nm and 280 nm (A_{260}/A_{280}) using a Biophotometer®D30 (Eppendorf). DNA was stored at -20°C, or at 4°C for immediate usage.

2.2.4 Total RNA isolation

Total RNA was extracted from $CD25^+$ and $CD25^-$ $CD4^+$ T cells using RNeasy Plus Mini Kit (Qiagen) according to the manufacturer's instructions. After washing with PBS, 1-3x10^6 T cells were lysed in 350 µl RLT buffer and homogenized by thorough vortexing. Homogenate was transferred to gDNA Eliminator Spin Columns placed in a 2 ml Collection Tube and centrifuged at 8000 rcf for 30 sec. Flow-though was mixed with 350 µl 70% ethanol and applied to a RNeasy Mini Spin Column placed in a 2 ml Collection Tube. After centrifugation at 8000 rcf for 15 sec, columns were washed with 700 µl RW1 Buffer followed by two washing steps with 500 µl RPE Buffer. While washing the flow-through was discarded and columns placed in a fresh Collection Tube. After the last washing step, columns were transferred to a fresh Collection Tube and centrifuged for 1 minute at full speed. For RNA elution, columns were transferred to 1.5 ml Eppendorf tubes, 30 µl RNeasy-free water was applied directly to the spin column membrane and centrifuged at 8000 rcf for 1 minute. All centrifugation steps were carried out in a 5415R microcentrifuge (Eppendorf) with a fixed angle rotor. RNA concentration and quality was assessed by analysing the absorbance ratio of 260 nm and 280 nm (A_{260}/A_{280}) using a Biophotometer®D30 (Eppendorf). RNA was stored at -20°C, or at 4°C for immediate usage.

2.2.5 Reverse transcription: complementary DNA (cDNA) synthesis

RNA was reversely transcribed into cDNA using AffinityScript QPCR cDNA Synthesis Kit (Agilent Technologies) according to the manufacturer's instructions. 100 to 250 ng RNA were reversely transcribed in RNase-free water in a total volume of 20 µl with 10 µl of First Strand Mastermix (2x), 3.0 µl Oligo(dT) primer and 1 µl AffinityScript RT / RNase Block enzyme mixture. Reaction was incubated for 5 minutes at 25°C for primer annealing, followed by 15 minutes at 42°C for cDNA synthesis. The last step with 5 minutes at 95°C terminated the cDNA synthesis. cDNA was stored at -20°C, or at 4°C for immediate usage.

2.2.6 Polymerase chain reaction (PCR)

10 ng DNA or 1 µl cDNA was used as template for PCR reactions. DNA fragments were amplified in a reaction volume of 25 µl. The reaction contained 1x PCR Buffer, 1x RediLoad™ Loading Buffer, 250 µM dNTPs, 0.5 µM Primermix, and 0.5 units AmpliTaq® DNA Polymerase (all from Life Technologies). Cycling parameters were as follows: 95°C 5 min, 35 cycles at 95°C 30 sec, 60°C 30 sec, 72°C 1 - 2 minutes, and a final extension at 72°C for 7 minutes on a 9800 Fast Thermal Cycler (Life Technologies). PCR products were stored at -20°C.

2.2.7 Real-time PCR

2.2.7.1 TaqMan gene expression assays

Real-time PCR for detection of gene expression levels was performed in duplicates using TaqMan Gene Expression Assays in a 7500 Fast Real-time PCR System (all from Life Technologies). A TaqMan Gene Expression Assay mix contains two unlabelled sequence specific primers (forward and reverse). Additionally, it contains a primer probe labelled with a reporter fluorescent dye at the 5' end and a non-fluorescent quencher plus a minor groove binder (MGB) attached at the 3' end. Primer probe is either 6-carboxyfluorescein (FAM) or 2′-chloro-7′-phenyl-1,4-dichloro-6-carboxy-fluorescein (VIC) labelled, with the reporter dye emission being quenched while the probe is intact. During amplification the endogenous 5′ exonuclease activity of the TaqMan DNA polymerase cleaves the probe, separating the dye from the quencher which increases the reporter dye signal. Each PCR cycle releases several dye molecules, resulting in an increase in fluorescence intensity in proportion to the amount of synthesized amplicon. 1 µl cDNA was used in a 10 µl reaction volume consisting of 3.5 µl RNease-free water, 5 µl 2x TaqMan Universal PCR Master Mix and 0.5 µl 20x TaqMan Gene Expression Assay Mix (all from Life Technologies). The thermal cycling steps were the following: hot enzyme activation at 95°C for 10 min, followed by 40 cycles of denaturation at 95°C for 10 seconds and annealing/extension at 60°C for 1 minute. Relative quantification was achieved by calculating the difference in cross-threshold values (ΔCt) of the gene of interest and actin beta according to the formula $2^{-\Delta Ct}$.

2.2.7.2 Analysis of allelic expression by allele-specific PCR

LRRC32 allelic expression was examined by allele-specific PCR analysis using assays-by-design for SNP genotyping (Thermo Fisher Scientific). SNP Genotyping assays consist of two unlabelled PCR primers (forward and reverse), one VIC/MGB labelled probe detecting the major allele sequence and one FAM/MGB labelled probe that detects the minor allele sequence. The reporter dye emission is quenched while the probe is intact. During amplification the endogenous 5′ exonuclease activity of the TaqMan DNA polymerase cleaves the probe, separating the dye from the quencher and increases the reporter dye signal. The PCR was run as triplicates with 0.25 µl cDNA in a 10 µl reaction volume consisting of 4.5 µl RNease-free water, 5 µl 2x TaqMan Universal PCR Master Mix and 0.25 µl 40x SNP Genotyping Assay Mix in a 7500 Fast Real-time PCR System (Life Technologies). The thermal cycling steps were the following: hot enzyme activation at 95°C for 10 min, 40 cycles of denaturation at 95°C for 15 seconds and

annealing/extension at 60°C for 1 minute. The dye emission was measured after 40 cycles in a 7500 Fast Real-time PCR System (Life Technologies).

2.2.8 Gene array

Mouse gene expression microarrays were used to analyse differences in gene expression in Garp-deficient and control Tregs. Transcriptome analysis was performed by Agilent on Whole Mouse Genome Oligo Microarray (Mouse GE 4x44K v2) (Agilent Technologies) using total RNA purified from FACS-sorted Garp-deficient and control Tregs with five mice per group. The RNA was extracted from Tregs using the RNeasy Plus Mini Kit (Qiagen) as described above. RNA was reverse-transcribed into double-stranded cDNA and labelled with Cy3 dye. Cy3-labelled cDNA was hybridised to Mouse GE 4x44K v2 Microarrays (Agilent Technologies). Fluorescently labelled target sequences that bind to their probe sequence generate a signal. The detected intensity data was subjected to quantile normalization. Fold changes of normalised data were calculated to identify genes with greater than twofold differential expression. Transcriptome and initial data analysis was performed by Agilent CrossLab. Treg relevant and apoptosis associated genes were analysed for fold changes and significant differences in expression. HDACs and HATs were analysed for fold changes and significant differences in expression. Normalised log2 median centred intensities of selected genes were visualized by Mayday (version 2.30) (Battke et al., 2010) using centring for display.

2.2.9 Agarose gel electrophoresis

1.2 % Agarose gel containing 1x SYBR Safe DNA Gel Stain (Life Technologies) was used for gel electrophoresis and analysis of DNA fragments. 3 µl of the PCR product containing 1x *Redi*Load™ Loading Buffer (Life Technologies) was loaded per well. 2 µl GeneRuler DNA ladder 100 bp (Fermentas) was loaded as marker. Gel electrophoresis was performed at 100 V for 40 minutes in 1x TAE Buffer. DNA bands were visualized and photographed using a UVT-28 MP transilluminator (Herolab).

2.2.10 Mice

Conditional Lrrc32 knock out mice (C57BL/6.Lrrc32$^{fl/fl}$;Cd4-Cre) were generated by genOway (Lyon, France) by flanking the third exon of Garp with loxP sites (C57BL/6.Lrrc32$^{fl/fl}$) and subsequent crossing homozygous floxed Garp mice with C57BL/6NTac-TgN(Cd4-Cre) mice (Taconic, Laven, Denmark) bearing the cyclization recombination (Cre)-recombinase cassette under the mouse Cd4 promoter. The genetic integrity of the homozygote Lrrc32 knock out mice, which were received from genOway, was routinely monitored by genotyping the breeding pairs. Control C57BL/6J (wild-type) and B6SJLF1/J mice expressing CD45.1 on T cells were purchased from Janvier (Le Genest-Saint-Isle, France). B6.129S7-Rag1^{tm1Mom}/J mice were obtained from The Jackson Laboratory (Bar Harbor, ME). Mice were housed under specific-pathogen-free conditions. Mice were used at 8 – 16 weeks of age and euthanized by carbon dioxide (CO_2) inhalation using compressed CO_2 gas. All efforts were made to minimize suffering, animal number, and stress / discomfort. All animal experiments were approved by the Regierung von Oberbayern and performed in compliance with the guidelines of the German Tierschutzgesetz.

2.2.11 Mice genotyping

For genotyping, DNA of C57BL/6.Lrrc32$^{fl/fl}$;Cd4-Cre mice breeding pairs was purified from ear punches using the High Pure PCR Template Preparation Kit (Roche) as described above. 4 ng DNA was analysed by PCR as described above. The Cre PCR detects the Cre-recombinase coding sequence in the Cre-recombinase cassette of C57BL/6.Lrrc32$^{fl/fl}$;Cd4-Cre mice, which is not present in wild-type C57BL/6J mice. The Cre PCR yields no amplification product for wild-type C57BL/6 mice. The flippase (Flp) PCR detects the non-recombined allele of wild-type C57BL/6 mice (0.5 kilobase (kb) (Figure 2 A) and the Flp-mediated excised locus (0.6 kb) containing the Flippase recognition target (FRT)-site of C57BL/6.Lrrc32$^{fl/fl}$;Cd4-Cre mice (Figure 2 B). FRT is a remnant of the excised FRT flanked neomycin selection cassette. PCR products were analysed by agarose gel electrophoresis as described above (Figure 2 C).

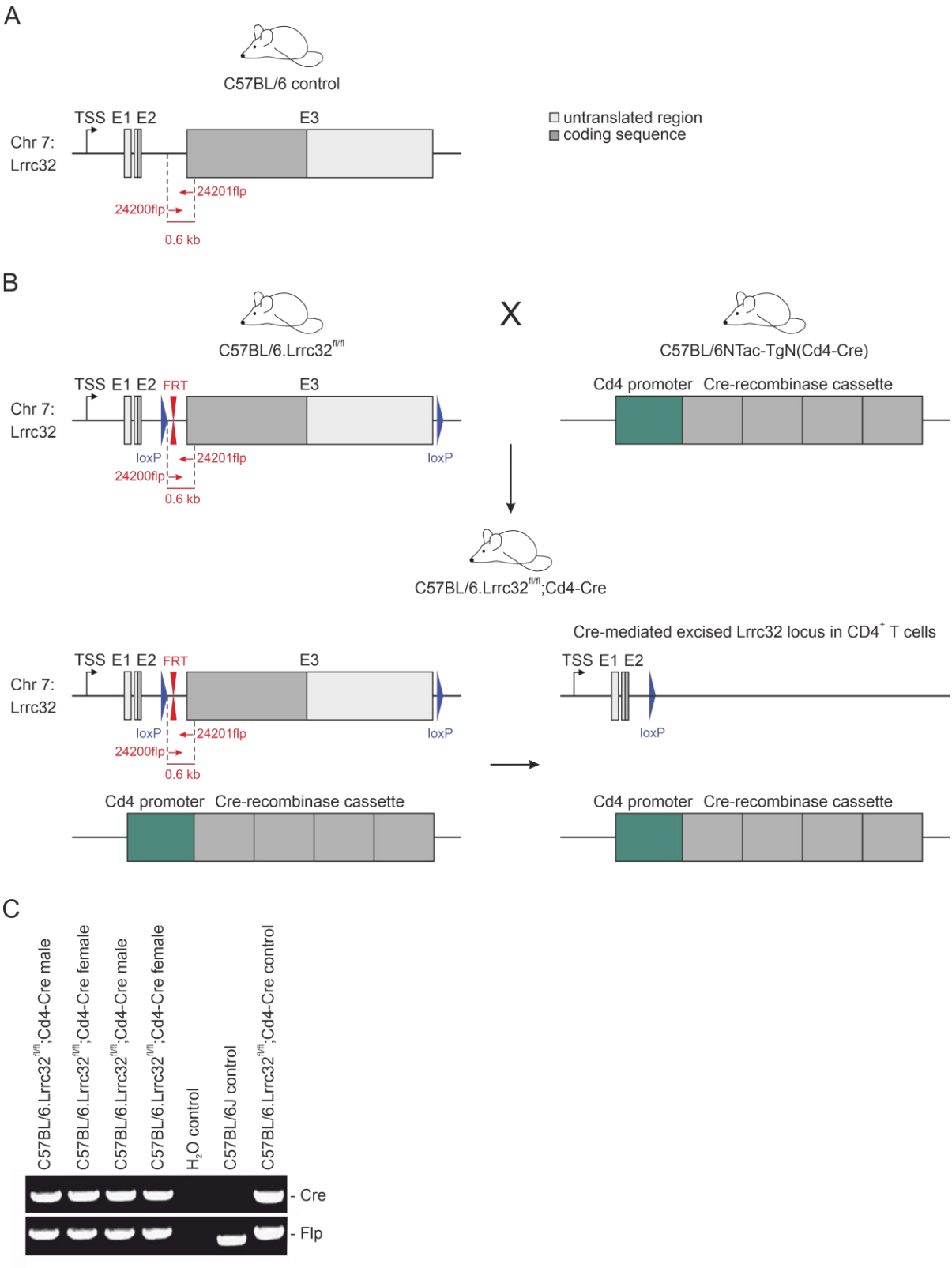

Figure 2 Representative genotyping of C57BL/6.Lrrc32$^{fl/fl}$;Cd4-Cre mice
(A) Schematic overview of endogenous Lrrc32 locus and Flp-excision of C57BL/6 mice. (B) Scheme of the breeding strategy for the generation of C57BL/6.Lrrc32$^{fl/fl}$;Cd4-Cre mice; Chr, chromosome; TSS, transcription start site; E, exon. (C) Agarose gel of representative genotype analysis for Cre and Flp of two C57BL/6.Lrrc32$^{fl/fl}$;Cd4-Cre breeding pairs and controls is demonstrated. PCR products from PCR without sample (H_2O), C57BL/6 mice and C57BL/6.Lrrc32$^{fl/fl}$;Cd4-Cre mice were used as control.

2.2.12 Cell purification

All centrifugation steps were performed using a Rotixa 50 RS centrifuge. For washing cells were centrifuged at 723 rcf for 5 minutes.

2.2.12.1 Isolation of human $CD4^+$ T cells

PBMCs were isolated by centrifugation of blood over a Ficoll (Biotest, Dreieich, Germany) layer. 10 ml Ficoll was loaded under 20 ml blood diluted with 20 ml PBS and centrifuged at 400 rcf for 20 minutes without forced stop at room temperature. PBMCs were harvested and washed once with PBS. CD4 positive T cells were purified by negative selection of PBMCs on the basis of magnetic activated cell sorting (MACS) using human $CD4^+$ T cell Isolation Kit (Miltenyi Biotec) according to the manufacturer's instructions. Cells were resuspended in 40 µl MACS buffer per 10^7 cells and incubated with 10 µl $CD4^+$ T cell Biotin-Antibody Cockail for 5 minutes at 4°C. Non-$CD4^+$ T cells were thus labelled with biotin-conjugated antibodies against CD8a, CD14, CD15, CD16, CD19, CD36, CD56, CD123, TCRγ/δ, and CD235a (Glycophorin A). Afterwards, another 30 µl MACS buffer per 10^7 cells and 20 µl of $CD4^+$ T cell MicroBead Cocktail were added. Cells were incubated with the antibody mixture for 10 minutes at 4°C. With this procedure, cells were magnetically labelled for negative selection by conjugation with magnetic anti-Biotin MicroBeads. After washing with MACS buffer cells were resuspended in 1 ml MACS buffer per 10^8 cells and applied onto a LS MACS column placed in the magnetic field. Magnetically labelled non-$CD4^+$ T cells resided in the column while the unlabelled $CD4^+$ cells were collected in the flow through by washing the column three times with 3 ml MACS buffer. $CD4^+$ T cell purity was assessed by flow cytometry and cells were used for experiments or further MACS separation. Routinely ≥95% of isolated T cells were CD3/CD4 positive.

2.2.12.2 Isolation of human $CD25^+$ and $CD25^-$ $CD4^+$ T cells

$CD25^+$ $CD4^+$ T cells were purified from $CD4^+$ T cells by MACS positive selection using human CD25 MicroBeads II (Miltenyi Biotec) following the manufacturer's instructions. $CD4^+$ T cells were resuspended in 90 µl MACS buffer per 10^7 cells and incubated with 10 µl of human CD25 MicroBeads II per 10^7 cells for 15 minutes at 4°C. After washing with MACS buffer the cells were resuspended in 500 µl MACS buffer per 10^8 cells and applied on a MS MACS column placed in the magnetic field. An estimated maximum of 10^7 CD25 positive cells are able to bind to the column, while unlabelled $CD25^-$ $CD4^+$ T cells were collected in the flow through by washing the column three times with 500 µl MACS buffer. The MS column was removed from the magnetic field and the magnetically labelled $CD25^+$ $CD4^+$ T cells were eluted with 1 ml

MACS buffer by firmly pushing the plunger into the column. The flow through containing the $CD25^-$ $CD4^+$ T cell fraction was transferred onto a LD column placed in the magnetic field to remove remaining $CD25^+$ T cells and washed three times with 3 ml MACS buffer. Purified cells were kept at 4°C until usage, their purity was assessed by flow cytometry. Routinely Tregs were ≥90% CD25 positive and effector T cells (Teffs) ≥98% CD25 negative.

2.2.12.3 Isolation of human $CD4^-$ $CD8^-$ PBMCs

Human PBMCs were isolated as described above. In a first step $CD8^+$ cells were depleted from PBMCs by MACS using CD8 MicroBeads (Miltenyi Biotec) following the manufacturer's instructions. Cells were resuspended in 80 µl MACS buffer per 10^7 cells and incubated with 20 µl CD8 MicroBeads (Miltenyi Biotec) for 15 minutes at 4°C. Cells were washed with MACS buffer and resuspended in 1 ml MACS buffer per 10^8 cells. 1 ml with up to 10^8 labelled cells was applied onto an LS MACS column placed in the magnetic field. CD8 positive cells bind to the column, while unlabelled CD8 negative cells were collected in the flow through by washing the column three times with 3 ml MACS buffer. In a second step $CD4^-$ cells were labelled with magnetic beads using the human $CD4^+$ T cell Isolation Kit (Miltenyi Biotec) as described above. Up to 10^8 CD8 depleted $CD4^-$ labelled PBMCs were applied onto a LS MACS column placed in the magnetic field. Magnetically labelled $CD4^-$ cells resided in the column while the unlabelled $CD4^+$ cells were separated and collected in the flow through by washing the column three times with 3 ml MACS buffer. The LS MACS column was removed from the magnetic field and the magnetically labelled $CD8^-$ $CD4^-$ cells were eluted with 5 ml MACS buffer by firmly pushing the plunger into the column.

2.2.12.4 Isolation of mouse $CD4^+$ T cells

Spleens were collected from mice and homogenized to a single-cell suspension in MACS buffer using gentleMACS™ C Tubes in gentleMACS™ Dissociator (Miltenyi Biotec). The cell suspension was filtered through 70 µm Nylon Cell Strainer (BD Falcon, Bedford, MA) and purified by MACS. $CD4^+$ positive T cells were purified by negative selection from splenocyte cells using mouse $CD4^+$ T cell Isolation Kit (Miltenyi Biotec) based on the manufacturer's instructions. 10^7 cells were resuspended in 40 µl MACS buffer and incubated with 10 µl $CD4^+$ T cell Biotin-Antibody Cocktail for 5 minutes at 4°C. Non-$CD4^+$ T cells were hereby labelled with biotin-conjugated antibodies against CD8a, CD11b, CD11c, CD19, CD45R (B220), CD49b (DX5), CD105, Anti-MHC Class II, Ter-119, and TCRγ/δ. Another 30 µl MACS buffer per 10^7 cells and 20 µl of $CD4^+$ T cell MicroBead Cocktail were added and incubated for 10 minutes at

4°C. Cells were washed with MACS buffer and resuspended in 1 ml MACS buffer per 10^8 cells. 1 ml was applied onto an LS MACS column placed in the magnetic field. Magnetically labelled non-$CD4^+$ T cells resided in the column while the unlabelled $CD4^+$ cells were collected in the flow through by washing the column three times with 3 ml MACS buffer. $CD4^+$ T cells were then used for experiments or further MACS separation. Routinely ≥95% of isolated T cells were CD3/CD4 positive.

2.2.12.5 Isolation of mouse $CD25^+$ and $CD25^-$ $CD4^+$ T cells

$CD25^+$ $CD4^+$ T cells were purified by MACS from $CD4^+$ T cells by positive selection using the mouse CD25 MicroBeads Kit (Miltenyi Biotec) following the manufacturer's instructions, or where indicated by fluorescence-activated cell sorting (FACS) at MoFlo (Beckman Coulter). $CD4^+$ T cells were resuspended in 100 µl MACS buffer per 10^7 total cells and incubated with 10 µl of CD25-PE antibody for 10 minutes at 4°C. After washing with MACS buffer, cells were resuspended in 90 µl MACS buffer per 10^7 cells and 10 µl Anti-PE MicroBeads. Cells were incubated for 15 minutes at 4°C. After washing with MACS buffer the cell pellet was resuspended in 500 µl MACS buffer per 10^8 cells and applied on an MS MACS column placed in the magnetic field. No more than 10^8 cells were applied on an MS MACS column. Unlabelled $CD25^-$ $CD4^+$ T cells were collected in the flow through by washing the column three times with 500 µl MACS buffer. The MS column was removed from the magnetic field and the magnetically labelled $CD25^+$ $CD4^+$ T cells were eluted with 1 ml MACS buffer by firmly pushing the plunger into the column. The flow through containing the $CD25^-$ $CD4^+$ T cell fraction was transferred onto a LD column placed in the magnetic field to remove remaining $CD25^+$ T cells and washed three times with 3 ml MACS buffer. Purified cells were kept at 4°C until usage, their purity was assessed by flow cytometry. Routinely Tregs were ≥90% CD25 positive and Teffs ≥98% CD25 negative.

2.2.13 Cell culture

All cells were cultured at 37°C in a humidified atmosphere containing 5% CO_2 in Heracell 240 CO_2 incubators (Thermo Scientific).

2.2.13.1 T cell culture

Freshly isolated human T cells were stimulated with plate-bound anti-CD3 (1 µg/ml) and soluble anti-CD28 (1 µg/ml) (BD Bioscience) in RPMI 1640 cell medium supplemented with 50 U/ml penicillin G, 50 µg/ml streptomycin, 2 mM L-glutamine (all from Life Technologies Invitrogen),

10% normal human serum (NHS) and 10U/ml IL-2 (Novartis) for indicated amount of time. For TCR stimulation with plate-bound anti-CD3 flat-bottom cell culture plates were incubated with anti-human CD3 (1 µg/ml) (BD Bioscience) in 50mM Tris-HCl (pH 9.5) over night at 4°C. Before use coated cell culture plates were washed three times with HBSS (Life Technologies Invitrogen). Cell concentrations of $0.5x10^6$ cells/ml were used.

Freshly isolated murine T cells were cultured unstimulated or stimulated with plate-bound anti-CD3 (2 µg/ml) and plate-bound anti-CD28 (10 µg/ml) (BD Bioscience) in RPMI 1640 cell medium supplemented with 50 U/ml penicillin G, 50 µg/ml streptomycin, 2 mM L-glutamine, 10% FCS (all from Life Technologies Invitrogen) and 10 ng/ml IL-2 (R&D Systems) for indicated amount of time. For TCR stimulation flat-bottom cell culture plates were incubated with anti-mouse CD3 (2 µg/ml) and anti-mouse CD28 (10 µg/ml) (all from BD Bioscience) in 50 mM Tris-HCl (pH 9.5) over night at 4°C. Before use coated cell culture plates were washed three times with HBSS (Life Technologies Invitrogen). 2 ng/ml mouse TGFβ1 (R&D Systems) was added when indicated. For serum starvation cells were incubated with serum free RPMI 1640 supplemented with 50 U/ml penicillin G, 50 µg/ml streptomycin, 2 mM L-glutamine (Life Technologies Invitrogen) and 10 ng/ml IL-2 (R&D Systems) for 20 hours. Cell concentrations of 10^6 cells/ml were used.

For cytokine analysis 10^6 freshly isolated murine Tregs were cultured in RPMI 1640 cell medium supplemented with 50 U/ml penicillin G, 50 µg/ml streptomycin, 2 mM L-glutamine, 10% FCS (all from Life Technologies Invitrogen) with 1ng/ml PMA, 2µM monensin (both from Sigma-Aldrich) and 0.5µM ionomycin (Merck) for five hours.

2.2.13.2 Maintenance of cell lines

HEK293 cells and T cell leukemia (Jurkat) cells were obtained from American Type Culture Collection (ATCC) (Manassas, VA). HEK293 cells were maintained and split every 2 to 3 days with DMEM cell medium supplemented with 50 U/ml penicillin G, 50 µg/ml streptomycin, 2 mM L-glutamine and 10% FCS (all from Life Technologies Invitrogen). For splitting and seeding HEK293 cells, the medium was removed, cells washed with PBS and the cell layer dissociated with Trypsin (Sigma-Aldrich). Trypsinisation was stopped by adding DMEM supplemented with 50 U/ml penicillin G, 50 µg/ml streptomycin, 2 mM L-glutamine and 10% FCS (all from Life Technologies Invitrogen) and cells were diluted to appropriate concentrations.

Jurkat cells were maintained at 0.25-1x10^6 cells/ml and split every 2 to 3 days with RPMI 1640 medium supplemented with 50 U/ml penicillin G, 50µg/ml streptomycin, 2 mM L-glutamine and 10% FCS (all from Life Technologies Invitrogen).

2.2.14 Analysis of Foxp3 protein stability

CHX (Sigma-Aldrich) was used to inhibit protein synthesis in Tregs to study Foxp3 protein stability. CHX is a fungicide produced by the bacterium Streptomyces griseus that interferes in the translocation step in protein synthesis and blocks translational elongation in eukaryotes (Ennis and Lubin, 1964). CHX was dissolved in ethanol (40 mg/ml) and diluted in PBS for working solutions. 6 µg/ml CHX (Sigma-Aldrich) was used in cell culture experiments to determine the half-life of Foxp3.

Murine $CD4^+$ T cells were cultured unstimulated or stimulated with plate-bound anti-CD3 (2 µg/ml) and plate-bound anti-CD28 (10 µg/ml) (BD Bioscience) in RPMI 1640 cell medium supplemented with 50 U/ml penicillin G, 50 µg/ml streptomycin, 2 mM L-glutamine, 10% FCS (all from Life Technologies Invitrogen) and 10 ng/ml IL-2 (R&D Systems) for 3, 6, 9 and 20 hours in the presence of CHX. Foxp3 protein half-life was calculated on normalised Foxp3 frequencies by linear regression.

Human $CD4^+$ T cells were stimulated with plate-bound anti-CD3 (1 µg/ml) and soluble anti-CD28 (1 µg/ml) (BD Bioscience) in RPMI 1640 cell medium supplemented with 50 U/ml penicillin G, 50 µg/ml streptomycin, 2 mM L-glutamine (all from Life Technologies Invitrogen), 10% NHS and 10U/ml IL-2 (Novartis) for 6, 20 and 48 hours in the presence of 6 µg/ml CHX. Foxp3 frequencies were assessed by intracellular flow cytometry. Foxp3 protein half-life was calculated on normalised Foxp3 frequencies by linear regression.

2.2.15 *In vitro* suppression assay

The inhibitory capacity of $CD25^+$ $CD4^+$ Tregs from PID patients and healthy controls was analysed by T cell proliferation assays. Freshly isolated human $CD25^-$ $CD4^+$ T cells were resuspended in PBS at concentration of 100x10^6/ml and labelled with 10 µM CFSE (Life Technologies Invitrogen) for 8 minutes at room temperature. Staining reaction was blocked with equal volume of NHS as PBS cell suspension. After labelling cells were washed twice and resuspended in 10% NHS/RPMI 1640 (Life Technologies Invitrogen). 50x10^3 CFSE-labelled CD25 negative $CD4^+$ T cells were stimulated in a 96-well round-bottom plate with 1 µg/ml

soluble anti-CD3 (OKT3) in the presence of $100x10^3$ CD4/CD8 negative PBMCs and descending amounts of Tregs ($50x10^3$, $25x10^3$, $12.5x10^3$ and no Treg cells) for four days. Teff to Treg ratios of 1:1, 2:1, 4:1 and 1:0 were used in triplicates for each condition. At the end of the experiment cells from three wells were combined and analysed by flow cytometry. CFSE is a cell permeable fluorescent cell staining dye that covalently couples to intracellular lysine residues and other amine sources via its succinimidyl group (Parish, 1999). CFSE fluorescence intensity is halved with each cell division. Proliferative capacity of Tregs was assessed by flow cytometry based on CFSE-dilution.

2.2.16 Transfection

2.2.16.1 Lipofectamine transfection

Lipofectamine transfection was performed to transfect HEK293 cells (ATCC) with plasmid DNA using Lipofectamin™ LTX (Life Technologies Invitrogen). $0.25x10^6$ cells were seeded in 12-well plates with 2.5 ml DMEM supplemented with 50 U/ml penicillin G, 50 µg/ml streptomycin, 2 mM L-glutamine and 10% FCS (all from Life Technologies Invitrogen) and transfected on the following day at a confluency of 70-90% with pcDNA3.1-GARPcds variants GARP_wt, GARP_c.741G>A, GARP_c.934C>T and GARP_c.1262G>A (Thermo Fisher Scientific) in complex with Lipofectamin™ LTX. An empty pcDNA3.1 vector in complex with Lipofectamin™ LTX was used as control. On the day of transfection 0.4 µg plasmid DNA was dissolved in 200 µl Opti-MEM and incubated with 3.5 µl Lipofectamin™ LTX (both from Life Technologies Invitrogen) for 30 minutes at room temperature. Medium of prepared HEK293 cells was removed and 1ml DMEM supplemented with 50 U/ml penicillin G, 50 µg/ml streptomycin, 2 mM L-glutamine and 10% FCS (all from Life Technologies Invitrogen) was added. 200 µl DNA/Lipofectamin complexes were then added to the cultured cells. On the following day the Medium was removed and 2.5 ml DMEM supplemented with 50 U/ml penicillin G, 50 µg/ml streptomycin, 2 mM L-glutamine and 10% FCS (all from Life Technologies Invitrogen) was added. The expression of GARP was analysed 48 hours post-transfection by extracellular flow cytometry.

2.2.16.2 Amaxa transfection

Amaxa transfection was performed to transfect Jurkat T cells by using the Nucleofector® II device and the Amaxa Cell Line Nucleofector kit V (both from Lonza) according to manufacturer's instructions. For transfection, 10^6 cells were resuspended in 82 µl Cell Line

Nucleofector® solution V and 12 µl supplement (both from Lonza). The pcDNA3.1-GARPcds variants GARP_wt, GARP_c.741G>A, GARP_c.934C>T and GARP_c.1262G>A (Thermo Fisher Scientific) an empty pcDNA3.1 or the pmaxGFP (Lonza) expression vector were used respectively. For transfection 1 µg plasmid DNA was directly added to the cell suspension and the cell/DNA suspension was transferred to a cuvette (Lonza). The cuvette was placed in the Nucleofector® II device (Lonza) and the appropriate program X-001 was selected. The cells were retrieved from the cuvette after the transfection by adding 0.5 ml of pre-warmed RPMI 1640 supplemented with 50 U/ml penicillin G, 50 µg/ml streptomycin, 2 mM L-glutamine (all from Life Technologies Invitrogen) and 10% NHS. Cells were transferred to a 12 well plate with a final volume of 1.5 ml per well. The empty vector was used as negative control for GARP expression, the pmaxGFP expression vector served as control for transfection efficiency. Expression of GARP variants and GFP was analysed 48 hours after transfection by extracellular flow cytometry.

2.2.16.3 Amaxa small interfering RNA (siRNA) transfection

Amaxa transfection was performed to transfect freshly isolated murine $CD4^+$ T cells with siRNA by using the Nucleofector® II device and the Amaxa Mouse T cell Nucleofector kit (both from Lonza) according to manufacturer's instructions. Briefly, $5x10^6$ $CD4^+$ cells were resuspended in 82 µl Mouse T cell Nucleofector® Solution and 12 µl supplement (both from Lonza). For transfection a final concentration of 100 nM Hdac9 siRNA (Thermo Fisher Scientific), 100 nM siGENOME Non-Targeting siRNA Control Pools (Thermo Fisher Scientific) or 2.5 µg/100µl pmaxGFP® Vector (Lonza) was used. The siRNA and the pmaxGFP® Vector (Lonza) were directly added to the cell suspension and transferred to a cuvette (Lonza). The cuvette was placed in the Nucleofector® II device (Lonza) using the appropriate program X-001. The cells were retrieved from the cuvette after the transfection by adding 0.5 ml of pre-warmed RPMI 1640 supplemented with 50 U/ml penicillin G, 50 µg/ml streptomycin, 2 mM L-glutamine, 10% FCS (all from Life Technologies Invitrogen) and 10 ng/ml IL-2 (R&D Systems) and transferred to a 12-well plate to a final volume of 2 ml medium per well. Amaxa advises T cell stimulation within 3 - 24 hours post transfection. Therefore, cells were incubated under non-stimulating conditions for 3 hours and then transferred to an anti-CD3 (2 µg/ml), anti-CD28 (10 µg/ml) (BD Bioscience) coated 24-well plate and incubated for one to four days. The pmaxGFP® Vector was used as control to assess the transfection efficiency in $CD4^+$ T cells. Cells transfected with siGENOME Non-Targeting siRNA Control Pools were used as negative control.

2.2.17 *In vivo* mice experiments

2.2.17.1 Collagen-induced arthritis (CIA)

The susceptibility and disease progression of Garp-deficient and control mice was examined in *in vivo* CIA experiments that were performed by colleagues of the group. Only the analysis of the results was conducted by me. CIA was induced in 12-week-old mice by intradermal injections of 200 µg chicken collagen (Chondrex) in complete Freund's adjuvant (Sigma-Aldrich) followed by a booster injection of 200 µg collagen in incomplete Freund's adjuvant (Sigma-Aldrich) on day 21. Mice were scored every two to three days assessing redness and swelling of each limb (0-3): 0, normal; 1, slight swelling and/or erythema; 2, pronounced edematous swelling; and 3, joint rigidity, allowing a maximum score of 12 per mouse. Hind paw thickness was assessed at the day of first injection (day 0) and the experimental endpoint (day 38). Cartilage damage, inflammation, lymphocyte infiltration and osteoclast differentiation were analysed in hind paws at the experimental endpoint by histological hematoxylin (Sigma-Aldrich) and eosin (Merck, Darmstadt, Germany) (H&E) stainings and Tartrate-resistant acid phosphatase (TRAP) stainings.

2.2.17.2 Experimental autoimmune encephalomyelitis (EAE)

Colleagues of the group performed EAE experiments to analyse the susceptibility and disease progression of Garp-deficient and control mice *in vivo*. Only the analysis of the results was conducted by me. EAE was induced by subcutaneous immunization of 12-week-old mice with 200µg MOG_{35-55} (R&D Systems) in complete Freund's adjuvant and 400 ng pertussis toxin (both from Sigma-Aldrich). On day 2 additional 400 ng pertussis toxin were administered by subcutaneous injection. Mice were scored daily for signs of paralysis starting from day 7 after immunization to the experimental endpoint (day 19). EAE clinical score was assessed as follows: 0, clinically normal; 1, limp tail; 2, weak hind limbs; 3, partially paralysed hind limbs; 4, complete hind limb paralysis; and 5, death.

2.2.17.3 DSS induced colitis

The disease progression of Garp-deficient and control mice was examined in *in vivo* DSS induced colitis experiments that were performed by colleagues of the group. Only the analysis of the results was conducted by me. Colitis was induced in 8-week-old mice by administration of 2% DSS (MP Biomedicals) in drinking water. Body weight was monitored daily for 9 days. On day 9 mice were sacrificed. Colon sections were prepared and hematoxylin (Sigma-Aldrich)

and eosin (Merck, Darmstadt, Germany) (H&E) stainings performed. Colon sections were evaluated for colitis clinical score using the The Jackson Laboratory scoring system (0-12): severity (0-3), ulceration (0-3), hyperplasia (0-3), area involved (0-3) (Bleich et al., 2004). Lymphocyte patch numbers were counted in ten 100 µm sequential sections.

2.2.17.4 Adoptive transfer

The inhibitory capacity of $CD25^+$ $CD4^+$ Tregs from Garp-deficient and control mice was analysed by *in vivo* T cell proliferation assays that were performed by colleagues of the group. Only the analysis of the results was conducted by me. $2x10^6$ $CD45.1^+$ $CD25^-$ $CD4^+$ T cells purified from B6SJLF1/J mice were injected intravenously into 12-week-old B6.129S7-$Rag1^{tm1Mom}$/J mice either alone or together with $5x10^5$ $CD45.2^+$ Tregs purified from control (C57BL/6J) or Garp-deficient (C57BL/6.$Lrrc32^{fl/fl}$;Cd4-Cre) animals with four to five animals per group. The injected $CD45.2^+$ Tregs were on average 70% $Foxp3^+$ cells for control and Garp-deficient Tregs. Splenocytes were analysed by flow cytometry seven days post-transplantation. Extracellular stainings of CD3, CD4, CD45.1 and CD45.2 provided information for CD3/CD4/CD45.1 positive effector T cell numbers and frequencies in spenocytes and respectively for the capacity of injected Tregs to suppress CD3/CD4/CD45.1 positive effector T cell proliferation. Extracellular staining of CD3, CD4 and CD45.1 and simultaneous intracellular staining of Foxp3 analysed CD45.1 negative CD3/CD4/Foxp3 positive Treg numbers and frequencies at the end of the experiment.

2.2.18 Flow cytometry

Fluorescence activated cell sorting (FACS) was performed to analyse the expression of cell surface molecules or intracellular proteins as well as protein modifications on a single cell level using a Cytomics FC500 flow cytometer (Beckman-Coulter). Fluorescence signals were determined using appropriate electronic compensation to exclude emission spectra overlap. Flow Cytometry of surface molecules

For extracellular stainings $0.05\text{-}0.2x10^6$ cells were washed with 500 µl FACS buffer, resuspended in 50 µl FACS buffer and incubated with suitable directly fluorochrome-conjugated antibodies (0.1 µg/stain) for 15 minutes at 4°C in the dark. Cells were washed with 500 µl FACS buffer, resuspended in 200 µl FACS buffer and analysed by flow cytometry. All centrifugation steps were performed with 3800 rcf for 2 minutes at 4°C in a 5427 R centrifuge (Eppendorf) with a fixed angle rotor.

2.2.18.1 Flow cytometry of intracellular proteins

For intracellular stainings of Foxp3 and acetylated lysine (AcK) 0.2-1x10^6 cells were fixed and permeabilized using the FOXP3 Fix/Perm buffer set (Biolegend) according to the manufacturer's instructions. Cells were resuspended in 50 µl Perm buffer and incubated with appropriate antibodies for 30 minutes at 4°C in the dark. Afterwards cells were washed once with 500 µl FACS buffer, resuspended in 200 µl FACS buffer and analysed by flow cytometry.

For intracellular stainings of phosphorylated SMAD2/3 10^6 cells were fixed and permeabilized using the Cytofix/Cytoperm™ Fixation and Permeabilization Solution with the Phosflow™ Perm Buffer III (both from BD Bioscience) according to the manufacturer's instructions. After fixation and permeabilization cells were washed and resuspended in 50 µl FACS buffer. Cells were incubated with appropriate antibodies for 30 minutes at 4°C in the dark and washed once with 500 µl FACS buffer, resuspended in 200 µl FACS buffer and analysed by flow cytometry. For indirect stainings cells were incubated with unlabelled primary antibodies for 30 minutes at 4°C in the dark and washed once with 500 µl FACS buffer. Cells were then resuspended in 50 µl FACS buffer and incubated with suitable fluorochrome-conjugated secondary antibodies for 30 minutes at 4°C in the dark. Cells were washed three times with 500 µl FACS buffer and resuspended in 200 µl FACS buffer for analysis. All centrifugation steps were performed with 3800 rcf for 2 minutes at 4°C in a 5427 R centrifuge (Eppendorf) with a fixed angle rotor.

2.2.18.2 Flow cytometry of cytokines

For cytokine stainings 10^6 cells were fixed with 4% paraformaldehyde (PFA) (Roth, Karlsruhe, Germany) in PBS (pH 7.4) for 10 minutes at 37°C and permeabilized using FACS buffer with 0.1% Saponin (Sigma-Aldrich). Cells were resuspended in 50 µl FACS buffer with 0.1% Saponin (Sigma-Aldrich) and incubated with appropriate antibodies for 30 minutes at 4°C in the dark. Cells were washed twice with 500 µl FACS buffer with 0.1% Saponin (Sigma-Aldrich) and resuspended in 200 µl FACS buffer for analysis. All centrifugation steps were performed with 3800 rcf for 2 minutes at 4°C in a 5427 R centrifuge (Eppendorf) with a fixed angle rotor.

2.2.18.3 Fluorescence resonance energy transfer (FRET)

FRET was used in flow cytometry experiments for the analysis of intracellular Foxp3 protein acetylation in Tregs from Garp-deficient and control mice. 10^6 cells were fixed and permeabilized with the True-Nuclear™ Transcription factor buffer set (Biolegend) according to the manufacturer's instructions. Cells were resuspended in 50 µl Perm buffer and incubated with

unlabelled primary antibodies for 30 minutes at 4°C in the dark. Cells were washed once with 500 µl Perm buffer and resuspended in 50 µl Perm buffer. Cells were incubated with suitable fluorochrome-conjugated secondary antibodies for 30 minutes at 4°C in the dark. Cells were washed three times with 500 µl FACS buffer and resuspended in 200 µl FACS buffer for analysis. All centrifugation steps were performed with 3800 rcf for 2 minutes at 4°C in a 5427 R centrifuge (Eppendorf) with a fixed angle rotor. For measurement of Foxp3 acetylation, a FRET antibody pair for Foxp3 detected with acceptor Alexa Fluor 594-labeled goat anti-rat IgG secondary antibody and AcK detected with donor Alexa Fluor 488-labeled goat anti-rabbit IgG secondary antibody (all from Thermo Fisher Scientific) were used. Isotype controls were used to set up the parameters for FRET signal detection. Total Foxp3 was additionally assessed in separate probes by indirect staining with Alexa Fluor 488-labeled goat anti-rat IgG as secondary antibody. The FRET donor Alexa Fluor 488 was excited using a single laser configuration (488nm). To optimize detection of the FRET signal for acceptor Alexa Fluor 594 emission, the filter block configuration was modified for signal detection at 600-620nm, replacing the 615 DSP with 645 DSP and 620 SP with 620 BP.

2.2.19 Histological staining

Histological stainings were performed by colleagues of the group. Only the analysis was conducted by me. Tissues from Garp-deficient and control mice were fixed in 4% PFA (Roth) 8-12 hours at room temperature and embedded in paraffin wax using standard histological procedures. Paws were decalcified in 10% EDTA (Sigma-Aldrich), pH 7.2 for two weeks at 4°C and washed over night in 70% ethanol prior embedment. 2 µm paraffin sections were prepared at -20°C using the rotary microtom Microm HM 340E (Thermo Fisher Scientific). Paraffin sections were stained with hematoxylin (Sigma-Aldrich) and eosin (Merck, Darmstadt, Germany) (H&E staining) for morphological assessment. Immunohistochemistry for CD3 cell infiltration was performed using unlabelled anti-CD3 antibodies and biotin-labelled secondary antibodies (all from DAKO). Bound Antibodies were detected with a streptavidin-biotinylated alkaline phosphatase complex (DAKO) and Fast Red as chromogenic substrate (Sigma-Aldrich). TRAP stainings were performed to analyse osteoclast differentiation using the Acid Phosphatase, Leukocyte (TRAP) Kit (Sigma-Aldrich) following the manufacturer's instructions. Stainings were examined and recorded by light microscopy (Keyence BZ 8100E).

2.2.20 Immunoprecipitation

Immunoprecipitation was performed to assess Foxp3 acetylation in Tregs from Garp-deficient and control mice. 5-10x10^6 $CD25^+$ $CD4^+$ Tregs were lysed in 0.5-1 ml RIPA buffer containing 50 mM Tris-HCl, pH 7.6, 150 mM NaCl (Merk), 10 mM EDTA (Sigma-Aldrich), 0.1% SDS (Merk), 0.5% NP-40 (Millipore), 1x cOmplete™ EDTA-free Protease Inhibitor Cocktail (Roche) and incubated for 30 minutes at 4°C under rotation. DNA was sheared with a 0.4 µm syringe and lysate centrifuged at full speed for 10 minutes. The Supernatant was incubated with 2 µg/ml unlabelled anti-Foxp3 monoclonal antibody (FJK-16s, ebioscience) in eppendorf tubes overnight at 4°C under rotation. For immunoprecipitation 50 µl Dynabeads® Protein G (Thermo Fisher Scientific) were washed with RIPA buffer and incubated with the cell lysate for 1 hour at 4°C under rotation. The beads were washed tree times with 200 µl RIPA buffer. For washing eppendorf tubes were placed on a magnet to remove the supernatant. The beads remained in the tube and were removed from the magnet and resuspended with RIPA buffer. For protein elution from the beads, the pellet was resuspended with 20 µl 2x SDS buffer and incubated for 10 minutes at 95°C.

2.2.21 SDS-polyacrylamide gel electrophoresis (SDS-PAGE) and Western Blot

Polyacrylamide gels for SDS-PAGE were prepared using the Mini-PROTEAN® Tetra Cell Casting Module (Bio-Rad). 20 ml 12.5% resolving gel was prepared for four plate sets containing 7.5 ml 1 M Tris-HCl (pH 8.8), 8.25 ml 30% acrylamide/bis-acrylamide, 3.95 ml H_2O, 200 µl 10% SDS, 20µl TEMED (all from Merk) and 200µl 10% APS (Sigma-Aldrich). After polymerization 10 ml 4% stacking gel was poured containing 1.25 ml 1 M Tris-HCl (pH 6.8), 1.32 ml 30% acrylamide/bis-acrylamide (Merk), 7.3 ml H_2O, 100 µl 10% SDS, 10 µl TEMED (all from Merk) and 100µl 10% APS (Sigma-Aldrich). Samples were boiled, centrifuged at 16000 rcf for 5 minutes and loaded onto the gel. To estimate the molecular weight of the bands prestained protein standard (11–245 kDa, New England Biolabs) and biotinylated protein ladder (9-200 kDa, Cell signalling) were loaded to each gel. Gel electrophoresis was performed with SDS-running buffer containing 25 mM Tris-HCl, 192 mM Glycine (Merk) and 0.1% SDS (Merk) for 30 minutes at 100 V followed by 90-120 minutes at 200 V.

2.2.22 Western Blot

For detection proteins were transferred from gel onto a Protean nitrocellulose membrane (Whatman, Maidstone, UK) using the EC140 Mini Blot Module (E-C Apparatus corporation,

Holbrook, UK). Transfer was run with SDS Transfer buffer containing 25 mM Tris-HCl, 192 mM Glycine (Merk), 0.2% SDS (Merk) and 20% methanol (Sigma-Aldrich) at 150 mA for 1.5 hours. After the transfer, membrane was washed with TBS buffer containing 20 mM Tris-HCl (pH 7.6), 140 mM NaCl (Merk) for 5 minutes and blocked with 5% nonfat milk powder (Real) in TBST buffer containing 20 mM Tris-HCl (pH 7.6) 140 mM NaCl (Merk) and 0.1% Tween-20 (Sigma-Aldrich) for 1 hour at room temperature. Membrane was then washed three times with TBST buffer for 5 minutes and incubated with primary antibody (1:200 – 1:1000 diluted in TBST buffer containing either 5% BSA (Merk) or 5% nonfat milk (Real) for 1 hour at room temperature or overnight at 4°C. After three washing steps the membrane was incubated with horseradish peroxidase (HRP)-conjugated secondary antibody (Santa Cruz) (1:10000 diluted in TBST buffer containing 5% non-fat milk (Real) for 1 hour at room temperature. After three additional washing steps with TBST buffer, membrane was incubated for 1 minute with 2 ml ECL western blotting detection reagent (1:1 mixture of reagent 1 and reagent 2, GE Healthcare) and developed 1-10 minutes using a FUJIFILM LAS-3000 (Fujifilm, Tokyo, Japan).

2.2.23 GARP promoter analysis for SMAD binding elements

Analysis of murine GARP promoter was performed by using MatInspector (Genomatix, Munich, Germany).

2.2.24 Molecular imaging

Molecular images were generated with PyMOL (The PyMOL Molecular Graphics System, Schrödinger, LLC) using the PDB file 6GFF as a template for the generation of visualisations for GARP protein variants. Mutations found in patients were introduced into the PDB structure using the mutation feature. The surface feature was used to identify solvent exposed residues.

2.2.25 Protein stability prediction

STRUM analysis was used to predict GARP protein destabilization (ΔΔG) introduced by mutations found in PID patients. Protein stability is defined by fold stability, which describes the difference in Gibbs free energy between the unfolded (Gu) and folded (Gf) states $\Delta G = Gu - Gf$. A high ΔG value indicates high stability against denaturation (Huang and Gromiha, 2010). How mutations alter protein stability can be measured by the free energy gap difference between wild-type ΔGw and mutated variants ΔGm as $\Delta\Delta G = \Delta Gm - \Delta Gw$. A ΔΔG below zero indicates a destabilization caused by mutation. STRUM is a method that was developed by the group of

Zhanglab at the university of Michigan to predict stability changes (ΔΔG) of proteins upon single-point mutation. STRUM adopts a gradient boosting regression approach by use of a variety of features at different levels of evolutionary information and structural resolution (Figure 3). The features of STRUM are the inclusion of sequence profile scores and combining different methods of multiple sequence alignment. Structural profile scores reflect the likelihood of a given amino acid or other properties at mutant position being found in the ensemble of a structurally similar protein, and different energy functions based on an Iterative Threading ASSEmbly Refinement (I-TASSER) model provide accurate environment information. I-TASSER is a hierarchical approach to protein structure prediction and structure-based function annotation. It identifies structural templates from the PDB by a multiple threading approach in a first step with full-length atomic models constructed by iterative template-based fragment assembly simulations. Then in a second step function insights of the target are derived by re-threading the 3D models through the protein function database BioLiP.

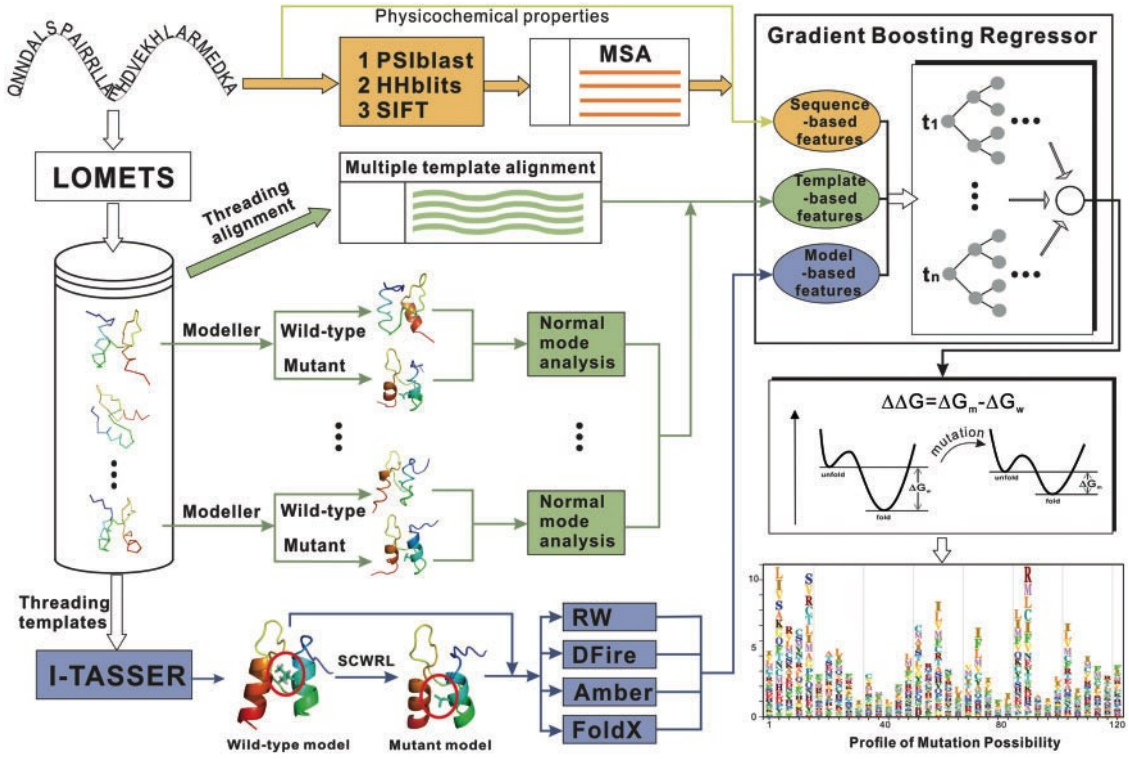

Figure 3 Flowchart of STRUM for mutation-induced stability change prediction.
Three sources of features from sequences (orange lines), threading alignments (green), and I-TASSER models (blue) are trained by gradient boosting regression for ΔΔG prediction. The final output is an all-to-all ΔΔG table and a visible mutation profile specifying the mutation probability to different amino acids at each position. Adapted from (Quan et al., 2016).

2.2.26 Statistical analysis

Statistical analysis was performed by using Student's t-test. Kolmogorov-Smirnov test was used for testing of normal distribution. *p* values less than 0.05 were considered statistically significant and are indicated as: * – $p < 0.05$, ** – $p < 0.01$, ***p – < 0.001, n.s. – not significant.

3 Results

3.1 Characterization of *LRRC32* mutations causing severe immundysregulation in PID patients

3.1.1 PID patients with *LRRC32* mutations

Colleagues from AG Grimbacher identified two patients, one male one female, with previously unknown *LRRC32* mutations (Figure 4A, Table 1) by screening their patients at the Center for Chronic Immunodeficiency using whole-exome sequencing. The patients demonstrated clinical symptoms of a severe immune dysregulation characterized by recurring life-threatening intestinal obstructions consecutive to chronic persistent mucosal autoinflammation in patient 1 (pt1) and by development of anti-granulocyte autoantibodies and subsequent leucopenia and opportunistic infections in patient 2 (pt2).

In Patient 1 (male) 135,084 variants were identified in relation to the reference genome (build hg38). Following filtering steps lead to 30 heterozygous candidate variants within genes that were associated with autosomal dominant conditions and 17 compound heterozygous or homozygous variants in genes that were previously not associated with a disease or autosomal recessive conditions. The most promising candidates among these were two heterozygous variants in the gene *LRRC32*. As shown in Figure 4B patient 1 has a nucleotide exchange (G→A) at position 741 leading to the exchange of the tryptophan codon at position 247 to a stop codon (p.Trp247Ter) and a nucleotide exchange (C→T) at position 934 leading to the amino acid exchange of arginine (Arg) 312 to cysteine (Cys) (p.Arg312Cys). The *LRRC32* variant p.Trp247Ter is a newly identified nonsense mutation. Variant p.Arg312Cys of *LRRC32* is a rare missense variant. In patient 1, the variants are located on the same allele according to Sanger sequencing. With both variants on the same allele the p.Arg312Cys mutation does not come into effect when the mutated GARP variant is expressed since the introduced stop codon p.Trp247Ter terminates protein translation beforehand.

In Patient 2 (female) 108,522 variants were identified regarding the reference genome. Further filtering led to 33 heterozygous candidate variants in genes that were associated with autosomal dominant conditions, as well as 29 compound heterozygous or homozygous variants in genes that were formerly not associated with a disease or with autosomal recessive conditions. The most promising candidates among these were two heterozygous variants in the gene *LRRC32*. As demonstrated in Figure 4B patient 2 has the same nucleotide exchange (C→T) at position 934 leading to the amino acid exchange of arginine 312 to cysteine at one *LRRC32* allele (p.Arg312Cys) and a nucleotide exchange (G→A) at position 1262 leading to the amino acid exchange of arginine 421 to glutamine (Gln) at the second allele (p.Arg421Gln). Sanger sequencing proved that these variants were on different alleles for patient 2.

Table 1. LRRC32 variants in PID patients

Pt.	Chromosomic change (hg38)	CDS change	Amino acid change	Variant type	dnSNP	AF gnomAD exomes	AC/AN gnomAD exomes
1	11-76660852-C-T	c.741 G>A	p.Trp247 Ter	stop_gained	-	-	-
	11-76660659-G-A	c.934 C>T	p.Arg312 Cys	missense_variant	rs143082901	0.00031237	78/249706
2	11-76660659-G-A	c.934 C>T	p.Arg312 Cys	missense_variant	rs143082901	0.00031237	78/249706
	11-76660331-C-T	c.1262 G>A	p.Arg421 Gln	missense_variant	rs200320285	0.00005036	12/238306

Nomenclature conforming to both Ensembl's canonical transcript ENST00000407242.6 and to RefSeq's canonical transcript NM_001128922.2. Pt.: patient; CDS: coding sequence; AF: allele frequency; AC: allele count; AN: allele number.

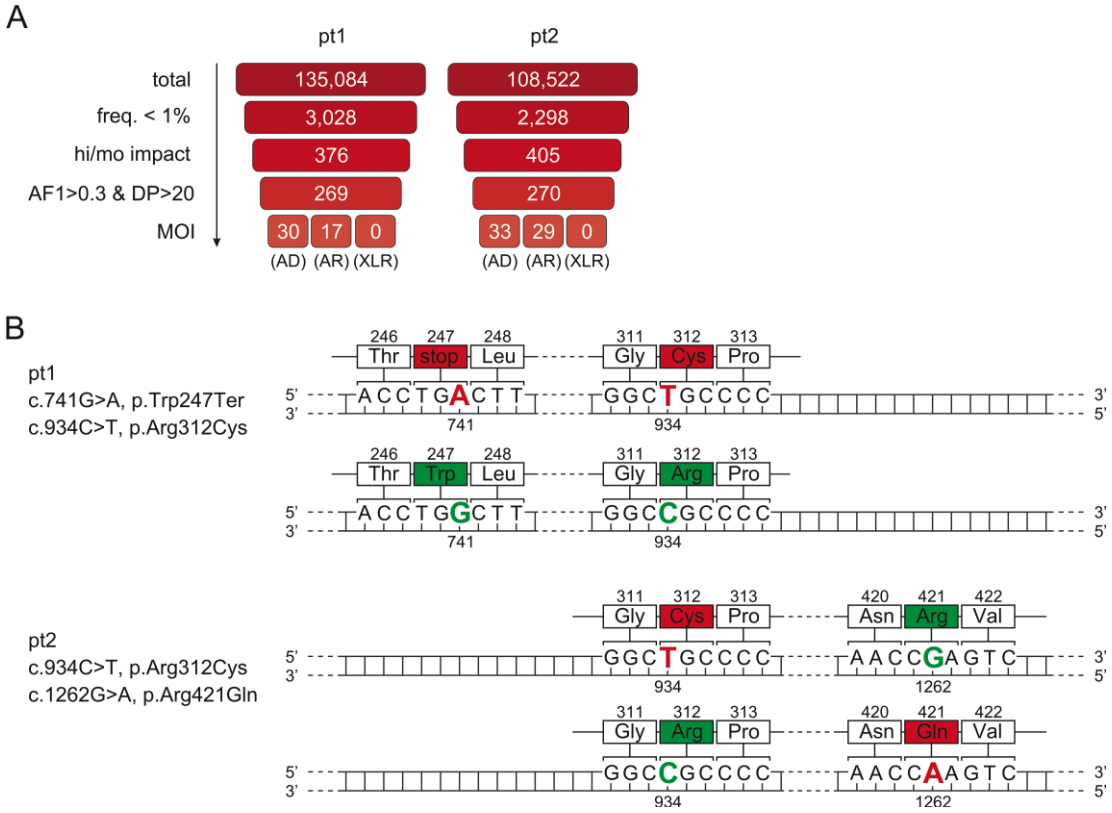

Figure 4 PID patients with mutated *LRRC32* variants
(A) Exome sequencing data is shown with indicated variant numbers at the respective filtering step. freq.: frequency in the internal cohort as well as in gnomAD exomes and genomes; hi/mo: high or moderate impact prediction of mutations regarding gene function or structure on the basis of the variant type (missense variant is predicted as "moderate", "stop_gained" variant as "high"); AF1: the frequency of readings including the alternative allele; DP: read depth (number of readings that cover that variant); MOI: mode of inheritance; AD: autosomal dominant; AR: autosomal recessive; XLR: X-linked recessive. (B) Schematic overview of the *LRRC32* alleles in patient 1 and patient 2. The affected nucleotides and the resulting amino acids as well as their respective positions are indicated. The wild-type variants are marked with green and the mutations variants with red. Based on (Lehmkuhl et al., 2021).

3.1.2 GARP mutation analysis and protein stability prediction

For a better understanding of the described GARP mutations found in patients, the mutated protein structures were predicted and visualized using PyMOL (Figure 5) on the basis of the crystal structure of the GARP:latent TGFβ1 complex, PDB entry 6GFF (Lienart et al., 2018). GARP variants p.Arg312Cys as well as p.Arg421Gln are depicted with the latent TGFβ1 complex (TGFβ1 and LAP dimer) as solved in the crystal structure. The linker and transmembrane domain of GARP are indicated. For the visualization, the described mutations were introduced into the solved wild-type structure using the mutation feature in PyMOL and are indicated by red arrows. The predicted protein structure of GARP variant p.Trp247Ter is a shortened protein variant missing a substantial segment of GARP, including the transmembrane domain (Figure 5). In patient 1 the stop codon introduced by the mutation leads to a premature end of protein translation. Therefore, the following mutation p.Arg312Cys that is located on the same allele does not come into effect in patient 1. Variant p.Trp247Ter, which lacks the

transmembrane domain, is expected to be unable to tether to the cell surface and to be non functional in terms of assisting in TGFβ1 activation. The predicted GARP protein variants for p.Arg312Cys and p.Arg421Gln are both full-length proteins. In GARP p.Arg312Cys a hydrophilic, positively charged arginine (Arg) at position 312 is exchanged to a uncharged cysteine (Cys). In GARP protein variant p.Arg421Gln a positively charged arginine (Arg) is exchanged to a uncharged glutamine (Gln). Based on the location the exchanged amino acids are unlikely to interfere with the binding interfaces of GARP to latent TGFβ1.

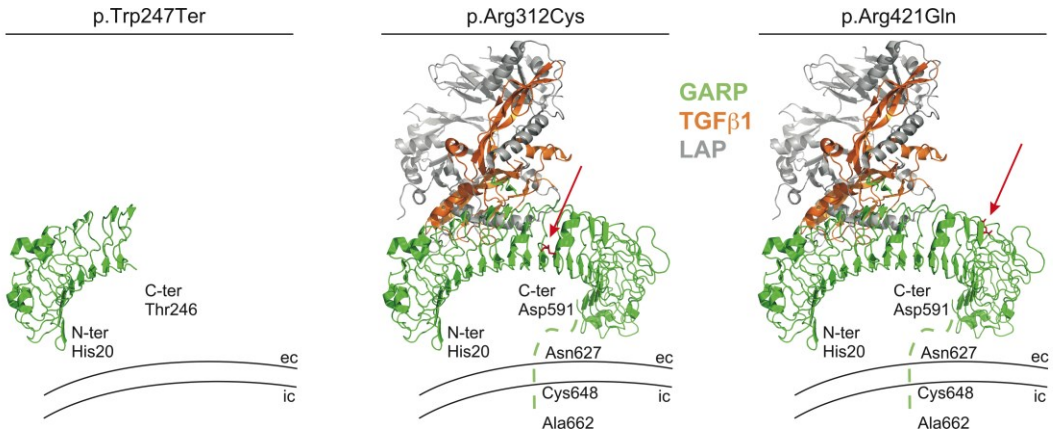

Figure 5 Predicted structure of GARP:TGFβ1 complex
Predicted protein structures for the GARP mutation variants are depicted in complex with TGFβ1 and LAP. GARP is coloured in green, TGFβ1 in orange, LAP in grey. The mutated amino acids are marked in red and pointed at by red arrows. The dashed line is a schematic representation of the transmembrane and the linker domain of GARP, which were not resolved in the 6GFF crystal structure. N-ter: N-terminus; C-ter: C-terminus; ec: extracellular; ic: intracellular. Based on (Lehmkuhl et al., 2021).

Further analysis was performed in PyMOL. To estimate the effect of the amino acid exchange introduced by the mutations the surface exposure of p.Arg312Cys and p.Arg421Gln was analysed. Utilising the PyMOL surface feature it was shown that both residues are solvent exposed (Figure 6). Arginine is a highly hydrophilic amino acid. Cysteine (p.Arg312Cys) and glutamine (p.Arg421Gln) in contrast have polar side chains and are not hydrophilic. Although these are not hydrophobic amino acids, the surface localization and solvent exposure of non-hydrophilic side chains can be unfavourable and lead to protein instability or folding issues for the mutated GARP variants (Figure 6).

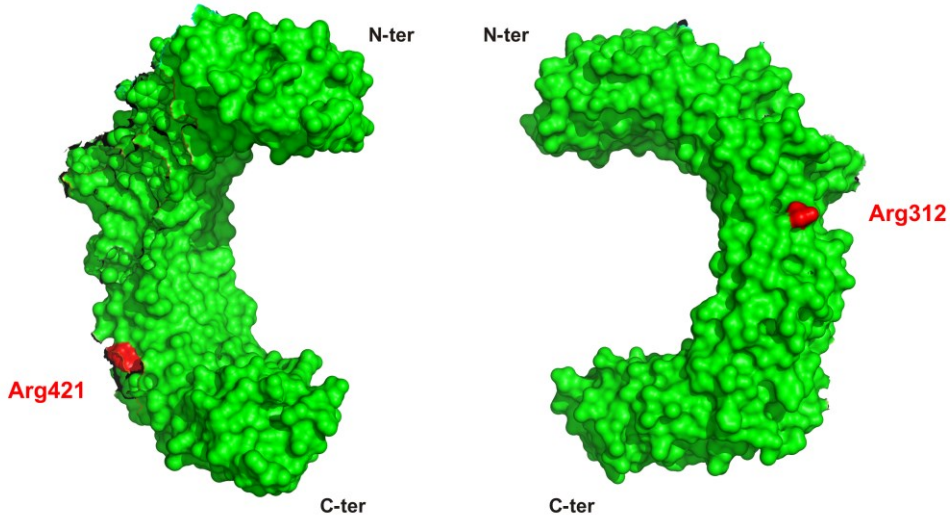

Figure 6 Surface structure of GARP variants
Surface representation of GARP based on crystal structure 6GFF visualized by PyMOL. GARP membrane domain is located at the C-terminus. Amino acids affected by GARP SNPs variants are indicated in red: p.Arg312Cys, p.Arg421Gln (patient 2).

Consequences of mutations can be assessed by changes in thermal stability of proteins. STRUM stability prediction (Zhanglab) was utilised to estimate the fold stability change ΔΔG introduced by the single-point mutations in GARP variants p.Arg312Cys- and p.Arg421Gln (Figure 7) (Quan et al., 2016). STRUM predicted a reduced protein stability for both GARP mutation variants. STRUM calculated a $\Delta\Delta G$ value of -2.93 Kcal/mol for p.Arg312Cys and -2.79 Kcal/mol for p.Arg421Gln. The average destabilization introduced by point mutations calculated by STRUM is around -0.5 Kcal/mol (Quan et al., 2016).

For more detailed insights an advanced STRUM analysis was performed, calculating ΔΔG for all possible single amino acid exchanges in the neighbouring regions (50 residue range) of the mutated residues. The analysis of possible mutations revealed that the positions 312 and 421 that were mutated in PID patients had the highest destabilization potential compared to the neighbouring residues (Figure 7A). An analysis of the residue positions 312 and 421 predicted ΔΔG values for all possible amino acid exchanges. The ΔΔG values for the mutations to Cysteine (312) and Glutamine (421) found in patients were close to the average of all possible amino acid exchanges (Figure 7B). Hydrophobic and non-hydrophilic amino acids were predicted to have the highest destabilization effect (negative ΔΔG values) for position 312 and 421 as would be expected due to solvent exposure. The STRUM analysis indicates that the position of the described mutations has a higher impact on to the destabilization than the nature of the amino acid exchange itself.

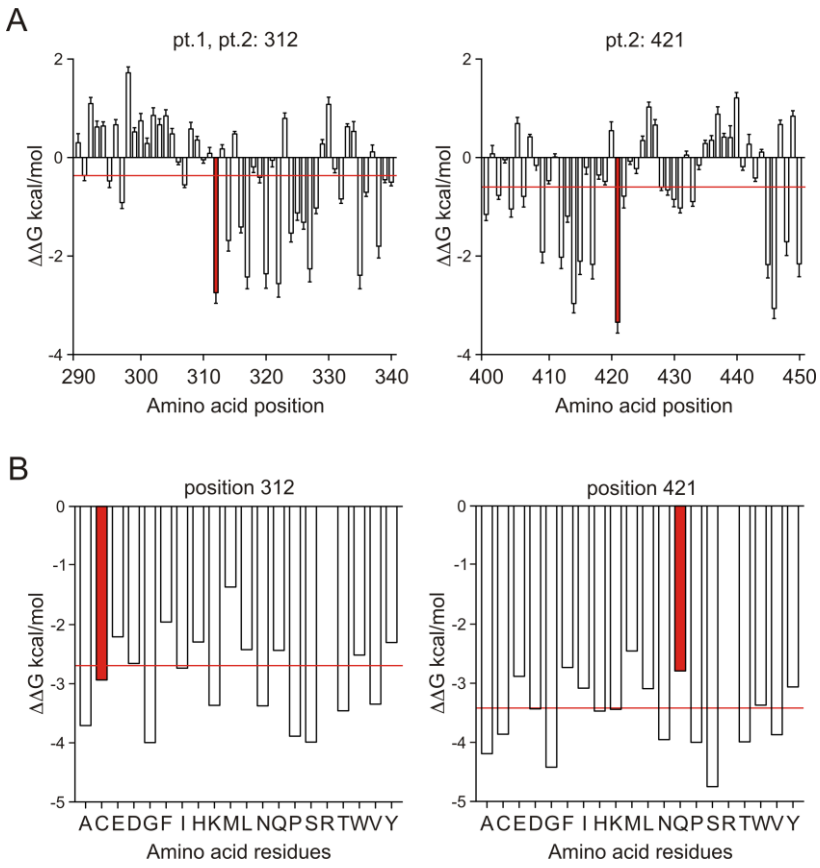

Figure 7 STRUM ΔΔG prediction
(A, B) The residues neighbouring the GARP mutations were analysed by STRUM for protein stability changes (ΔΔG). (A) Bars show means of predicted ΔΔG values for each amino acid exchange and indicate SEM for residues 290-340 (left) and 400-450 (right). Mutations found in patients in position 312 and 421 are highlighted in red. Mean of all positions is indicated as a red line. (B) The predicted ΔΔG value for each potential amino acid exchange for residue 312 (left) and 421 (right) is visualized as bars. The mutations found in patients Cysteine "C" and Glutamine "Q" are highlighted in red. Mean of all amino acids is indicated as a red line.

3.1.3 Expression of human GARP variants in HEK293 cells

The analysis by STRUM showed that the residue positions where the mutations occurred had the highest potential to introduce destabilization compared to their neighbouring residues. The mutated GARP variants found in patients were transfected and expressed in HEK293 cells to examine a potential reduction in protein stability. Flow cytometry analysis of mutated GARP variants showed no detectable protein expression for the GARP p.Trp247Ter encoding construct and reduced GARP expression for p.Arg312Cys and p.Arg421Gln compared to wild-type GARP (wt) (Figure 8). The mutation variants displayed a lower percentage of GARP expression as well as lower GARP protein levels as indicated by low MFI values. A corresponding empty vector (empty) was used as control. Assuming comparable transfection efficiency, this data suggests that the examined GARP mutations result in a decreased protein stability.

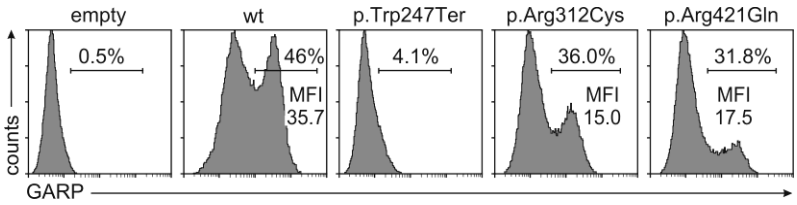

Figure 8 Protein expression of GARP variants
Surface expression of wild-type GARP and GARP mutation variants was analysed in transfected HEK293 cells by flow cytometry. GARP staining histograms of a representative experiment are demonstrated. In total three independent experiments were performed with similar results. empty: empty vector; wt: wild-type. Based on (Lehmkuhl et al., 2021).

3.1.4 Clinical characteristics of PID patients

Patient 1 was a 65-year-old male. At the time of the investigation he was suffering from reduced IgG levels, that resulted in a recurrent sepsis and severe intestinal obstructions. At age 54 he was diagnosed with common variable immunodeficiency (CVID). Lymphocyte infiltration was identified in the gut mucosa, but the infiltration was not as severe as usually observed with enterocolitis that is associated with CVID. The patient was in therapy with intravenous immunoglobulin substitution and supplementation with prophylactic antibiotics at the time of blood collection. Patient 2 was a 49-year-old female who developed reoccurring infections of the upper respiratory tract and suffered from diarrhoea. The symptoms resulted from chronic autoimmune granulocytopenia caused by autoantibodies directed against granulocytes. Although prescribed, she was not receiving prophylactic antibiotics at the time of blood collection.

3.1.5 Allelic expression of *LRRC32* variants in PID patients

To investigate whether both *LRRC32* variants were expressed in the PID patients, Tregs were purified from blood of healthy controls (hc) and the patients and the allelic expression of *LRRC32* was analysed (Figure 9). Allele-specific PCR assays were generated by Thermo Fisher Scientific for the GARP variants c.741G>A and c.1262G>A and utilised for the analysis of *LRRC32* messenger RNA (mRNA) expression. Unfortunately, due to the characteristics of the nucleotide sequence of c.934C>T it was not possible to generate an assay for this variant. Nonetheless, by duplexing the probes used for wild-type and mutant alleles it was still possible to analyse the allelic *LRRC32* expression completely, since both VIC (wild-type variant) and FAM (mutant variant) emissions were detected in the GARP c.741G>A assay in Tregs from patient 1 and in the GARP c.1262G>A assay in Tregs from patient 2. It was concluded that the transcription of *LRRC32* occurred in both patients from both alleles. The GARP wild-type and the p.Trp247Ter GARP mutant variant were expressed in Tregs from patient 1. In the case of patient 2, expression of the p.Arg312Cys- and the p.Arg421Gln GARP mutant variant was observed in Tregs.

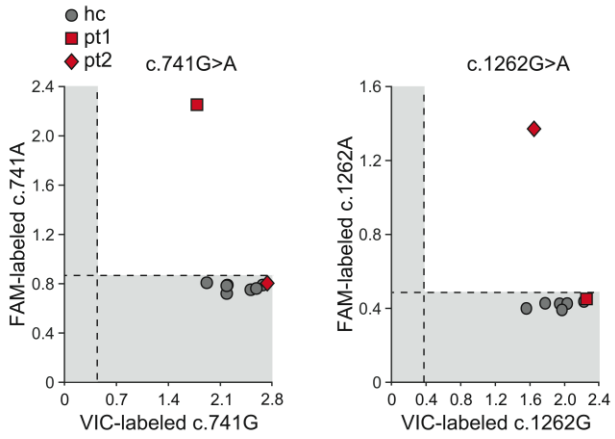

Figure 9 Allelic *LRRC32* expression in PID patients
Analysis of *LRRC32* variant and wild-type expression. Tregs were purified and total mRNA extracted. mRNA was analysed by allele-specific PCR for the GARP variants c.741G>A and c.1262G>A and their wild-type counterpart. Mean values of triplicates are shown. The means of the patients are highlighted in red. The means of seven healthy controls (hc) are indicated in grey. The probes for wild-type variants were labelled with VIC. The probes of the mutant variants were labelled with FAM. Both probes were duplexed in one reaction. The shaded area indicates the background fluorescence of the probes. Based on (Lehmkuhl et al., 2021).

3.1.6 Immune and T cell populations in PID patients

Blood of patients was analysed for white blood cell types. In both patients, $CD3^+$ and $CD4^+$ T cells were severely diminished (Figure 10A). Figure 10A (right side) shows laboratory values from the Universitätsklinikum Freiburg compared to normal range. Figure 10A (left side) shows results from flow cytometry staining performed at our laboratory compared to healthy controls (hc). The frequency of Foxp3 positive Tregs in purified $CD4^+$ T cells was analysed by intracellular flow cytometry. Interestingly, both patients displayed reduced Foxp3 frequencies compared to health controls (Figure 10B).

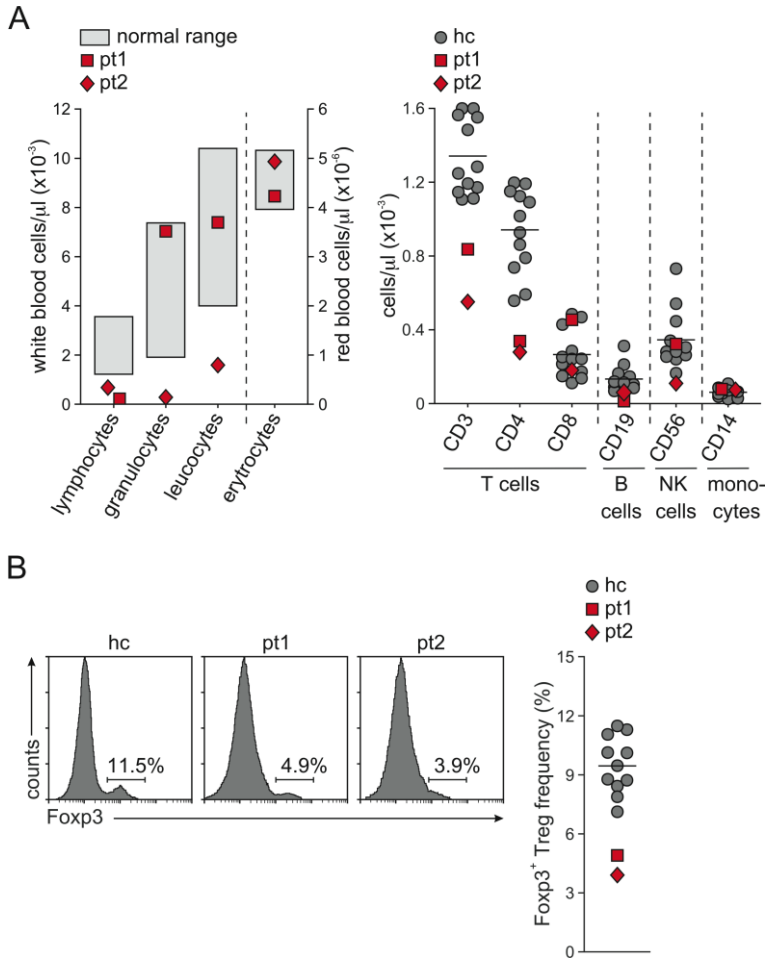

Figure 10 PID patient bloodcell analysis
(A) Left panel: Cell counts of red and white blood cells in the peripheral blood were analysed by a central laboratory. The respective normal ranges as they are defined by the central laboratory for clinical tests are depicted. Right panel: T cell, B cell, natural killer (NK) cell and monocyte cell counts were analysed in the peripheral blood by flow cytometry. The results from the patients are highlighted in red. Individual results from 12 healthy controls and their mean values are indicated in grey. (B) Treg frequency within $CD4^+$ T cells was determined by intracellular flow cytometry for Foxp3. Left panel: Foxp3 stainings of both patients and a representative staining of a healthy control are demonstrated. Right panel: The results from the patients are highlighted in red. Individual results from 11 healthy controls and their mean value are indicated in grey. Based on (Lehmkuhl et al., 2021).

3.1.7 Regulatory T cells of PID patients

GARP protein expression is upregulated on the surface of Tregs in response to TCR stimulation (Zhou et al., 2013). Therefore, GARP expression was analysed by extracellular flow cytometry on two-day-activated Tregs of patients and healthy controls. GARP expression was also measured in freshly isolated Tregs to identify potential basal activation, which was not detected (Figure 11A). LAP forms a complex with TGFβ and can associate with GARP that facilitates its surface localisation in Tregs (Miyazono et al., 1991; Stockis et al., 2009; Tran et al., 2009). LAP detection is indicative for the presence of latent TGFβ on the cell surface. Therefore, the surface expression of LAP was also analysed in these Tregs. The GARP levels on the surface of Tregs were notably reduced in both patients. Correspondingly, LAP expression on Tregs was also lower in both patients compared to healthy controls. Interestingly, in contrast to the reduced surface expression of GARP, *LRRC32* mRNA expression of the patients was rather increased in freshly isolated Tregs (day 0) and at the upper end of the normal range after two days (day 2) (Figure 11B).

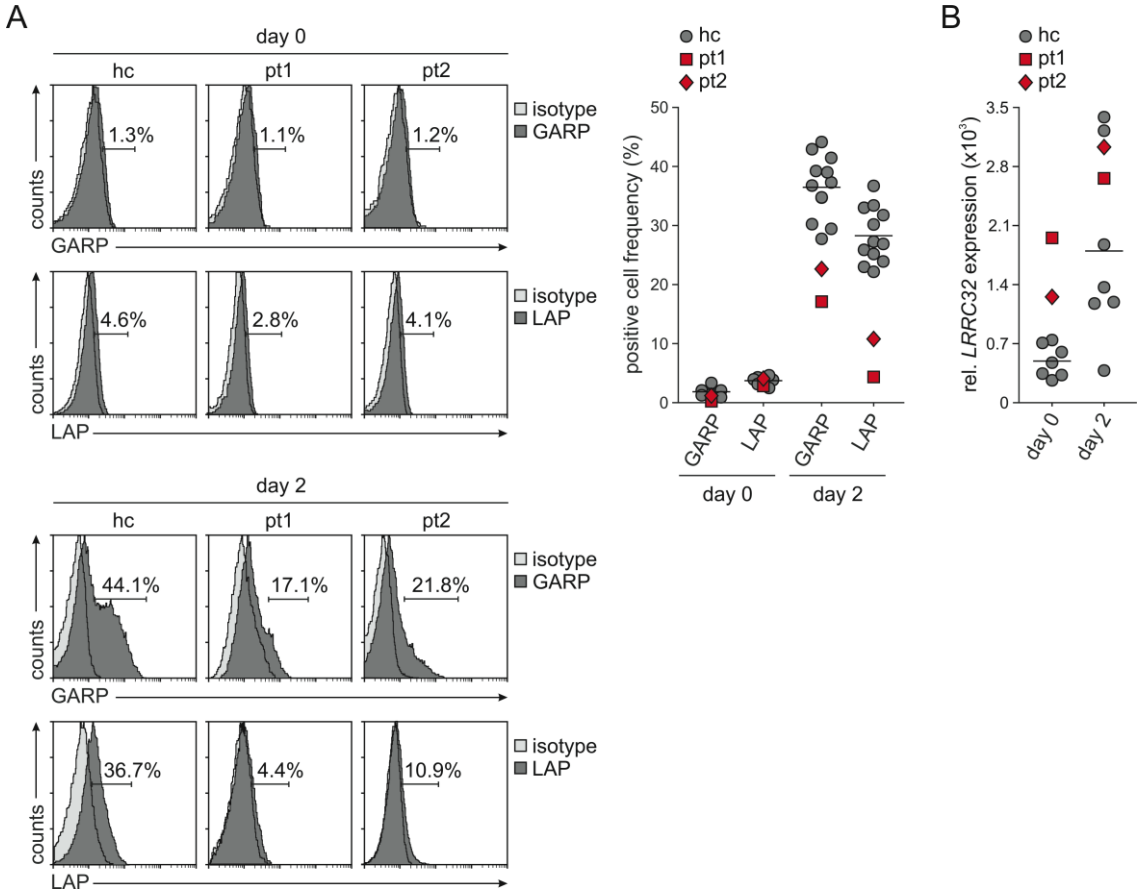

Figure 11 GARP and LAP expression in Tregs from patients with *LRRC32* mutations
(A) GARP and LAP cell-surface expression was assessed by flow cytometry in freshly isolated Tregs (day 0) and after two-day stimulation with anti-CD3 and anti-CD28 (day 2). Representative staining histograms are shown for both patients and a healthy control. The graph displays results from 11 healthy controls in grey and their mean value. Patients are indicated in red. (B) *LRRC32* mRNA expression was analysed by real-time PCR in duplicates and is shown in relation to *ACTB* expression. Results of seven healthy controls and their mean value are demonstrated. Patients are indicated in red. Based on (Lehmkuhl et al., 2021).

As GARP regulates the surface localization of latent TGFβ and thereby its processing and the release of mature TGFβ (Rifkin, 2005; Wang et al., 2012), TGFβ signalling was analysed in Tregs of PID patients and healthy controls. It was expected that TGFβ signalling, which is defined by SMAD2/3 phosphorylation, would be reduced in patients with lower GARP expression (Schmierer and Hill, 2007). Basal phosphorylation levels of SMAD2/3 were analysed by intracellular flow cytometry and were indeed diminished in Tregs of PID patients (Figure 12). As a control, total SMAD3 protein levels were also analysed and showed no differences in Tregs from patients compared to Tregs from healthy controls (Figure 12). This indicates that reduced GARP expression results in reduced TGFβ availability and signalling as seen in patients with *LRRC32* mutations.

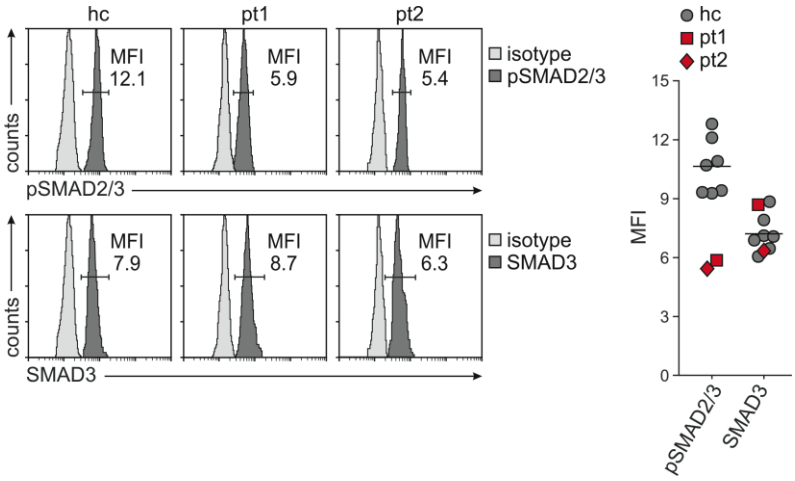

Figure 12 SMAD2/3 phosphorylation in Tregs
Basal SMAD2/3 phosphorylation levels and total SMAD3 expression was assessed by intracellular flow cytometry in freshly isolated Tregs. Representative staining histograms of a healthy control and stainings of both patients are demonstrated. The graph shows results from seven healthy controls and their mean value. Patients are indicated in red. MFI; mean fluorescence intensity. Based on (Lehmkuhl et al., 2021).

In a next step, Treg mediated suppression of effector T cell proliferation was analysed *in vitro* (Figure 13A, B). Teffs in the presence of Tregs from patients showed an increased proliferation compared to healthy controls, suggesting that Tregs with reduced GARP expression and diminished TGFβ signalling exhibit a lower suppressor function. It is therefore assumed that the newly identified mutations in *LRRC32* resulting in reduced GARP levels are responsible for the reduction and dysfunctionality of Tregs that have clinical manifestations of severe immune dysregulation.

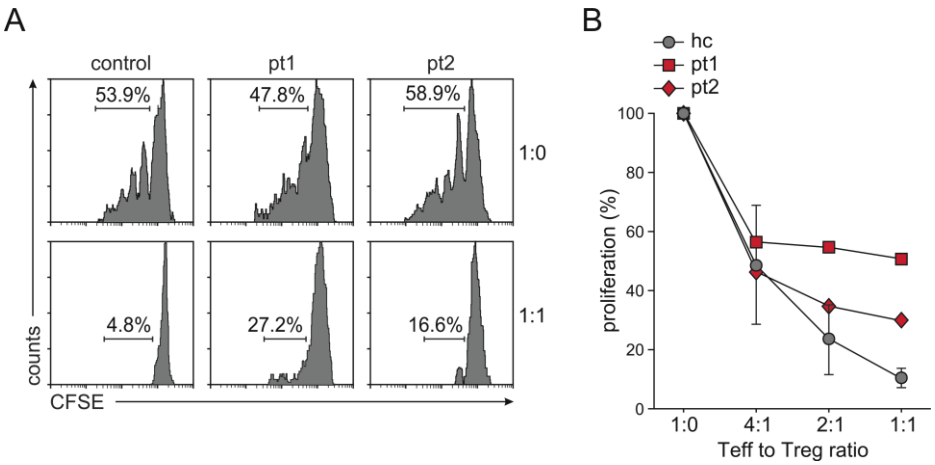

Figure 13 Treg mediated suppression
(A, B) The suppressive capacity of Tregs on the proliferation of CFSE-labelled CD25 negative CD4 positive Teffs was analysed by flow cytometry after four days of cell culture in different Teff to Treg ratios with anti-CD3 stimulation. (A) Representative staining histograms for Teffs in absence of Tregs and in a 1:1 Teff to Treg ratio are demonstrated. (B) The proliferation rate of Teffs in the absence of Tregs (1:0) was set to 100%. The proliferation rate of Teffs in the presence of Tregs (4:1, 2:1, 1:1) was calculated respectively. The mean ± SD of the proliferation in eight individual healthy control T cell cultures is demonstrated in grey. Proliferation results of T cell cultures from patients are indicated in red. Based on (Lehmkuhl et al., 2021).

3.2 Analysis of molecular mechanisms defining the phenotype of Garp-deficient Tregs

3.2.1 TGFβ signalling in Garp-deficient Tregs

Since the expression of GARP was markedly diminished on the Treg surface of PID patients, conditional GARP knock out mice (C57BL/6.Lrrc32$^{fl/fl}$.Cd4-Cre) were analysed to gain a deeper understanding of the molecular mechanisms that lead to Treg dysfunction when GARP expression is impaired. Flow cytometry stainings and real-time PCR analysis that were performed by colleagues of our group showed that Tregs from Garp-deficient mice did not express GARP. GARP expression could not be detected on the cell surface of activated Garp-deficient Tregs (Figure 14A). Correspondingly, Garp-deficient Tregs did not bear LAP on the cell surface. Real-time PCR analysis of freshly isolated and activated CD4$^+$ CD25$^+$ Tregs and CD4$^+$ CD25$^-$ Teffs confirmed the knock out of GARP in CD4$^+$ T cells. It also showed the Treg specificity of GARP. CD4$^+$ CD25$^-$ Teffs from wild-type (control) mice did not express GARP (Figure 14B).

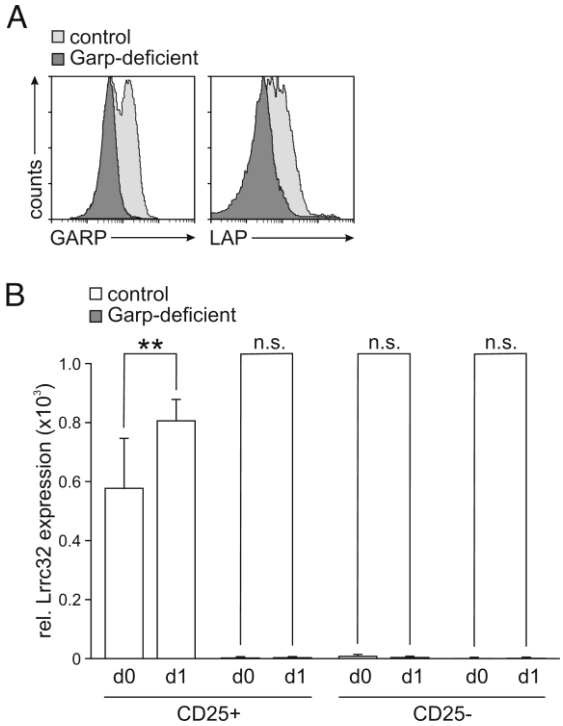

Figure 14 Confirmation of GARP knock out in mice
(A) The surface expression of GARP and LAP was analysed in activated Tregs. Representative flow cytometry. stainings are displayed. (B) Lrrc32 mRNA levels relative to *Actb* expression were analysed by real-time PCR in freshly isolated (d0) and stimulated (d1) Tregs (CD25+) and Teffs (CD25-). Results of six independent experiments are demonstrated as mean ± SD. Based on (Lehmkuhl et al., 2021).

With a successful knockout of GARP and the lack of detectable LAP on the surface of Garp-deficient Tregs, a reduced bioavailability of latent TGFβ and diminished processing and release of active TGFβ is expected (Cuende et al., 2015; Edwards et al., 2014; Stockis et al., 2017). Therefore, TGFβ signalling was analysed by intracellular flow cytometry. It was shown that Garp-deficient Tregs have indeed a significantly lower basal SMAD2/3 phosphorylation than Tregs from healthy controls. The total SMAD3 protein expression in Garp-deficient Tregs was unaltered compared to controls (Figure 15).

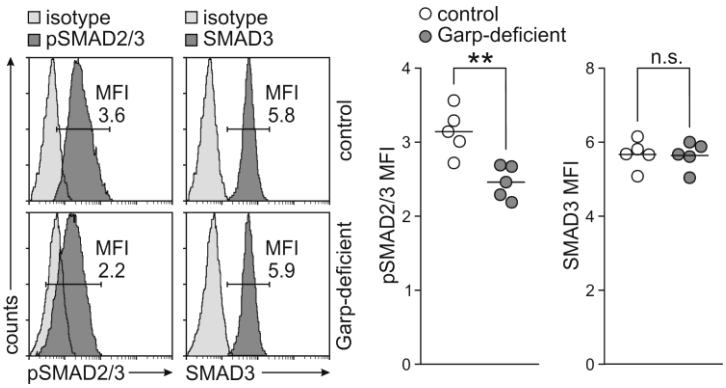

Figure 15 SMAD2/3 phosphorylation in Tregs
(A) Basal phosphorylation levels of SMAD2/3 and SMAD3 protein expression was assessed in freshly isolated Tregs by intracellular flow cytometry. Representative staining histograms for SMAD2/3 phosphorylation (pSMAD2/3) and SMAD3 expression are shown for Garp-deficient and control Tregs. The results of one representative experiment with five mice per group out of two independent experiments with five mice per group are demonstrated. Mean values are indicated by horizontal lines. MFI: mean fluorescence intensity. Based on (Lehmkuhl et al., 2021).

The deregulation of TGFβ signalling in Garp-deficient Tregs is consistent with results seen in PID patients with LRRC32 mutations. This indicates that the mutations and reduced GARP and LAP expression in patients have similar effects on basal phosphorylation of SMAD2/3 as the complete lack of GARP in Garp-deficient Tregs. They have, however, no effect on total SMAD3 protein levels, both in mice and humans.

3.2.2 T cell populations in Garp-deficient mice

To define the phenotype of Garp-deficient mice splenocyte T cell populations were analysed. Interestingly, and in contrast to results seen in patients, the frequencies of Foxp3$^+$ Tregs in the CD4$^+$ T cell population were not decresed in Garp-deficient mice compared to control mice (Figure 16A); instead Tregs expressed lower protein levels of Foxp3. Stainings of CD3, CD4 and CD8 positive T cells demonstrated reduced CD3/CD4 T cell counts and unaltered CD8 T cell counts in Garp-deficient mice compared to control mice (Figure 16B). These results are consistent with findings from patients. Further, immunohistochemical stainings of tissue samples were performed by colleagues form our group. Analysis of samples revealed spontaneous intestinal inflammation indicated by more pronounced lymphocyte infiltrations in lung liver and gut of Garp-deficient mice (Figure 15C).

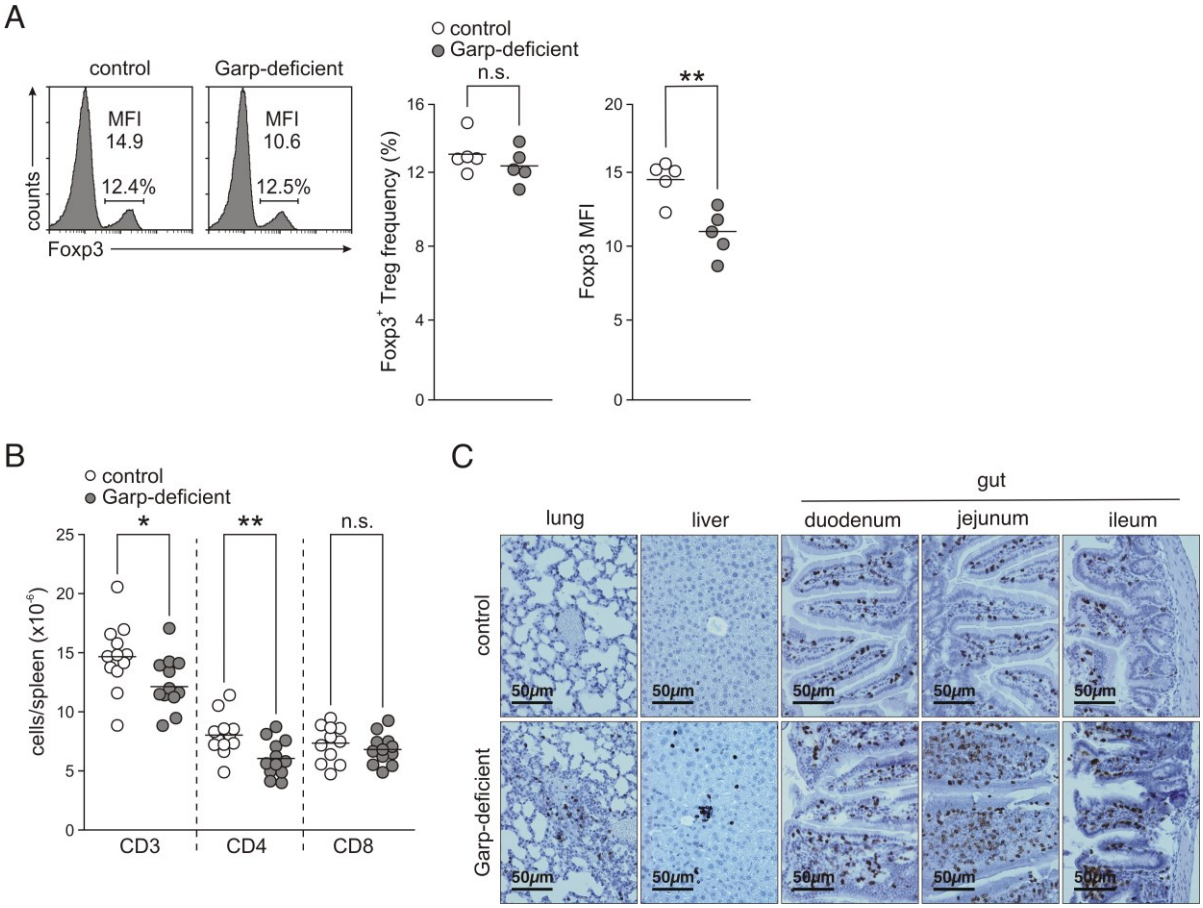

Figure 16 Phenotype of Garp-deficient mice
(A) Foxp3 frequencies in CD4$^+$ T cell populations were determined by intracellular flow cytometry. Representative stainings and results of one representative experiment with five mice per group out of four independent experiments with five mice per group are demonstrated. Mean values are indicated by horizontal lines. MFI: mean fluorescence intensity. (B) Cell counts of CD3, CD4 and CD8 T cells in spleens from 12 Garp-deficient and 12 control 12-week-old mice are demonstrated. Mean values are indicated by horizontal lines. (C) Lung, liver and gut from 10- to 12-week-old Garp-deficient and control mice were stained for CD3. Representative tissue sections are shown. Based on (Lehmkuhl et al., 2021).

3.2.3 Garp-deficiency in mice results in an inflammatory phenotype

Garp-deficient mice while living in a controlled pathogen free environment showed no obvious phenotype. To investigate whether Garp-deficiency correlates negatively with the suppressive capacity of Tregs and the maintenance of immune homeostasis, the immune system of Garp-deficient mice was challenged by performing CIA, EAE and colitis *in vivo* experiments. These experiments were performed by colleagues from our group and analysed by me. The susceptibility of mice to develop autoimmune disorders was analysed. Garp-deficient mice showed more pronounced symptoms and disease progression than control mice.

Garp-deficient mice, were unlike the control mice, susceptible to collagen-induced arthritis (CIA) (Figure 17A) and developed severe aggravating arthritis (Figure 17B) apparent by an increase in paw thickness (Figure 17C). Joint inflammation assessed by arthritis clinical scores was significantly higher in Garp-deficient mice than in control mice at the indicated time points reaching a maximum of 10.25 at day 35. Control mice did not develop severe arthritis and displayed a maximum score of only 1.9 on day 26 (Figure 17B). Measurements of hind paws at the start of the experiment compared to measurements performed at the experimental end point showed a significantly higher increase in paw thickness in Garp-deficient mice than in control mice (Figure 17C). At the end of the experiment, paws were analysed by histological TRAP stainings. The stainings confirmed the severe inflammation that was observed in Garp-deficient mice. The stained sections of Garp-deficient mice displayed cartilage damage, increased osteoclast differentiation and severe lymphocyte infiltration into the joint cleft (Figure 17D).

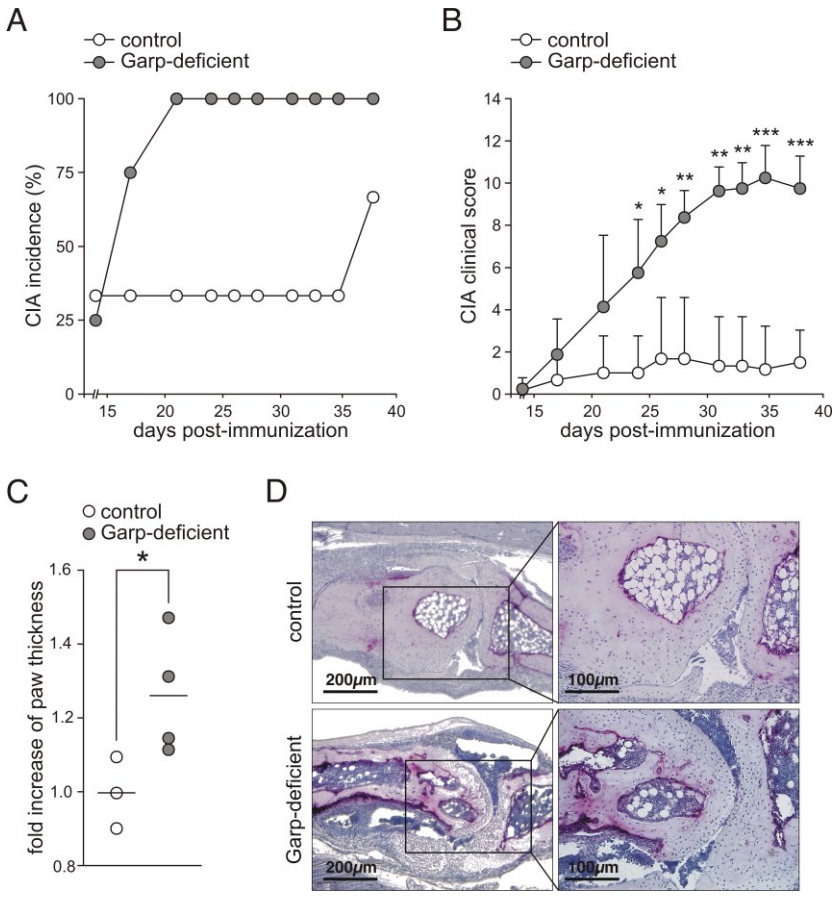

Figure 17 Collagen-induced arthritis in Garp-deficient mice.
(A) The graph shows the incidence frequency of collagen-induced arthritis. (B) The graph demonstrates the mean ± SEM values of the assessed arthritis clinical scores. (C) Changes in paw thickness were analysed my measurements at the first and final day post-immunization. (D) Representative TRAP staining are demonstrated of paws at day 38. The results of one representative experiment with three to four mice per group out of three independent experiments with three to five mice per group are demonstrated. Based on (Lehmkuhl et al., 2021).

Comparable to results seen in CIA experiments, Garp-deficient mice displayed a 100% susceptibility to experimental autoimmune encephalomyelitis (EAE) and developed severe paralysing disease (Figure 18A, B). Both control and Garp-deficient mice showed notable EAE development with a maximal clinical score at day 9. Garp-deficient mice however developed harsher symptoms represented by consistently higher clinical scores and significantly higher scores from day 11 to day 13 post immunization. The recovery of both groups started on day 10 but the control mice group reached total recovery two days earlier on day 17 and symptoms reduced to half the value of the maximal score on day 11 compared to day 15 in Garp-deficient mice (Figure 18B).

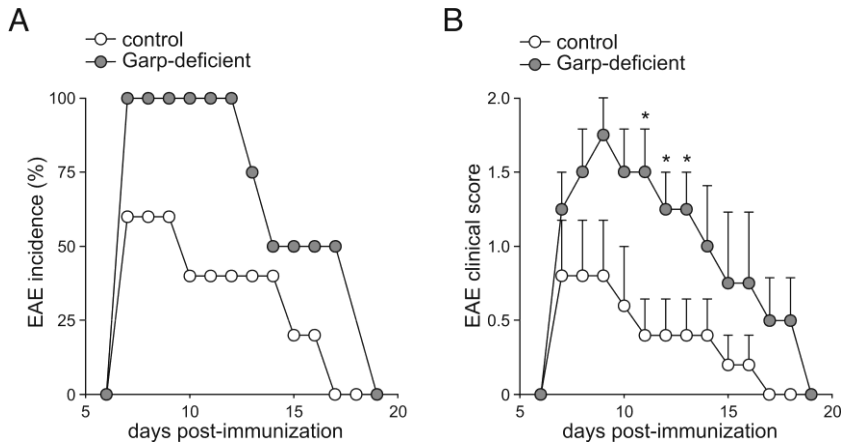

Figure 18 Experimental autoimmune encephalomyelitis in Garp-deficient mice.
(A) Incidence frequency of paralysis during EAE experiments is shown. (B) EAE clinical scores are demonstrated as mean ± SEM (B). Results of one representative experiment with three to four mice per group out of three independent experiments with three to five mice per group are displayed. Based on (Lehmkuhl et al., 2021).

In addition, DSS-induced colitis experiments were performed by colleagues of our group monitoring the body weight, clinical symptoms and evaluating colonic inflammation by histology at the end of the experiment. Following DSS administration, Garp-deficient mice developed severe colitis, resulting in a higher body weight loss, most apparent at day 8 and 9 of the experiment; a significantly higher clinical score and increased lymphocyte infiltrations into the mucosa in Garp-deficient mice (Figure 19A-D).

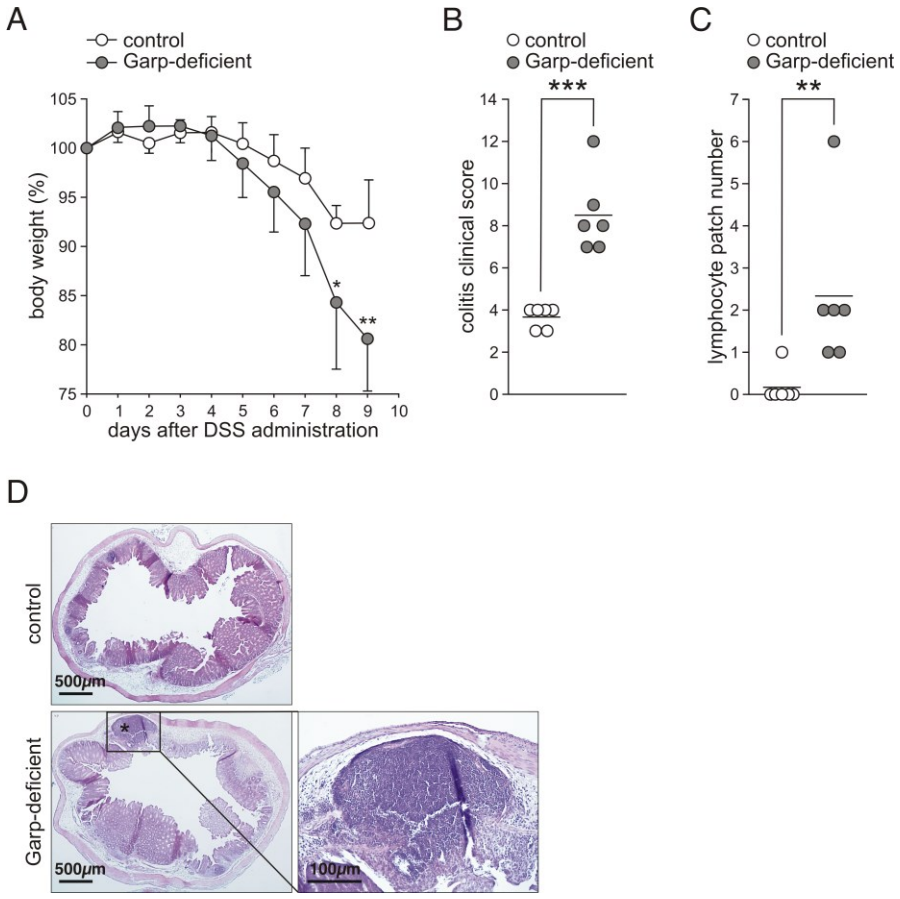

Figure 19 DSS-induced colitis in Garp-deficient mice.
(A-D) DSS-induced colitis. (A) The body weight of GARP-deficient and control mice was monitored for nine days, results are demonstrated as mean ± SEM. (B) The graph shows the clinical scores assessed at the last day of analysis. (C) The graph displays the number of colonic lymphocyte patches in ten 100 µm sequential sections. (D) A representative H&E colon staining is shown for GARP-deficient and control mice. A magnification of the lymphocyte patch found in the colon section of the GARP-deficient mice is displayed. Results of one representative experiment with six mice per group out of five independent experiments with five to six mice per group are shown. Mean values are indicated as horizontal lines. Based on (Lehmkuhl et al., 2021).

In conclusion, the absence of GARP in Tregs from Garp-deficient mice similar to the reduced GARP surface expression in Tregs of patients resulted in immune dysregulation.

3.2.4 GARP controls Treg phenotype stability

In a next step, the regulatory capacity of Garp-deficient Tregs was investigated in *in vivo* reconstitution experiments with Rag1-deficient mice. This experiment was performed by colleagues from our group and analysed by me. $CD45.2^+$ $CD25^+$ $CD4^+$ Tregs were isolated from control or Garp-deficient mice and injected into Rag1-deficient mice with $CD45.1^+$ $CD25^-$ $CD4^+$ Teffs. As a control, a group of mice were injected with Teffs only. Around 70% of the transferred control and Garp-deficient Tregs expressed Foxp3 (Figure 20A). The proliferation of $CD45.1^+$ $CD25^-$ $CD4^+$ Teffs was analysed after seven days in spleens (Figure 20B). As demonstrated in Figure 20C a strong Teff proliferation was observed in mice without the co-transfer of Tregs. The expansion of Teffs was significantly inhibited when Tregs from control mice were present. Meanwhile, the transfer of Garp-deficient Tregs had only small effects on controlling Teff proliferation. Furthermore, the ineffective inhibition of Teff proliferation by Garp-deficient Tregs was accompanied by a reduced recovery of Garp-deficient Tregs (Figure 20D). Both cell count and Tregs frequency were reduced in the analysed spleens of Rag1-deficient mice when Garp-deficient Tregs were transferred compared to control Tregs.

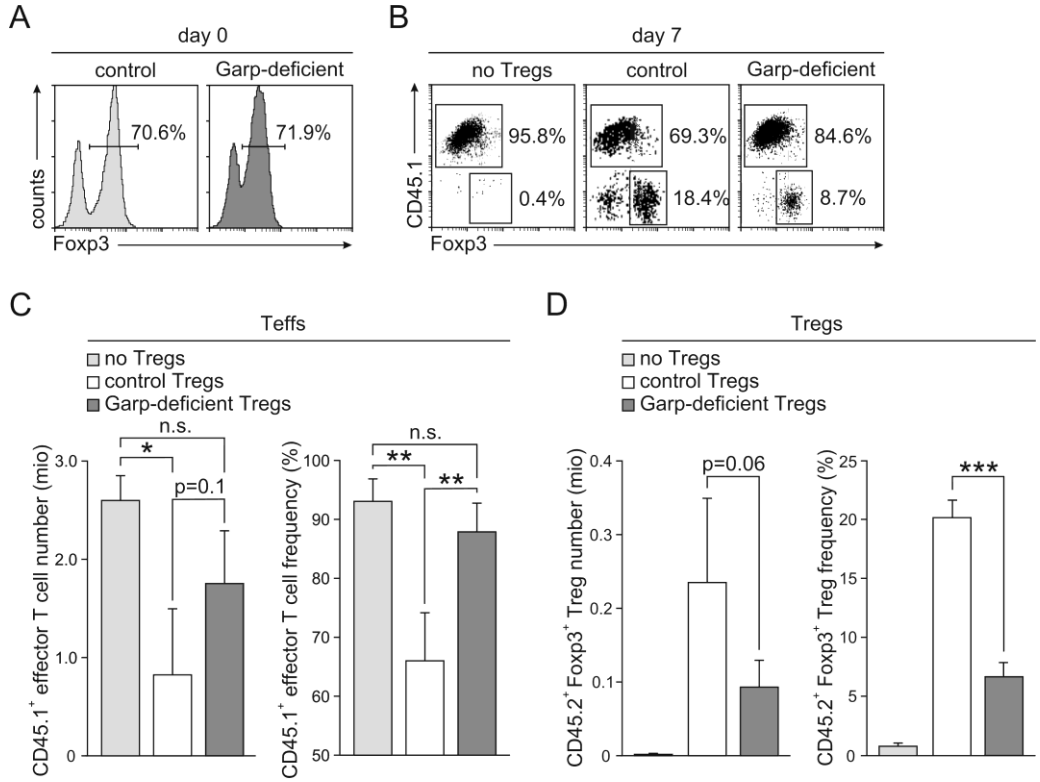

Figure 20 Proliferation suppression of Garp-deficient Tregs *in vivo*.
(A) Representative Foxp3 staining histograms of isolated CD45.2$^+$ CD25$^+$ CD4$^+$ Tregs. (B-D) Adaptive transfer of CD45.1$^+$ CD25$^-$ Teffs into Rag1-deficient recipient mice in absence or with Garp-deficient or control Tregs. Results of one representative experiment out of four independent experiments with four to five mice per group are demonstrated. (B) Representative CD45.1 und Foxp3 stainings of CD4$^+$ T cells recovered from spleens. (C) Cell counts and frequencies of CD45.1$^+$ CD4$^+$ T cells in recovered spleens seven days after the adoptive transfer. Results are demonstrated as mean ± SD. (D) Cell counts and frequencies of CD45.2$^+$ Foxp3$^+$ CD4$^+$ T cells in recovered spleens seven days after the injection. Results are demonstrated as mean ± SD. Based on (Lehmkuhl et al., 2021).

In a next step, colleagues analysed the suppressor function of Tregs from Garp-deficient and control mice *in vitro* using CFSE labelled CD4$^+$ CD25$^-$ effector T cells (Figure 21). In contrast to *in vivo* experiments, the suppressive capacity of Garp-deficient and control Tregs to limit effector T cell proliferation showed no differences *in vitro*.

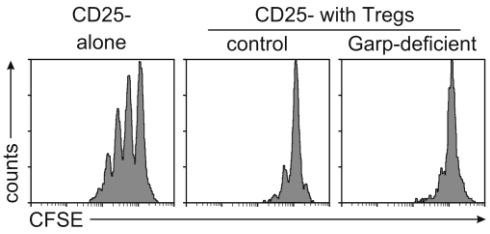

Figure 21 Suppressive capacity of Garp-deficient Tregs *in vitro*.
The suppressive capacity of Garp-deficient Tregs and control Tregs towards the proliferation of CFSE-labelled CD4$^+$ CD25$^-$ effector T cells was analyses by flow cytometry. Representative staining histograms are shown for proliferating CD4$^+$ CD25$^-$ T cells in the absence of Tregs and in the presence of control or Garp-deficient Tregs in a 1:1 Teff to Treg ratio.

To characterize the Treg phenotype stability, the frequency of apoptosis was analysed in different cell types by colleagues from our group. I*n vitro* experiments showed an increase in early apoptotic cells within the $CD25^+$ $CD4^+$ T cell population. $CD25^-$ $CD4^+$ T cells and $CD19^+$ B cells originating from Garp-deficient mice displayed no differences to control mice (Figure 22A). It was further demonstrated that the amount of Tregs that entered late apoptosis after one and two days in cell culture were higher in Garp-deficient Tregs compared to Tregs from control mice (Figure 22B).

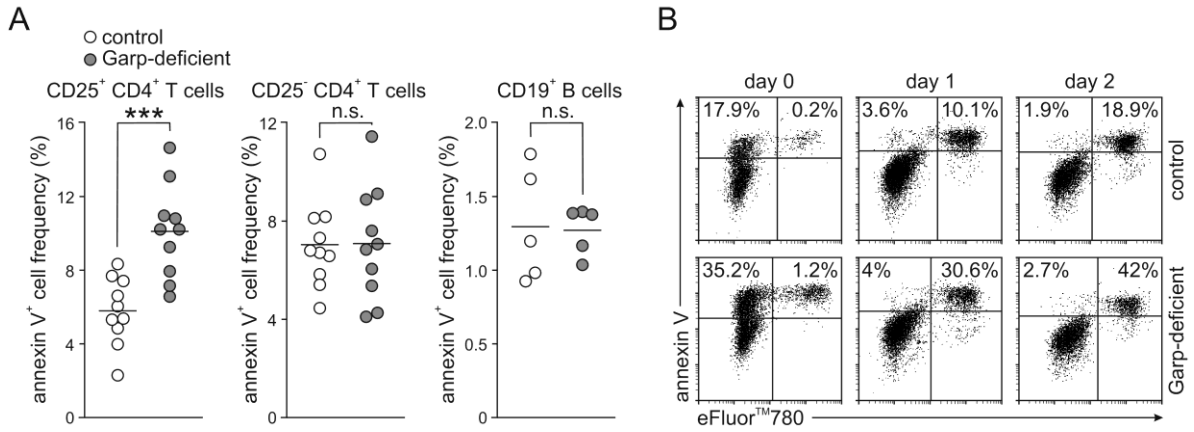

Figure 22 Apoptosis of Garp-deficient Tregs.
(A) Annexin V^+ frequencies of freshly isolated $CD25^+$ $CD4^+$ T cells, $CD25^-$ $CD4^+$ T cells and $CD19^+$ B cells. Mean values are indicated by horizontal lines. (B) The apoptosis rate of FACS-sorted Tregs stimulated with anti-CD3 and anti-CD28 for two days was assessed by flow cytometry using annexin V and cell viability dye. One representative experiment out of two independently performed experiments is demonstrated. Based on (Lehmkuhl et al., 2021).

3.2.5 Transcriptome analysis of Garp-deficient Tregs

To broaden the mechanistic understanding how GARP might regulate the Treg phenotype, transcriptomes of freshly isolated and one day stimulated Garp-deficient and control Tregs were compared and alterations in expression analysed (Figure 23). mRNA of five mice per group was purified from FACS-sorted Tregs by colleagues from our group and provided to the Agilent CrossLab to perform a Whole Mouse Genome Oligo Microarray (Mouse GE 4x44K v2) transcriptome analysis. Agilent CrossLab provided initial data analysis by identifying genes with greater than two-fold differential expression, further analysis was performed by me. Volcano plots were generated to present an overview on differently expressed genes. Coloured dots above the -log10 threshold of 2 (dotted line) are statistically significantly differently expressed genes with a fold change ratio greater than two. The knocked out Lrrc32 gene of Garp-deficient Tregs is indicated.

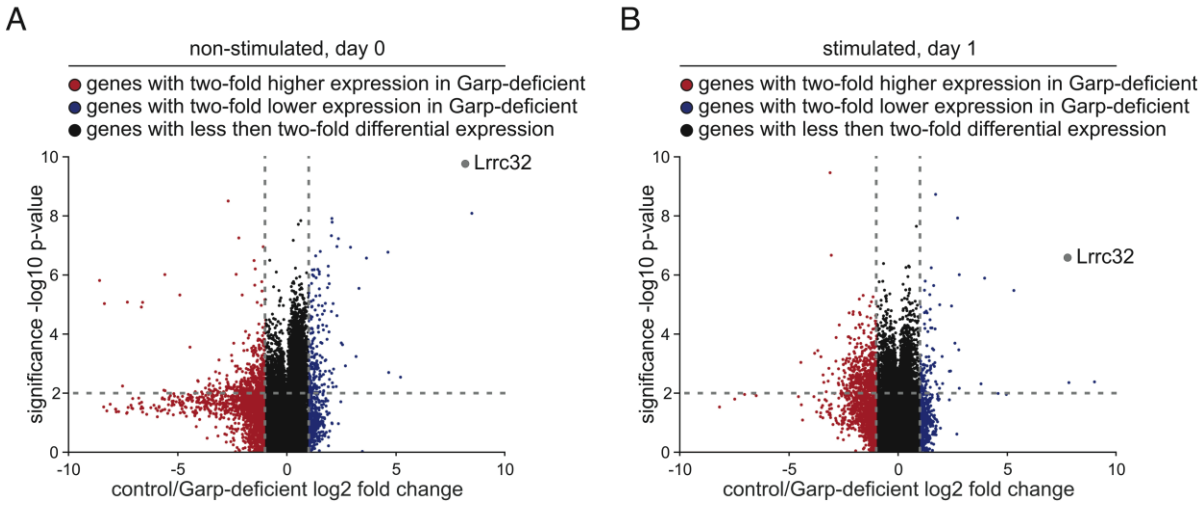

Figure 23 Volcano plots Whole Mouse Genome Oligo Microarray
Transcriptome analysis of mRNA purified from FACS-sorted control and Garp-deficient Tregs with five mice per group was performed on a Whole Mouse Genome Oligo Microarray (Mouse GE 4x44K v2). Tregs were either analysed (A) directly after purification or (B) after one day of stimulation. The intensity data were subjected to quantile normalization. Fold changes of normalised data and significances were calculated for freshly isolated and stimulated Tregs. Fold change is defined by the ratio of the median of the groups. Statistical analysis was performed by using Student's t-test. Horizontal dotted line indicates the -log10 p-value of 2 which equals a p-value of 0.01 and is defined as statistically significant in microarray data. Vertical dotted lines indicate the log2 fold change between -1 to 1 that equal fold change ratios between 0.5 and 2. Based on (Lehmkuhl et al., 2021).

In order to identify mechanisms that lead to the increased apoptosis rates, which were seen in Garp-deficient Tregs, the microarray data was analysed for genes associated with apoptosis and cell cycle regulation (Figure 24A). Consistent with the apoptosis data, a significantly reduced expression of Bcl2 was observed. Bcl2 encodes an anti-apoptotic molecule and reduced Bcl2 expression can promote apoptosis (Marsden et al., 2002). Additionally, the pro-apoptotic factor Bik showed an increased expression in Garp-deficient Tregs and the expression of several caspase genes, which are essential for apoptosis, was higher in Garp-deficient Tregs than in control Tregs (Figure 24A) (Elangovan and Chinnadurai, 1997; Nunez et al., 1998). Garp-deficient Tregs also displayed deregulations in multiple genes that are associated with cell cycle regulation. Genes with two-fold or higher differential expression are shown in Figure 24B. The microarray data indicates a deregulation in cell cycle control and apoptosis in Garp-deficient Tregs that is consistent with the previously demonstrated flow cytometry results showing increased apoptosis in Garp-deficient Tregs.

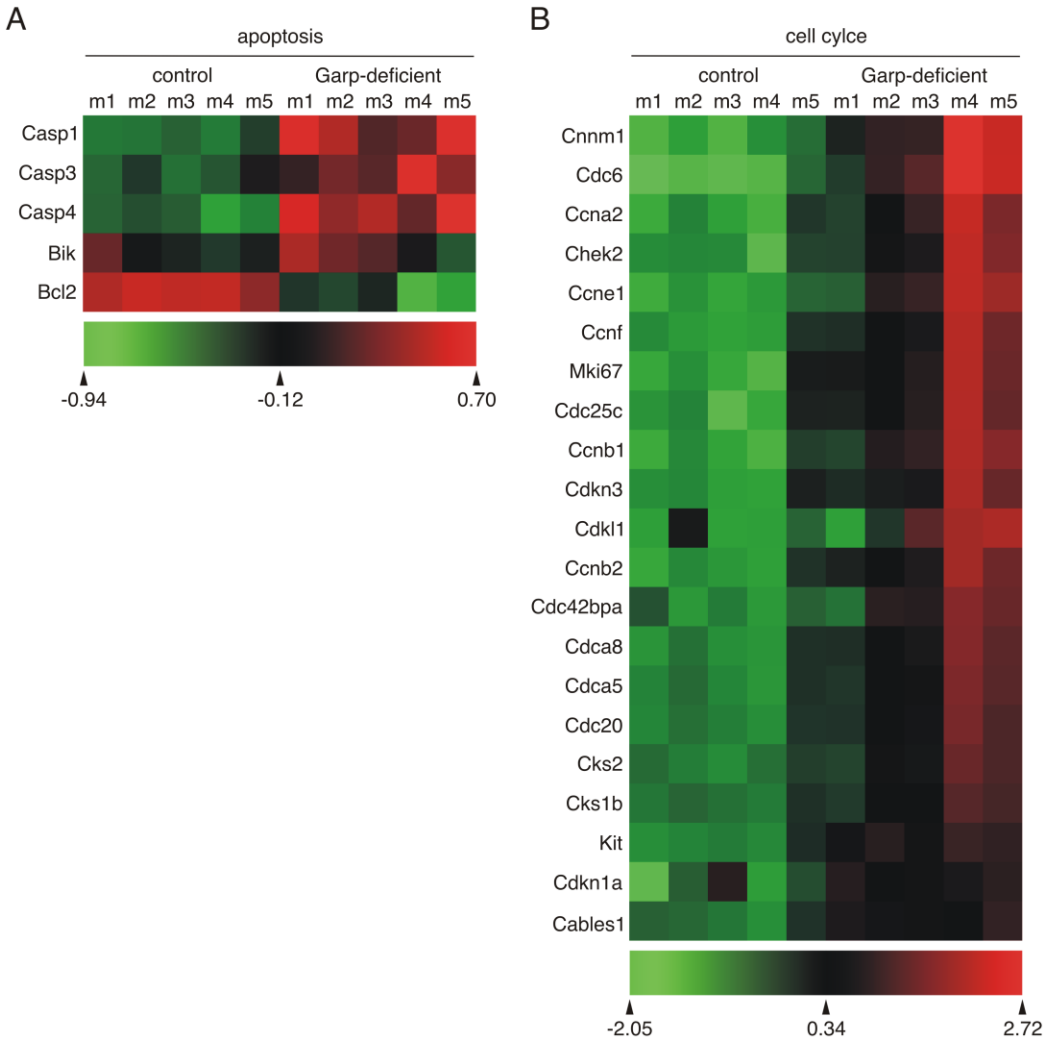

Figure 24 Microarray analysis of genes involved in apoptosis and cell cycle regulation
(A) Heat maps show apoptosis related genes with a statistically significant difference in expression (B) Heat maps of statistically significant and above two-fold differentially expressed genes involved in cell cycle regulation. Based on (Lehmkuhl et al., 2021).

Moreover, stimulation of Garp-deficient Tregs resulted in an increase in several effector cytokines compared to stimulation of control Tregs (Figure 25). This indicates a broad deregulation of cytokine expression as a consequence of missing GARP expression in Tregs.

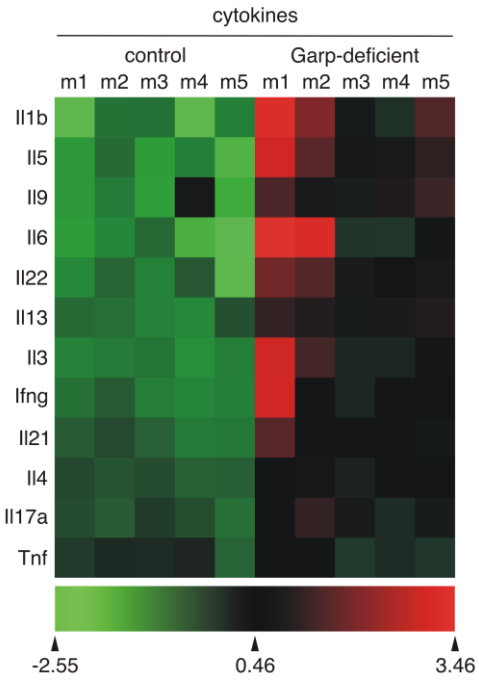

Figure 25 Microarray analysis of cytokines
Heat map of statistically significant and above two-fold differentially expressed cytokines in stimulated control Tregs and stimulated Garp-deficient Tregs. Based on (Lehmkuhl et al., 2021).

Further, Treg-characteristic genes were analysed. CD25, Nrp1, CTLA4 and IL-10 displayed significantly diminished expression levels in freshly isolated Garp-deficient Tregs (Figure 26A). However, the most striking observation was the significantly increased expression of Hdac9 in Garp-deficient Tregs (Figure 26A). Hdac9 is a Treg specific histone deacetylase that regulates Treg function and stability by the deacetylation of Foxp3 (Tao et al., 2007). It is therefore plausible that increased Hdac9 expression in Garp-deficient Tregs results in reduced Foxp3 stability due to higher rates of Foxp3 deacetylation. To follow up on the discovered deregulation of Hdac9 expression, other histone deacetylases as well as histone acetyltransferases (p300 and TIP60) were analysed (Figure 26B). Interestingly, neither of the analysed non-Treg specific histone deacetylases nor histone acetyltransferases displayed significant differences in gene expression between Garp-deficient and control Tregs (Figure 26B).

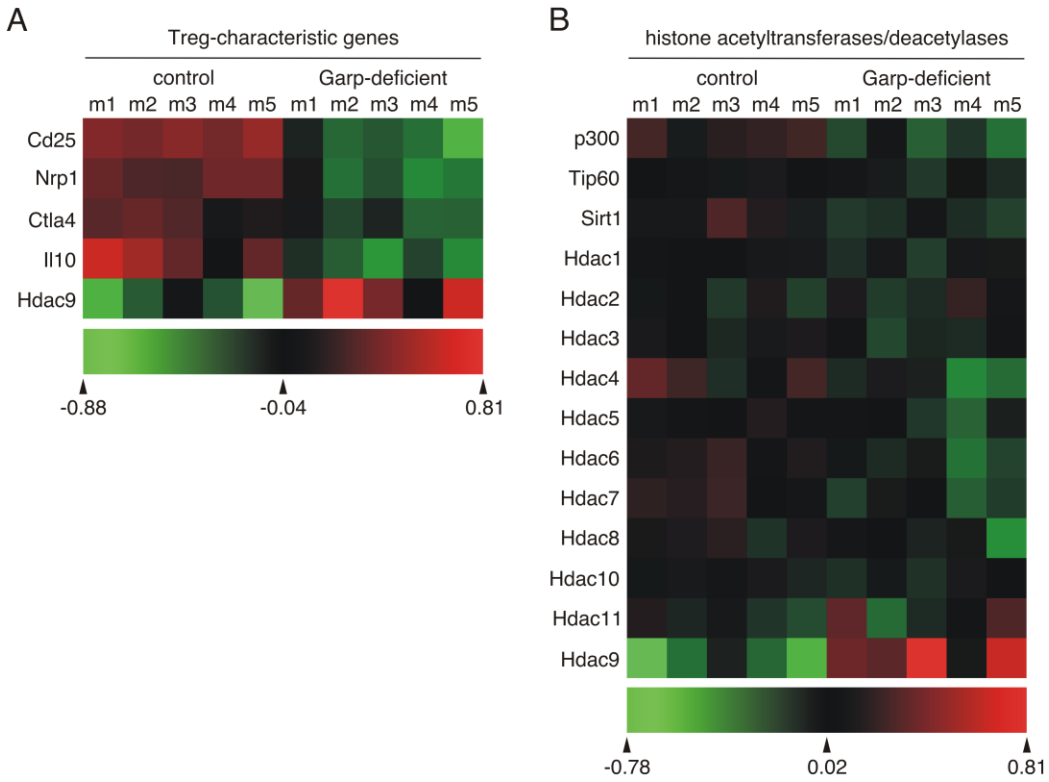

Figure 26 Microarray analysis of characteristic Treg genes, Hats and Hdacs
(A) Heat map of statistically significant differentially expressed genes characteristic for Treg phenotype. (B) Heat map of gene expression of histone deacetylases and histone acetyltransferases. Based on (Lehmkuhl et al., 2021).

To confirm microarray results that identified differentially expressed Treg specific genes in Garp-deficient Tregs, intracellular flow cytometry experiments were performed. Indeed, significantly diminished protein expression of CD25, NRP1 and CTLA4 was observed in Garp-deficient Tregs (Figure 27A-C). The expression of these proteins was analysed in Foxp3 positive Tregs. IL-10 expression was assessed using freshly isolated Tregs after stimulation with PMA, ionomycin and monensin. Corresponding to the mRNA microarray data, the frequency of IL-10 producing Tregs was significantly higher in control Tregs than in Garp-deficient Tregs (Figure 27D).

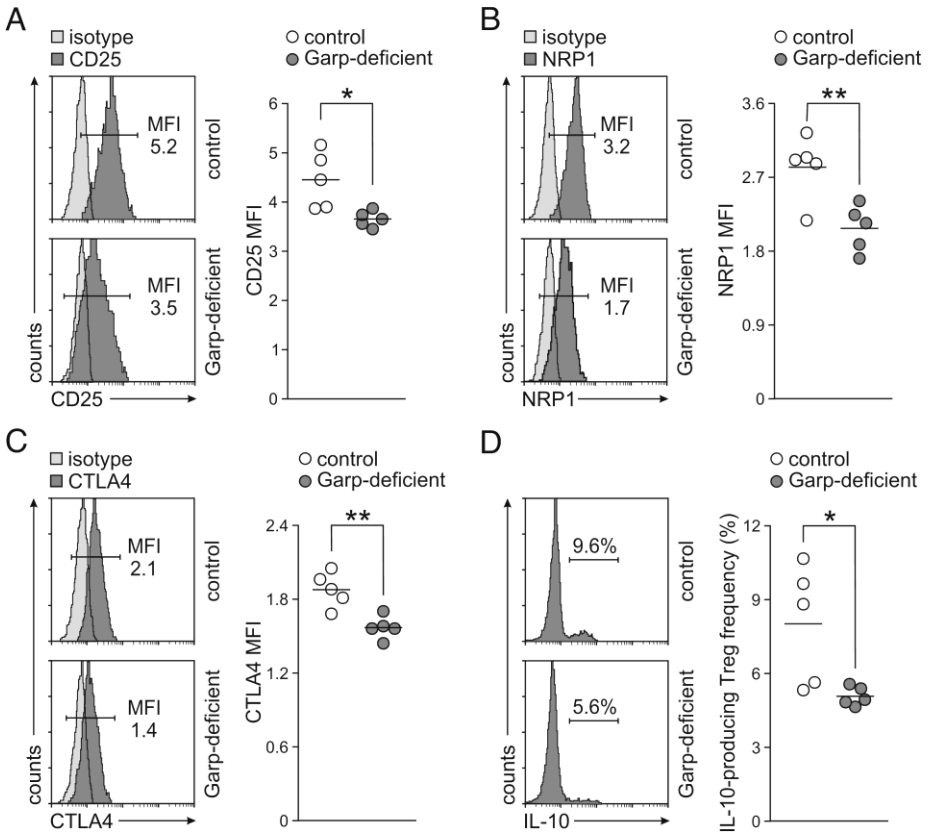

Figure 27 Expression of proteins characteristic for Treg
(A-D) Analysis of CD25, NRP1, CTLA4 and IL-10 expression by flow cytometry. (A-C) CD25, NRP1 and CTLA4 protein expression was analyzed in freshly isolated $CD4^+$ T cells after gating for Foxp3 expression. (D) IL-10 expression was assessed in freshly isolated Tregs after stimulation with PMA, ionomycin and monensin. Representative staining histograms are demonstrated with results of one representative experiment with five mice per group out of two independent experiments with five mice per group. Mean values are indicated by horizontal lines. MFI; mean fluorescence intensity. Based on (Lehmkuhl et al., 2021).

To gain further confirmation for the microarray results, expression of Hdacs was analysed in real-time PCR experiments performed by colleagues from our group. Only the analysis of the results was performed by me. mRNA of purified Tregs from Garp-deficient and control mice were analysed and showed a twofold higher Hdac9 expression in Garp-deficient Tregs (p=0.06) (Figure 28). This result matches the microarray data. Further analysis of other Hdacs showed no differences in Tregs from Garp-deficient and control mice, which is also consistent with the results from the microarray.

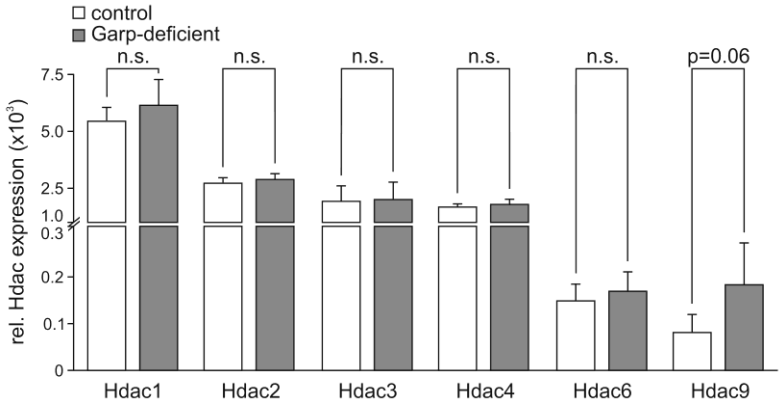

Figure 28 Hdac expression
Real-time PCR analysis of indicated histone deacetylases. mRNA levels are shown in relation to *Actb*. Results of four independent experiments are displayed as mean ± SD. Based on (Lehmkuhl et al., 2021).

3.2.6 Foxp3 protein acetylation

Protein acetylation of Foxp3 is defined by the activity of HATs and HDACs (Zhang et al., 2012). The deregulation of the Treg specific histone deacetylase HDAC9 that was observed in Garp-deficient Tregs is expected to lead to decreased Foxp3 protein acetylation. Since the expression of p300 and TIP60 was unaltered, it can be assumed that increased HDAC9 expression shifts the balance of acetylation and deacetylation for Foxp3 and promotes deacetylation. Protein acetylation increases protein stability by protecting from ubiquitination (Drazic et al., 2016). Therefore, decreased Foxp3 protein acetylation would result in unstable Foxp3. Thus, decreased protein stability of Foxp3 is a possible explanation for the decreased MFI of Foxp3 that was observed in Garp-deficient Tregs. In order to assess Foxp3 protein acetylation directly and to confirm this expectation different methods were tested.

3.2.6.1 Foxp3 acetylation analysis by immunoprecipitation

In a first step, analysis of Foxp3 protein acetylation in Tregs was attempted by immunoprecipitation of Foxp3 and consecutive western blot staining for AcK. The immunoprecipitation (IP) and supernatant (SN) was analysed, $CD4^+$ $CD25^-$ T cells were used as control and beta-actin served as a housekeeping protein. Despite all efforts, this method did not allow to quantify basal Foxp3 acetylation. The sensitivity remained insufficient with both of the used antibodies for AcK(Figure 29A, B).

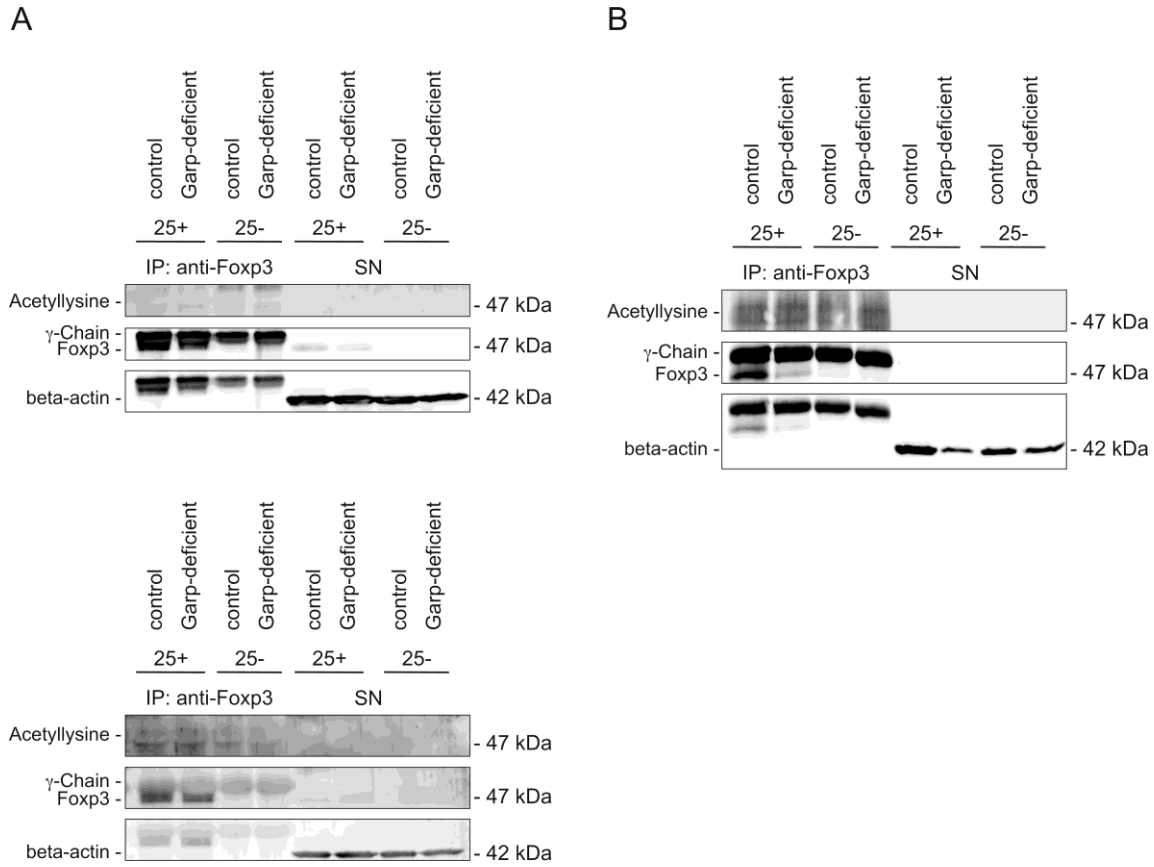

Figure 29 Foxp3 acetylation immunoprecipitation
(A, B) Lysates of $10x10^6$ $CD4^+$ $CD25^+$ Tregs (25+) and $CD4^+$ $CD25^-$ T cells (25-) were immunoprecipitated (IP) with anti-Foxp3 antibodies, western blots were probed for AcK, Foxp3 and beta-actin. Supernatant (SN) of lysed cells was analysed. Anti-AcK antibodies (A) from abcam and (B) from cell signalling were used respectively. Abcam anti-AcK antibodies were either incubated in milk (A top) or BSA (A bottom).

3.2.6.2 Development of a FRET based FACS staining for Foxp3 acetylation

As an alternative to immunoprecipitation an intracellular FACS assay utilising FRET was established to differentiate acetylated and unacetylated Foxp3 protein. CD4 positive T cells were purified and stained by intracellular flow cytometry. Sequential staining with primary unconjugated antibodies for AcK and Foxp3 followed by secondary antibodies with the specifically selected fluorochrome FRET pair Alexa 488 (A488) for AcK and Alexa 594 (A594) for Foxp3 generated a FRET signal upon excitation of the donor A488 when the acceptor A594 was in high vicinity. Using a single excitation laser at 488nm, the detector (FL3) was set up for detection at 600-620nm, optimized for the emission maximum of A594 at 617nm (Figure 30). The donor fluorochrome A488 that binds to AcK residues is directly excited by the 488nm laser. The dotted lines highlight the FL3 detector region of 600-620nm. A488 alone has a low emission in the FL3 detector range. The acceptor fluorochrome A594 emits strongly at this detector range, but is not excited by the 488nm laser. In order to excite A594 bound to Foxp3 a FRET signal originating from A488 is necessary. With this experimental setup a FRET signal detected in FL3 represents acetylated Foxp3.

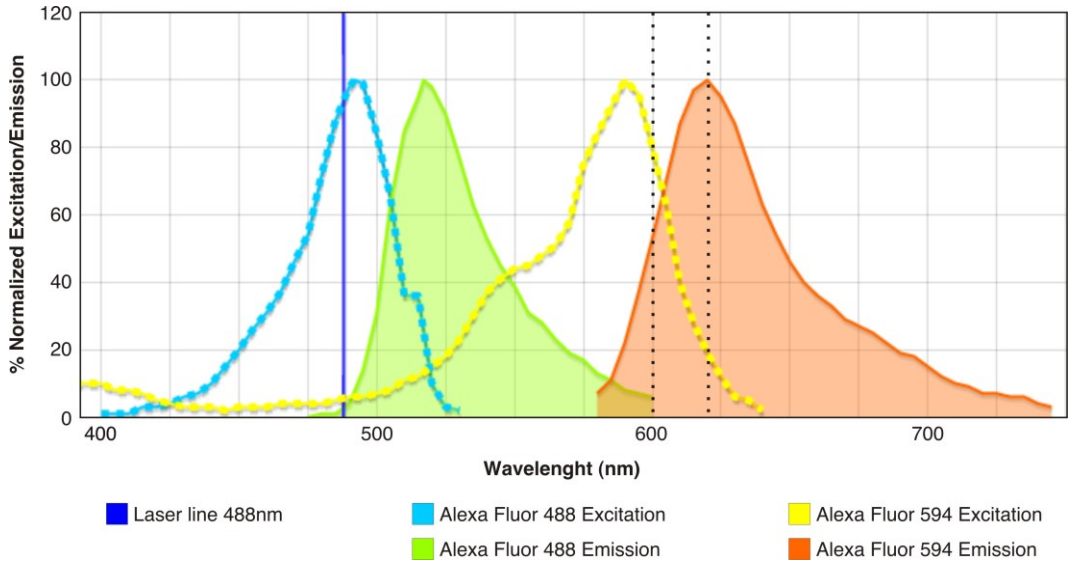

Figure 30 FRET detection scheme
Schematic overview of fluorochrome excitation and emission spectra and FRET signal detection. FRET donor A488 is directly excited by the 488nm laser line (blue line); FRET acceptor A594 relies on nonradiative transfer of energy from the excited donor for fluorescent emission. FRET detection from 600-620nm is indicated by dotted black lines. Illustration generated by Fluorescence Spectra Analyser (Biolegend).

In an initial proof of principle experiment, a very strong FRET signal was detected when freshly purified $CD4^+$ T cells were stained with anti-AcK antibodies and both secondary antibodies (A488, A595) were directed at AcK (Figure 31). Controls with single use of secondary antibody showed low levels of A488 signal bleedthrough into the FL3 FRET detection channel (MFI 17.6); in addition, low emission of A594 (MFI 17.6) was detected. The FRET signal emission by A594 located in proximity to excited A488 (A488 + A594) reached an MFI of 135.1. These results demonstrated that the chosen secondary antibody pair A488 + A594 can emit a FRET signal effectively (Figure 31).

Donor quenching of A488 was observed in the presence of A594. It reduced the signal of A488 in the FL1 detector (505-545nm) from MFI 159.7 to a MFI of 81.4 (Figure 31). This effect of donor quenching is expected, but the lower signal in FL1 when both secondary antibodies are present might be accentuated by the fact that these antibodies compete with each other to bind the primary anti-AcK antibody, which reduced the total amount of A488 binding AcK compared to single use of A488 secondary antibody. A594 secondary antibody that binds to AcK does not emit in FL1.

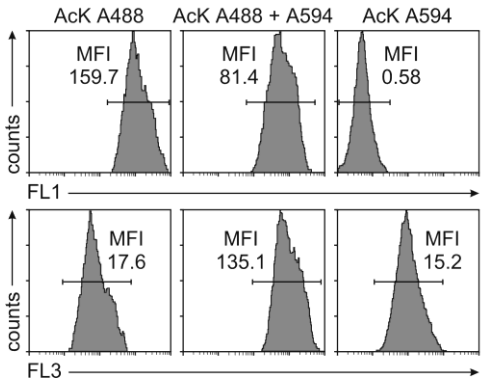

Figure 31 FRET staining proof of principle
A positive control for FRET was performed by targeting anti-AcK antibody with both secondary antibodies (A488 and A594). Representative staining histograms for FL1 and FL3 detection are demonstrated.

In a next step, FRET signal detection for Foxp3 protein acetylation was established. AcK with secondary antibody A488 served as FRET donor and Foxp3 with secondary antibody A594 as FRET acceptor (Figure 32). Three controls were used for each analysis: Isotype control for AcK (Iso AcK) detected by A488 with Isotype control for Foxp3 (Iso Foxp3) detected by A594 (lower left), Iso Ack detected by A488 with Foxp3 detected by A594 (upper left) and AcK detected by 488 with Iso Foxp3 detected by A594 (lower right). FRET signal of acetylated Foxp3 positive cells was detected by staining of AcK wtih A488 and Foxp3 with A594 (upper right). Detection of the FRET signal requires that an anti-Foxp3 antibody and an anti-AcK antibody bind to their targets in close proximity. The signal from Foxp3 with A594 in absence of AcK primary antibody (Iso AcK detected by A488 with Foxp3 detected by A594) was still detectable due to the calculated 8% excitation efficiency by the 488nm Laser for A594. However, this background signal was much weaker than the FRET signal of acetylated Foxp3 (Figure 32). Hence, this established method proved to be effective to quantify the frequency of acetylated Foxp3 positive Tregs.

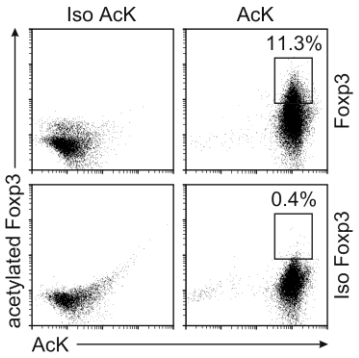

Figure 32 FRET staining acetylated Foxp3
Assessment of Foxp3 acetylation and controls. Representative stainings are demonstrated for the FRET antibody pair AcK with Foxp3 and the controls Iso AcK with Iso Foxp3, Iso AcK with Foxp3 and AcK with Iso Foxp3. AcK: acetylated lysin.

3.2.7 Foxp3 acetylation in Garp-deficient Tregs

Foxp3 acetylation was assessed in freshly isolated $CD4^+$ T cells by intracellular flow cytometry using the newly established protocol for FRET detection. The frequency of Tregs with acetylated Foxp3 was significantly lower in Garp-deficient Tregs than in control Tregs (Figure 33). This suggests that the up-regulation of Hdac9 in Garp-deficient Tregs results in diminished Foxp3 acetylation.

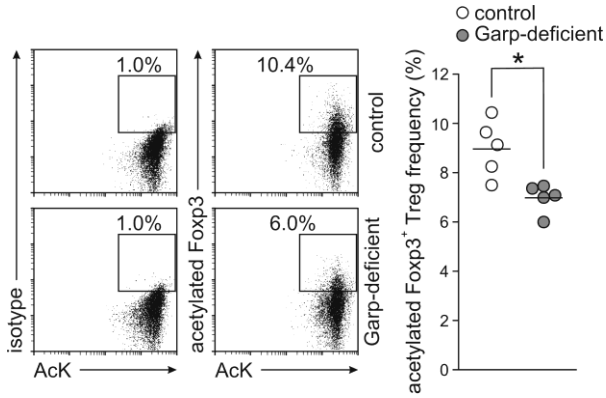

Figure 33 Foxp3 acetylation
Foxp3 acetylation was analysed in freshly isolated $CD4^+$ T cells by intracellular flow cytometry using a FRET antibody pair for Foxp3 and AcK. Representative stainings and results from one representative experiment with five mice per group out of four independent experiments with five mice per group are demonstrated. Mean values are indicated by horizontal lines. AcK: acetylated lysin. Based on (Lehmkuhl et al., 2021).

Moreover, total protein acetylation was also significantly lower in Garp-deficient Tregs than in control Tregs (Figure 34). This could indicate that the increased Hdac9 expression that was seen in Garp-deficient Tregs is sufficient to reduce the total acetylation level in Garp-deficient Tregs.

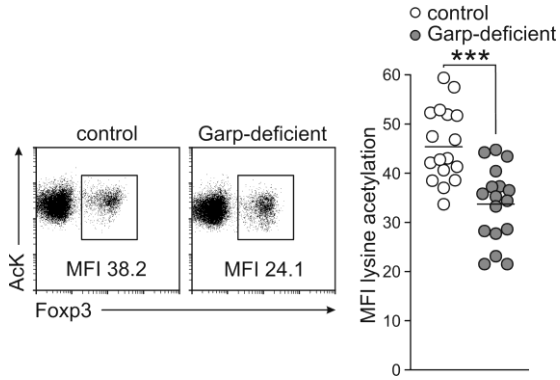

Figure 34 Total lysine acetylation
Total lysine acetylation of Foxp3 positive Tregs was analysed by flow cytometry. Left panel demonstrates representative stainings of control and Garp-deficient $CD4^+$ T cells. Right panel shows a summary of total lysine acetylation in Foxp3 positive Tregs, the results of three independently performed experiments with five mice per group are demonstrated.

3.2.8 Analysis of acetylation-mediated Foxp3 protein stability

As it was shown that reduced HDAC9 expression in Garp-deficient Tregs correlates with diminished Foxp3 acetylation, the protein stability of Foxp3, which is defined by its acetylation state, was investigated. Experiments performed by colleagues from our group analysing the Foxp3 expression of FACS sorted Tregs over the course of four days showed that Garp-deficient Tregs had a more rapid decline of Foxp3 expression compared to control Tregs (Figure 35). 61.4% of control but only 39.9% of Garp-deficient Tregs expressed Foxp3 after one day of cell culture.

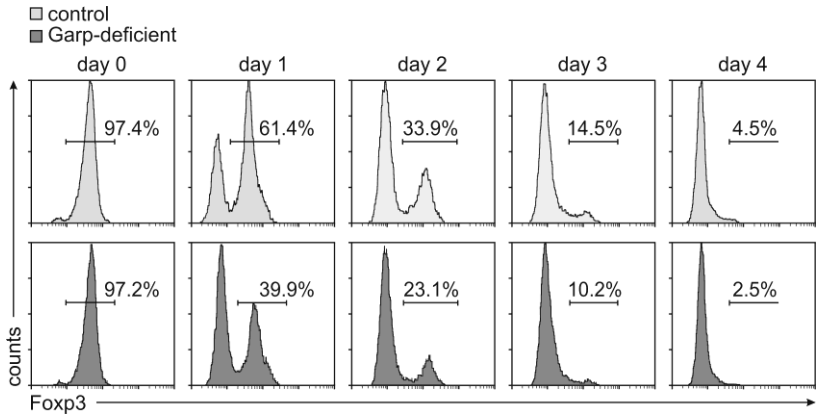

Figure 35 Treg stability
Tregs were purified by FACS-sorting from $CD4^+$ T cells of five to ten mice and stimulated with anti-CD3, anti-CD28 for one to four days. Foxp3 expression was analysed by intracellular flow cytometry. Staining histograms of one representative experiment out of two independent experiments are demonstrated. Based on (Lehmkuhl et al., 2021).

The detection of the frequency of Foxp3 positive Tregs and their decline is dependent on Foxp3 protein expression and Foxp3 protein stability. To eliminate the influence of Foxp3 expression and to focus on protein stability CHX, a protein synthesis inhibitor, was used in following cell culture experiments. Since the protein stability of Foxp3 is defined by its acetylation (van Loosdregt et al., 2010), it was expected that Garp-deficient Tregs lose their Foxp3 phenotype more rapidly than control Tregs.

The half-life of Foxp3 was determined by analysing the stability of Foxp3 positive Treg frequencies in purified $CD4^+$ T cell populations. CHX was added to the cell media. Observed Foxp3 frequencies were normalised and Foxp3 protein half-life was calculated by linear regression. It was demonstrated that the half-life of Foxp3 was significantly lower in Garp-deficient Tregs than in control Tregs. The half-life of Foxp3 was 11.9±1.0 hours in non-stimulated Garp-deficient Tregs and 14.9±0.56 hours in non-stimulated control Tregs (p=0.02) (Figure 36A). In Garp-deficient Tregs, anti-CD3 and anti-CD28 stimulation did not stabilize Foxp3, on the contrary stimulation emphasized the difference between Garp-deficient and control Tregs. Activated Garp-deficient Tregs had a half-life of Foxp3 of 12.1±0.47 hours as compared to activated control Tregs with 18.4±0.56 hours (p<0.005) (Figure 36B). In regard to the function of Foxp3 as the key transcription factor of Tregs, these results indicate that GARP is important for the protein stability of Foxp3 and thereby for the phenotype stability of Tregs.

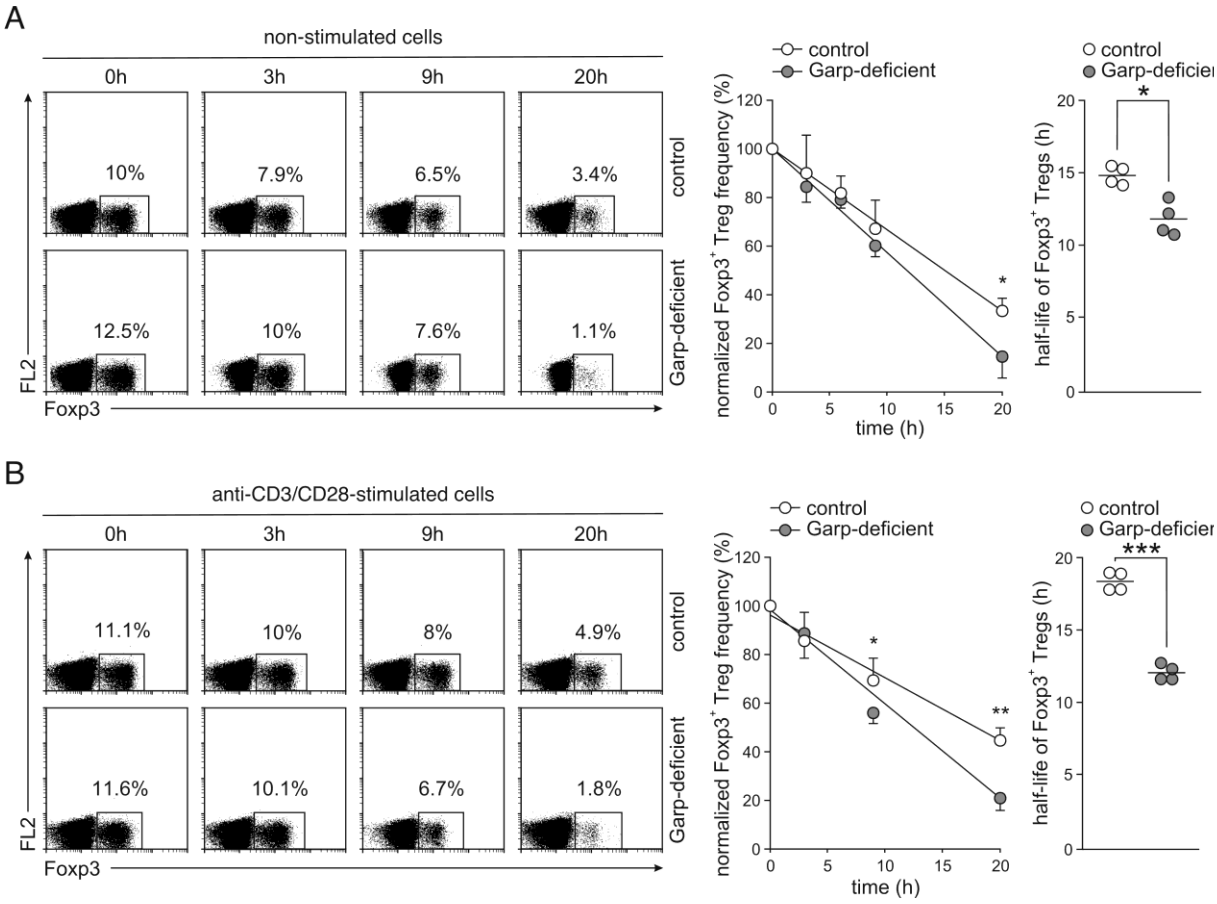

Figure 36 Treg stability in presence of CHX
(A, B) Treg stability was analysed by assessing the frequency of $Foxp3^+$ Tregs within $CD4^+$ T cells using intracellular flow cytometry. $CD4^+$ T cells were cultured for 20 hours (h) in the presence of CHX without stimulation (A) or with anti-CD3 and anti-CD28 stimulation (B). In the left panels representative stainings of one experiment out of four independent experiments are demonstrated for the indicated time points. The graphs on the right show the linear regression of normalised $Foxp3^+$ Treg frequencies of four independent experiments displayed as means ± SD and the individual results of Foxp3 half-lifes. Mean values are indicated by horizontal lines. Based on (Lehmkuhl et al., 2021).

3.2.8.1 Foxp3 protein stability in PID patients with LLRC32 mutations

After identifying deregulated HDAC9 expression and diminished Foxp3 protein stability in Garp-deficient Tregs in mice, Tregs from patients with *LRRC32* mutations and low GARP expression were further analysed using real-time PCR and flow cytometry (Figure 37A, B). Real-time PCR analysis of mRNA isolated from Tregs showed elevated *HDAC9* expression in the patients compared to health controls (Figure 37A).

In addition, purified $CD4^+$ T cell were cultured with CHX under stimulating conditions with anti-CD3 and anti-CD28 to analyse the stability of Foxp3 positive Tregs of patients and healthy controls. Tregs from patients with *LRRC32* mutations displayed a reduced Foxp3 half-life. The half-life of Foxp3 in patient 1 was 46.28h and in patient 2 41.64 hours as compared to 92.59±25.58 hours that was observed in Tregs from healthy controls. These results are consistent with observations made in Garp-deficient mice. The results indicate that the reduced GARP expression on Tregs affects TGFβ1 availability and results in decreased Foxp3 protein stability and Treg function.

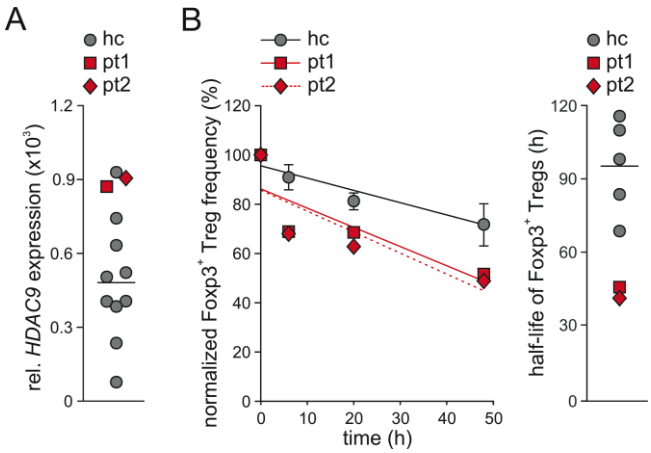

Figure 37 *HDAC9* expression and Treg stability in human Tregs with *LRRC32* mutations
(A) Real-time PCR analysis of *HDAC9* in freshly purified Tregs. Relative *HDAC9* mRNA levels are demonstrated in relation to *ACTB*. Results of 10 healthy controls are displayed in grey, patients are indicated in red. (B) Treg stability was analysed by assessing the frequency of $Foxp3^+$ Tregs within $CD4^+$ T cells using intracellular flow cytometry. $CD4^+$ T cells were cultured for 50 hours (h) in the presence of CHX with anti-CD3 and anti-CD28 stimulation. Linear regression of normalised $Foxp3^+$ Treg frequencies of patients are indicated in red, linear regression of mean values of five healthy controls are displayed in grey as means ± SD. Individual results of Foxp3 half-lifes of patients and healthy controls are shown on the right. Mean values are indicated by horizontal lines. Based on (Lehmkuhl et al., 2021).

3.2.8.2 Manipulation of acetylation-mediated Foxp3 protein stability

To modulate Foxp3 acetylation and Foxp3 protein stability, the histone deacetylase inhibitor TSA was used in *in vitro* cell culture experiments. Various TSA concentrations were tested and

their effect on total lysine acetylation and Foxp3 expression was analysed in control and Garp-deficient Tregs by flow cytometry (Figure 38A, B). High TSA concentrations ranging from 0.5-50 µM were effective to increase total lysine acetylation to up to sevenfold of the basal acetylation within 20 hours of cell culture (Figure 38A). However, as a side effect of TSA and the increased acetylation, Foxp3 frequencies were unfortunately diminished. To prevent the loss of Foxp3 expression and induction of apoptosis by TSA lower concentrations ranging from 0.5-50 nM were tested in a following experiment (Figure 38B). The 50 nM TSA concentration was still effective to increase the overall acetylation level in Tregs but again at cost of Foxp3 frequency, which TSA was supposed to stabilize by promoting Foxp3 acetylation and protein stability. The lower TSA concentrations (0.5 nM and 5 nM) did however, not affect acetylation or Foxp3 frequency (Figure 38B).

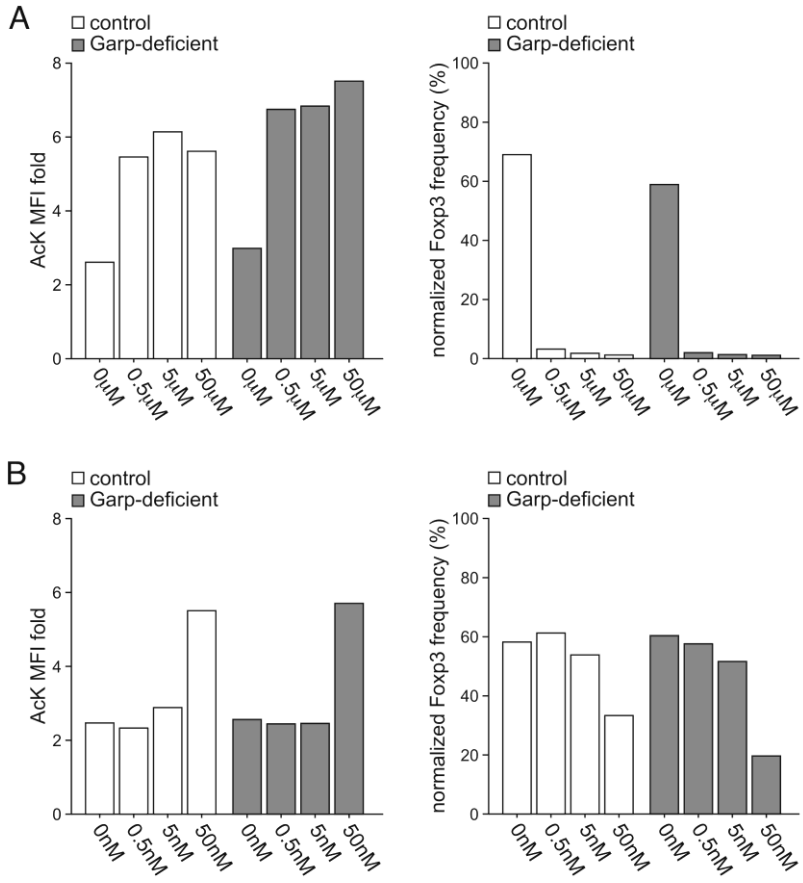

Figure 38 Acetylation and Foxp3 modulation by TSA
(A, B) CD4$^+$ T cells were cultured for 20 hours with various TSA concentrations and anti-CD3 and anti-CD28 stimulation. Foxp3 expression and total lysine acetylation was analysed by intracellular flow cytometry. Foxp3 frequency was normalised to the Foxp3 frequency of freshly isolated CD4$^+$ T cells. AcK MFI was normalised to the AcK MFI of freshly isolated CD4$^+$ T cells and displayed as fold change.

In a next step, TSA concentrations were further adjusted (6.25 nM to 50 nM). A dose dependent increase of total lysine acetylation was observed without the side effect of diminishing Foxp3

frequencies (Figure 39A). Since Foxp3 frequencies seemed similar at different TSA concentrations, Foxp3 protein levels were further analysed in Tregs by Foxp3 MFI values (Figure 39B). In negative correlation to increased acetylation, a dose dependent decrease of Foxp3 protein levels was observed in control and Garp-deficient Tregs (Figure 38B).

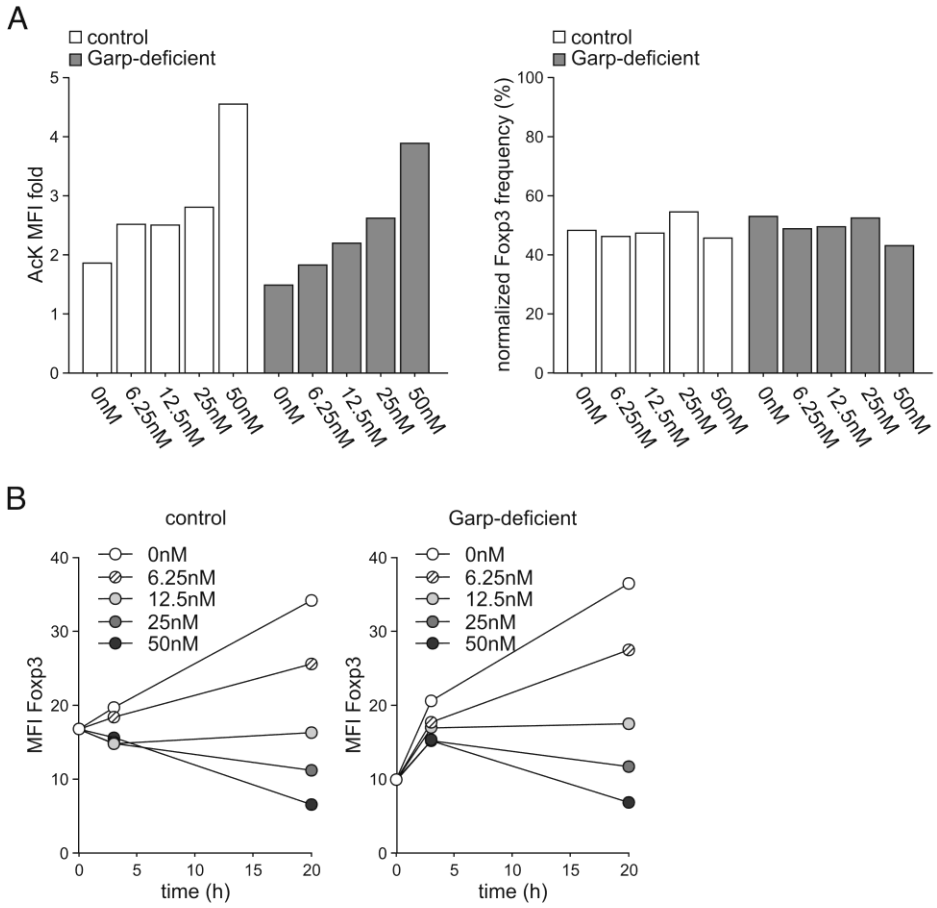

Figure 39 Acetylation and Foxp3 modulation by TSA
(A, B) $CD4^+$ T cells were cultured for 20 hours with various TSA concentrations and anti-CD3 and anti-CD28 stimulation. Foxp3 expression and total lysine acetylation was analysed by intracellular flow cytometry. (A) Foxp3 frequency was normalised to the Foxp3 frequency of freshly isolated $CD4^+$ T cells. AcK MFI was normalised to the AcK MFI of freshly isolated Tregs and demonstrated as fold change. (B) Foxp3 MFI of control and GARP-deficient Tregs is demonstrated for the various TSA concentrations at different time points.

To circumvent the side effects of TSA, CD4 positive T cells were incubated with TSA for only three hours to increase acetylation. After the incubation period the cells were washed to remove TSA from the medium to prevent the induction of apoptosis by long exposure to TSA. Cells were then cultured in presence of CHX for 20 hours and Foxp3 frequencies were analysed. Short exposure to TSA increased the overall lysine acetylation in Tregs but acetylation declined quickly after washing; and no stabilization of Foxp3 frequencies were observed with this approach. Additionally to TSA, HDAC inhibitors Vorinostat, EX-527 and NAM were tested at different concentrations. Alternative HDAC inhibitors showed similar results with strong side

effects diminishing Foxp3 frequencies in concentrations that were high enough to increase total acetylation.

In summary, it has been shown that inhibition of HDACs in *in vitro* cell culture experiments did not increase the stability of Foxp3 positive Tregs by inhibition of HDAC9 and promotion of Foxp3 acetylation. On the contrary: while increasing total lysine acetylation effectively, Foxp3 frequencies and Foxp3 protein levels were reduced by the presence of TSA and other HDAC inhibitors. It is known that HDAC inhibitors can induce cell cycle arrest (Marks et al., 2001) and activate intrinsic apoptotic pathways (Xu et al., 2006), which is why they are used in Cancer therapies and studies (Dokmanovic et al., 2007). Studies examining cell viability IC_{50} of TSA and Vorinostat for SH-SY5Y cells showed an IC_{50} of 0.598 µM for TSA and 1.264 µM for Vorinostat (Lauffer et al., 2013).

TSA and Vorinostat are HDAC class I + II inhibitors that block the activity of HDACs (1-10). A study by Lauffer et al. determined the inhibition IC_{50} values of TSA and Vorinostat for individual HDACs (Lauffer et al., 2013). Their results show that HDAC9 (3.7 µM) and HDAC4 (2.4 µM) have the highest IC_{50} value for TSA, while HDAC1,2,3,5,6,7,8,10 are inhibited by much lower TSA concentrations IC_{50}: 0,000141-0,871 µM. Vorinostat was the least effective in inhibiting HDAC class IIa (HDAC4,5,7,9) with an IC_{50}>10 and more potent to inhibit HDAC1,2,3,6,8,10; IC_{50}: 0,00944-0,827 µM. This indicates that TSA and Vorinostat have the least effect on HDAC9 and the observed increase in total lysine acetylation is more likely caused by inhibition of other HDACs that are more sensitive to these inhibitors.

Selisistat and NAM are HDAC class III inhibitors that block the activity of Sirt1. Inhibition of Sirt1 was reported to have positive effects on Foxp3 expression (Beier et al., 2011). Overall high inhibitor concentrations that increased overall lysine acetylation effectively resulted in loss of Foxp3 expression and induction of apoptosis that was detected by Annexin V stainings. The required inhibitor concentration to effectively inhibit HDAC9 is in conflict with the cell viability IC_{50}. However, lower inhibitor concentrations that did not reduce Foxp3 frequencies by induction of apoptosis were still not effective to promote Foxp3 protein stability in these experiments.

Since HDAC class I + II inhibitors are not only specific for HDAC9, siRNA experiments were performed to reduce HDAC9 expression in Tregs and to stabilize Foxp3 by promoting Foxp3 acetylation. After transfection with HDAC9 specific siRNA $CD4^+$ T cells were cultured for three

days and Foxp3 frequencies were analysed by flow cytometry. Unfortunately, the stress of the transfection procedure had negative effects on Foxp3 frequencies in Tregs and Foxp3 could not be stabilized.

3.3 GARP controls autocrine TGFβ1 signalling in Tregs

Diminished TGFβ signalling in Garp-deficient Tregs appears to be the most immediate effect of low or missing GARP expression on Tregs. Our hypothesis is therefore that the decrease in Foxp3 acetylation that leads to a reduction of Foxp3 protein stability in Garp-deficient Tregs is a consequence of deregulated TGFβ1 signalling. To compensate for the diminished TGFβ signalling, control and Garp-deficient Tregs were treated with exogenous TGFβ1 and its effects were analysed.

In a first step the responsiveness of Tregs to exogenous TGFβ1 was assessed by flow cytometry (Figure 40). Cells were serum starved for 20 hours followed by 30 minutes of TGFβ1 stimulation. Upon TGFβ1 stimulation control and Garp-deficient Tregs showed no longer differences in SMAD2/3 phosphorylation. In contrast, freshly isolated and serum starved Garp-deficient Tregs without TGFβ1 stimulation displayed significantly diminished SMAD2/3 phosphorylation (Figure 40).

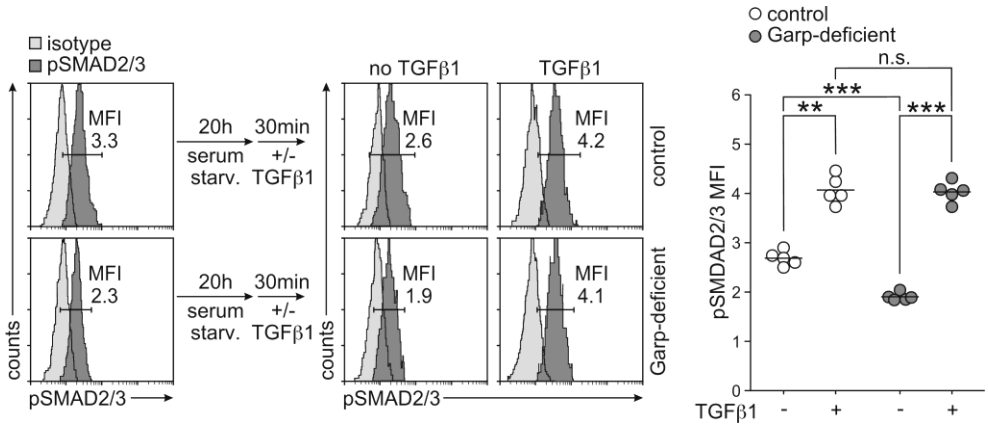

Figure 40 TGFβ signalling in response to exogenous TGFβ1
SMAD2/3 phosphorylation was analyzed by intracellular flow cytometry. Control and Garp-deficient $CD4^+$ T cells were starved in serum free RPMI 1640 for 20h followed by 30 minutes in the presence or absence of TGFβ1 while stimulated with anti-CD3 and anti-CD28. Results of one representative experiment with five mice per group out of two independent experiments with five mice per group are demonstrated. Mean values are indicated by horizontal lines. Serum starv.: serum starvation. Based on (Lehmkuhl et al., 2021).

As it was possible to modulate TGFβ signalling in control and Garp-deficient Tregs by exogenous TGFβ1 to reach similar levels, the effects of exogenous TGFβ1 and its potential to

resolve the deregulation of HDAC9 expression, Foxp3 acetylation and Foxp3 protein stability as seen in Garp-deficient Tregs was analysed.

Colleagues from our group stimulated control and Garp-deficient Tregs in presence and absence of TGFβ1 for 20 hours and analysed Hdac expression by real-time PCR (Figure 41A, B). In response to exogenous TGFβ1 the gene expression of Hdac9 was significantly reduced in control and Garp-deficient Tregs. This indicates that high Hdac9 expression in Garp-deficient Tregs is a consequence of a disruption in TGFβ1 signalling (Figure 41A). Interestingly, Hdac9 is the only deregulated Hdac in Garp-deficient Tregs and it is also the only Hdac that showed responsiveness to TGFβ1 with a reduction in relative gene expression up to 50% in control and Garp-deficient Tregs (Figure 41B). Hdac1-4 and Hdac6 displayed no significant alteration in their gene expression in response to TGFβ1 stimulation (Figure 41B).

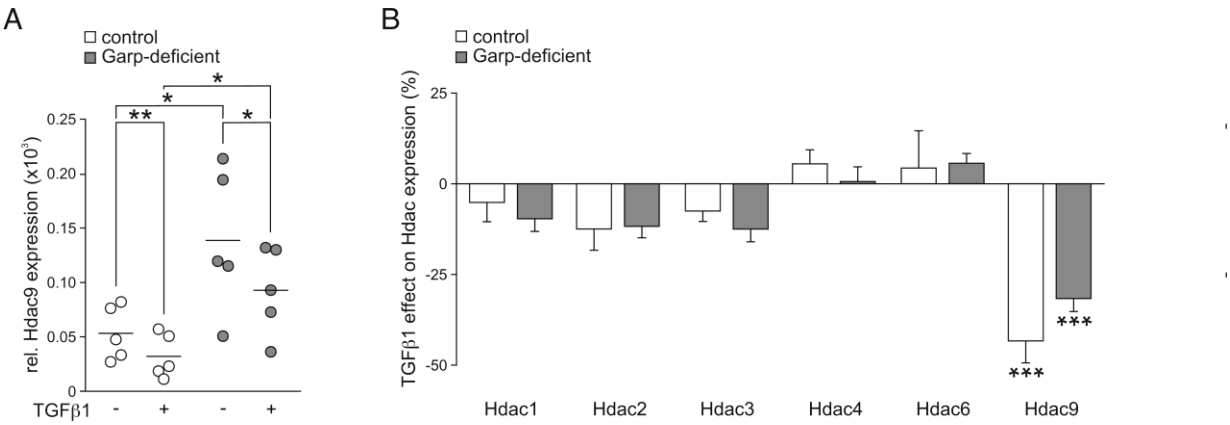

Figure 41 TGFβ1 effect on Hdac expression
(A, B) Real-time PCR analysis of different Hdacs in relation to Actb expression. mRNA was isolated from purified Tregs after 20 hours in the presence or absence of TGFβ1 with anti-CD3 and anti-CD28 stimulation. Results of five independent experiments are shown. (A) Mean values are indicated by horizontal lines. (B) Hdac1-4, Hdac6 and Hdac9 expression modulations upon TGFβ1 stimulation of five independent experiments were normalised and are demonstrated as mean ± SD. Based on (Lehmkuhl et al., 2021).

To further investigate the responsiveness of Hdac9 expression to TGFβ1 stimulation, *in silico* analysis of the Hdac9 promoter region was performed. Hdac9 promoter analysis confirmed the results by predicting a binding site for the TGFβ signalling mediators SMAD3 and SMAD4, supporting the finding that the expression of Hdac9 is regulated by TGFβ (Figure 42).

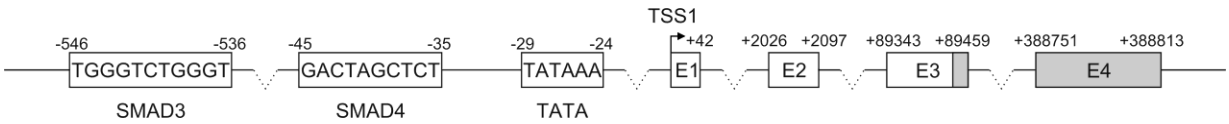

Figure 42 Hdac9 promoter region analysis
Schematic overview of SMAD3 and SMAD4 binding elements prior the Hdac9 transcription start site (TSS). Binding elements were identified by promoter analysis of murine Hdac9 using MatInspector by Genomatix.

As HDAC9 regulates Foxp3 acetylation, the reduction of HDAC9 expression in Tregs upon TGFβ1 stimulation was further investigated. $CD4^+$ T cells from Garp-deficient and control mice were cultured for 20 hours in the presence or absence of TGFβ1. The frequency of Tregs expressing acetylated Foxp3 was significantly increased by TGFβ1 in Garp-deficient and control Tregs (Figure 43). Moreover, the incubation with exogenous TGFβ1 increased the frequency of acetylated Foxp3 in Garp-deficient Tregs to the same frequency as observed in control Tregs (Figure 43). This strengthens the hypothesis that the reduced Foxp3 acetylation in Garp-deficient Tregs is a result of increased HDAC9 expression and that HDAC9 defines Foxp3 acetylation in Tregs. The data suggests that exogenous TGFβ1 is able to restore Foxp3 acetylation by reducing HDAC9 expression.

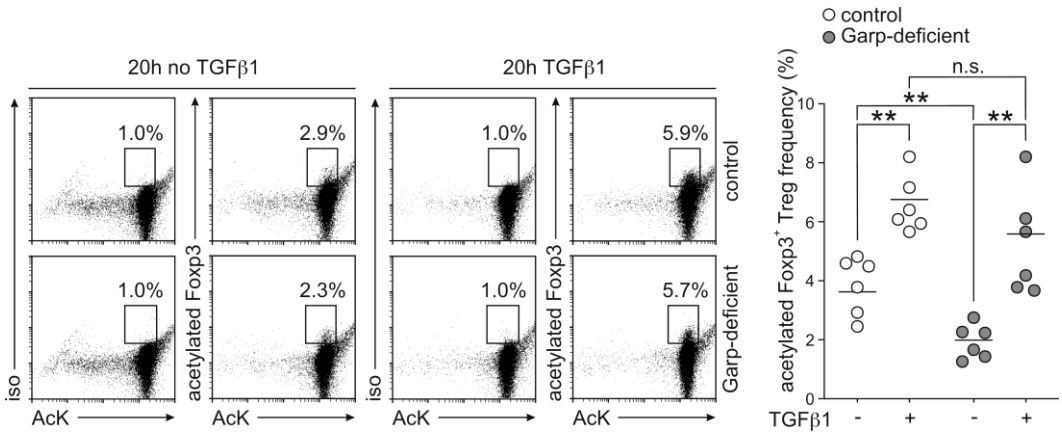

Figure 43 TGFβ1 effect on Foxp3 acetylation
Foxp3 acetylation was analysed in $CD4^+$ T cells after 20 hours of anti-CD3 and anti-CD28 stimulation in the presence or absence of TGFβ1 by intracellular flow cytometry using a FRET antibody pair for Foxp3 and AcK. Representative stainings and a summary of six independent FRET assay experiments with pooled $CD4^+$ T cells from two mice per group are demonstrated. Mean values are indicated by horizontal lines. AcK: acetylated lysine. Based on (Lehmkuhl et al., 2021).

In addition, total lysine acetylation was assessed in Foxp3 positive Tregs in response to exogenous TGFβ1. $CD4^+$ T cells were cultured for 20 hours with anti-CD3 and anti-CD28 stimulation in the presence or absence of TGFβ1 and analysed by intracellular flow cytometry using directly labelled antibodies for AcK and Foxp3. Interestingly, exogenous TGFβ1 also resulted in a significant increase in total lysine acetylation in control and Garp-deficient Tregs (Figure 44).

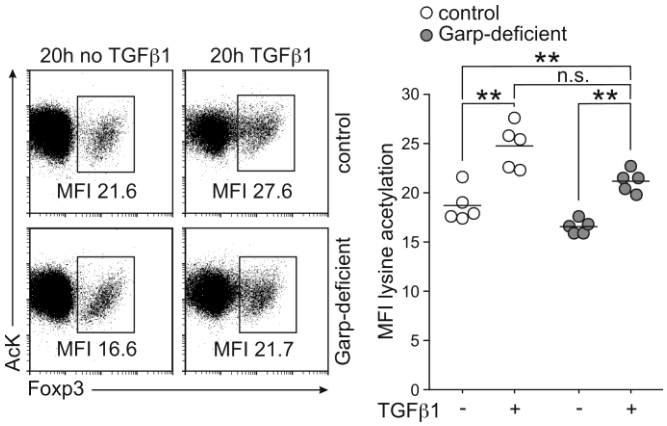

Figure 44 TGFβ1 effect on total acetylation
Total lysine acetylation of Tregs was assessed by intracellular flow cytometry. $CD4^+$ T cell populations gated for Foxp3 were analysed after 20 hours of anti-CD3 and anti-CD28 stimulation in the presence or absence of TGFβ1. Left panel demonstrates representative stainings of control and GARP-deficient $CD4^+$ T cells. Right panel shows summarized staining results from one representative experiment with five mice per group out of three independent experiments with five mice per group. Mean values are indicated by horizontal lines.

With regard to the elevated Foxp3 acetylation after TGFβ1 stimulation, Foxp3 protein stability was analysed using CHX following an incubation period in presence or absence of TGFβ1. The half-life of Foxp3 was indeed normalised in Garp-deficient Tregs (23.83±2.26 hours) compared to control Tregs (23.59±2.31 hours) (Figure 45, right panel), when they were cultured with TGFβ1 before the CHX incubation. When cells were preincubated without TGFβ1 prior to CHX incubation, Foxp3 half-life was still significantly shorter in Garp-deficient Tregs (17.95±1.28 hours) than in control Tregs (14.33±1.36 hours) (Figure 45, left panel), as previously demonstrated in experiments with no preincubation period (Figure 36). The restoration of acetylation-mediated Foxp3 protein stability in Garp-deficient Tregs by exogenous TGFβ1 indicates that the decreased Foxp3 stability observed in these Tregs in comparison to control Tregs was a result of deregulated TGFβ signalling.

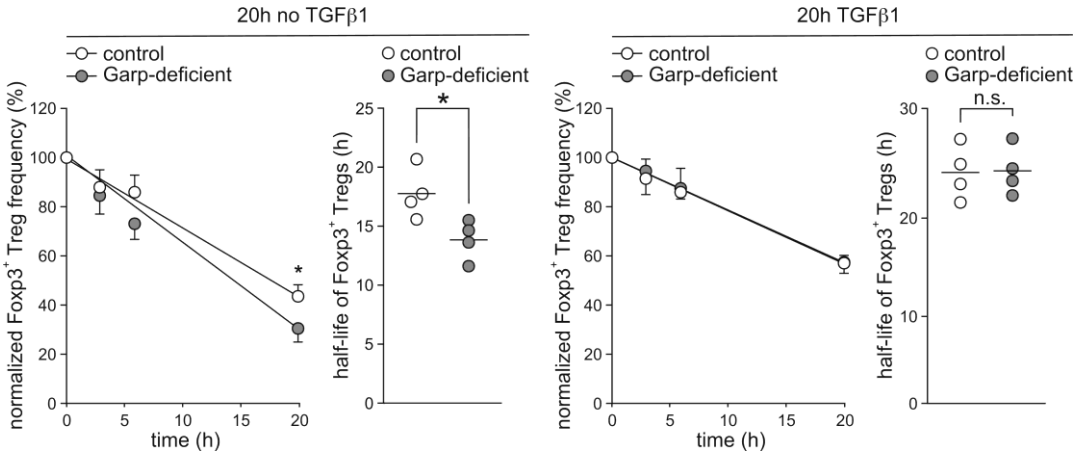

Figure 45 TGFβ1 restores Foxp3 stability defect in GARP-deficient Tregs
$CD4^+$ T cell were cultured for 20 hours with anti-CD3 and anti-CD28 in presence or absence of TGFβ1 before CHX was added. Cells were incubated for another 20 hours and frequency of Foxp3 positive T cells was assessed by intracellular flow cytometry. Linear regression and Foxp3 half-life were calculated based on normalised frequencies of Foxp3. Left panel demonstrates data acquired after preincubation in the presence of TGFβ1; right panel - in the absence of TGFβ1. Results from four independent experiments are demonstrated as mean ± SD. Mean values are indicated by horizontal lines. Based on (Lehmkuhl et al., 2021).

The positive effect of exogenous TGFβ1 on acetylation-mediated Foxp3 stability was not apparent when T cells were incubated with TGFβ1 and CHX simultaneously, without a pre-incubation period with TGFβ1 alone (Figure 45). CHX inhibits protein translation, preventing any alterations in protein levels introduced by TGFβ1 including HDAC9. Foxp3 half-life in control Tregs (without TGFβ1 15.97±0.38 hours *vs.* 15.89±0.82 hours with TGFβ1) and in Garp-deficient Tregs (without TGFβ1 13.22±0.15 hours *vs.* 13.17±0.31 hours with TGFβ1) (Figure 46) was not increased and restored by TGFβ1 in this experimental setup. This result demonstrates that TGFβ1 cannot directly influence the stability of Foxp3 when protein translation is inhibited.

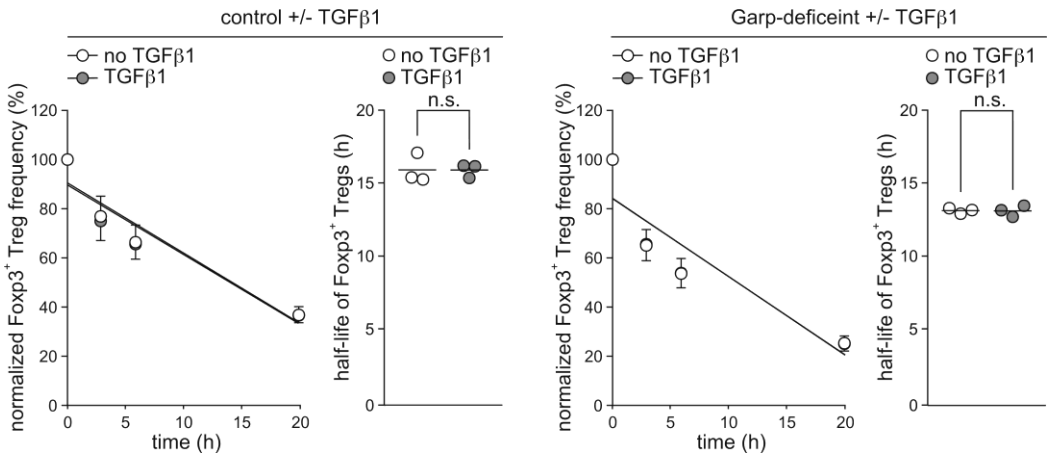

Figure 46 TGFβ1 has no effect in presence of translation inhibitor CHX
$CD4^+$ T cells were cultured for 20 hours with anti-CD3, anti-CD28 and CHX in the presence or absence of TGFβ1. Frequency of Foxp3 in $CD4^+$ T cells was analysed by intracellular flow cytometry. Linear regression and half-life of Foxp3 were calculated based on normalised Foxp3 frequencies. Left panel shows data of control T cells, right panel data of Garp-deficient T cells. Results from three independent experiments are demonstrated as mean ± SD. Mean values are indicated by horizontal lines.

Further experiments studied the effect of exogenous TGFβ1 on the stability of Foxp3 in absence of CHX. Colleagues from our group purified Tregs and examined Foxp3 frequencies for three days in presence and absence of TGFβ1 in control and Garp-deficient Tregs by intracellular flow cytometry. Only the analysis of this experiment was performed by me. Both Garp-deficient and control Tregs showed significantly higher Foxp3 frequencies in presence of TGFβ1 (Figure 47). In absence of TGFβ1 Foxp3 expression was lost faster in Garp-deficient Tregs than in control Tregs, as shown in Figure 35. Interestingly, Garp-deficient Tregs had similar frequencies of Foxp3 in the presence of TGFβ1 as control Tregs without exogenous TGFβ1 (Figure 47). Hence, it was concluded that the lack of GARP expression limits TGFβ signalling in Garp-deficient Tregs which is needed for maintaining a stable Treg phenotype.

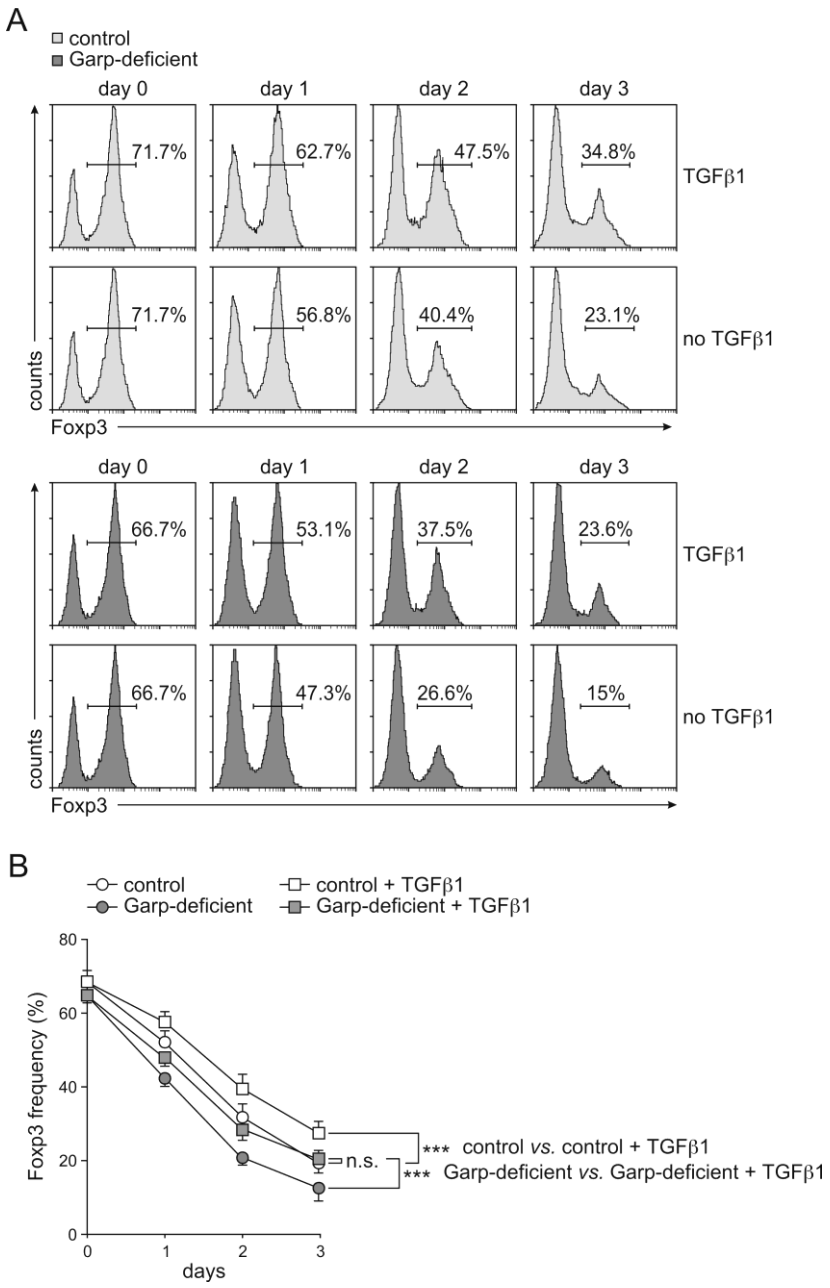

Figure 47 TGFβ1 effect on Foxp3 stability in Treg
(A) Purified Tregs from Garp-deficient and control mice were stimulated with anti-CD3 and anti-CD28 for one to three days in the presence or absence of TGFβ1. Foxp3 expression was analysed by intracellular flow cytometry. Representative staining histograms of one out of five independent experiments are shown. (B) Results of five independent experiments are demonstrated as mean ± SD. Statistical analysis was performed using two-way analysis of variance (ANOVA). ***$p < 0.001$, n.s. not significant.

4 Discussion

Regulatory T cells are essential to control immune responses to pathogens and to sustain homeostasis and immunological self-tolerance (Ohkura et al., 2013). Lack of stability or function of Tregs can result in unchecked effector T cell expansion and production of pro-inflammatory cytokines, leading to autoimmune diseases (Pesce et al., 2013). GARP binds and presents latent TGFβ1 on the cell surface of Tregs and is a critical factor for the activation of TGFβ1 (Stockis et al., 2017; Wang et al., 2012). This study shows in PID patients with mutated *LRRC32* and Lrrc32 knockout mice that diminished or absent GARP expression is a factor that contributes to immune dysregulation by diminished TGFβ availability, Foxp3 protein stability and suppressor function in Tregs.

4.1 PID patients with *LRRC32* mutations

It was evident that the immune systems of both PID patients with LRRC32 mutations are unable to properly resolve an immune response. This resulted in chronically perpetuating inflammation, a breakthrough of peripheral tolerance and in disease manifestation. In patient 1 persisting inflammation of gut mucosa was observed over the course of decades. In patient 2 development of auto-neutrophilic antibodies were apparent that resulted in a complete elimination of neutrophils.

Within a cohort of PID patients, we identified two patients with mutations in *LRRC32.* Whereas variants c.934C>T and c.1262G>A were already observed in the general population, variant c.741G>A was characterized as a novel mutation. The data suggests that the mutations contribute to a decrease of GARP expression on the Treg surface in both patients. The reduction of GARP expression was also apparent in diminished TGFβ availability. Accordingly, it is assumed that Treg require a certain amount of GARP on their surface to function properly. This concept is supported by previous findings of our group that showed diminished GARP expression on Tregs from patients suffering from rheumatoid arthritis (Haupt et al., 2016). Moreover, Manz et al. reported in 2016 that *LRRC32* missense mutations lead to reduced GARP expression in patients with atopic dermatitis (Manz et al., 2016). Tregs from PID patients in our study showed signs of reduced suppressor function and Foxp3 protein stability that could explain the observed immune dysregulation. The suppressor function was evaluated by proliferation experiments. Although the patients displayed increased proliferation in the presence of Tregs compared to healthy controls, the method could be criticised for its overall rather low proliferation rate of effector

T cells in absence of Tregs. Furthermore, patient 2 displayed only minor differences in effector T cell proliferation in the Teff to Treg ratios 4:1, 2:1 and 1:1 (Figure 13) which is unusual even for Tregs with decreased inhibitory capacity.

In mice it has been demonstrated that GARP lacking Tregs can still facilitate anti-tumor immunity but cannot suppress pathogenic T cell responses in an experimental colitis model with T cell transfer, indicating that Tregs without GARP have impaired suppressive capabilities (Salem et al., 2019). Finally, it was demonstrated that overexpression of GARP increased inhibitory Treg function (Wang et al., 2008) and that downregulation of GARP impairs suppressor function associated with a downregulation of Foxp3 (Probst-Kepper et al., 2009; Probst-Kepper et al., 2009).

Several reasons for the diminished GARP protein expression resulting from *LRRC32* mutations can be discussed. Patient 1 expresses a wild-type GARP variant on one allele and a p.Trp247Ter variant on the other allele. The introduction of a stop codon by this mutation lead to the expression of a truncated protein missing the trans-membrane region that could not be detected when expressed in HEK293 cells. This short variant is expected to be non functional and unable to bind to the cell surface. Since both alleles are expressed, as shown in the allelic expression analysis, the mutation results in a reduction in total GARP levels on the cell surface of activated Tregs in patient 1.

Patient 2 has *LRRC32* mutations in both alleles, expressing GARP variants p.Arg312Cys and p.Arg421Gln. GARP variant protein stability predictions calculated a negative free energy change ($\Delta\Delta G$) of -2.93 Kcal/mol for p.Arg312Cys and -2.79 Kcal/mol for p.Arg421Gln (Quan et al., 2016). The values indicate a strong reduction of protein stability for both GARP mutation variants.

Position 312 is a solvent exposed residue, the mutation p.Arg312Cys introduces a cysteine instead of a strongly hydrophilic arginine. Although the sulfhydryl group of free cysteine is polar, cysteine behaves like a strongly hydrophobic residue in proteins and is typically located in hydrophobic clusters like methionine, tryptophan and tyrosine (Nagano et al., 1999). An amino acid exchange to a residue with hydrophobic properties at a solvent exposed location introduces protein destabilization. Further analysis showed that the affected residues displayed the highest average $\Delta\Delta G$ of potential amino acid exchanges compared to the neighbouring regions. Thereby the STRUM protein stability predictions indicated a special relevance of the affected residues

for GARP stability that could explain the reduced GARP levels on Treg surface of patient 2 and the reduced GARP levels seen in HEK293 cells transfected with the GARP mutation variants compared to GARP wild-type transfection. The HEK293 transfection experiments were analysed assuming equal transfection efficiency for each construct. To take potential differences in transfection efficiency into account the co-expression of a reporter gene would have been a more sophisticated approach.

Both patients developed their autoimmune disorders with age indicating that similar to classic autoimmune diseases environmental factors were involved as triggers in the disease manifestations. This conclusion was strongly supported by the observation that Garp-deficient mice do not display a spontaneous phenotype but rather develop severe autoimmune disorders in response to triggers. This indicates that *LRRC32* might be a genetic factor that determines the susceptibility to inflammatory disorders and is important to maintain the integrity of the immune system.

4.2 TGFβ signalling in Garp-deficient Tregs and Tregs from PID patients

The data suggests that the reduced availability of active TGFβ in Tregs with diminished or lacking GARP expression was responsible for the observed immunological phenotype. The function of GARP as a Treg specific latent TGFβ-binding protein (LTBP) and its importance for TGFβ maturation was confirmed by the diminished basal TGFβ signalling that was observed in Tregs of patients with mutated *LRRC32* and in Tregs of Garp-deficient mice. Diminished TGFβ signalling was apparent in reduced SMAD2/3 phosphorylation. Tregs from Garp-deficient mice that completely lack GARP also lacked LAP on their cell surface. Patients with GARP mutations and reduced GARP expression on the surface of activated Tregs displayed reduced levels LAP consistent with significantly diminished basal SMAD2/3 phosphorylation compared to healthy controls. LAP detection is indicative for the presence of latent TGFβ on the cell surface of human and murine Tregs. These results suggest that no alternative pathways are able to compensate for the absence or reduction of GARP to facilitate surface localization of latent TGFβ in Tregs which is critical for the maturation of TGFβ (Stockis et al., 2017). The reduced levels of GARP/latent-TGFβ complexes on activated Tregs in patients are in contrast to increased basal *LRRC32* mRNA levels. The increased *LRRC32* expression in patients could be attributed to a compensational effect for the lack of functional GARP in Tregs.

Cuende et al. also highlighted the importance of functional GARP for TGFβ maturation by utilising an inhibitory anti-hGARP antibody in human Tregs. The antibody was able to disrupt GARP dependent TGFβ maturation as shown by western blots analysis for pSMAD2 (Cuende et al., 2015). Disruptions in the maturation process of TGFβ have a similar effect as a complete lack of TGFβ. Edwards et al. demonstrated in TGFβ1 dependent Treg-mediated Th17 differentiation experiments that Tgfβ1- and Furin-deficient Tregs were completely unable to provide active TGFβ1 and to drive Th17 differentiation of co-cultured naïve $CD4^+$ T lymphocytes. Further they showed that the induction of Th17 differentiation in the presence of Garp-deficient mice was reduced by ~75% compared to control Tregs (Edwards et al., 2014).

Furin is not sufficient for the activation of TGFβ, but it is necessary for the first instance of TGFβ maturation by the cleavage of precursor pro-TGFβ. After the cleavage LAP remains non-covalently bound to TGFβ and requires GARP for further processing of this complex to release mature TGFβ. Although Garp-deficiency did not show the same effect as Tgfβ1- or Furin-deficiency, however, it demonstrated, that cell surface-bound GARP/latent-TGFβ complexes provide a significant portion of activated TGFβ1 that mediates Th17 induction. Similar to Th17 induction, the induction of Foxp3 expression of naïve T cells in co-culture experiments with activated Tregs was very ineffective when Garp-deficient Tregs were used (Edwards et al., 2013). While GARP alone is not sufficient to activate TGFβ1, it is required for the production of active TGFβ1 in murine and human Tregs. Integrin $\alpha_v\beta_8$ has been reported to associate with the GARP/latent-TGFβ complex and to be essential for the release of active TGFβ (Edwards et al., 2014; Stockis et al., 2017; Wang et al., 2012). Similar to anti-hGARP antibody inhibition, antibodies against β_8 block TGFβ1 activation in human Tregs (Cuende et al., 2015; Stockis et al., 2017). Antibody-mediated inhibition of GARP and Integrin $\alpha_v\beta_8$ showed additionally to reduced TGFβ1 signalling an impairment of Treg suppressor function in *in vivo* graft versus host disease (GVHD) experiments (Cuende et al., 2015; Stockis et al., 2017). Anti-hGARP antibody inhibition also led to diminished suppression in *in vitro* experiments (Cuende et al., 2015). This highlights the importance of GARP and TGFβ1 maturation for the suppressor function of Tregs and confirms the results we observed in Tregs from PID patients with mutations in *LRRC32* and in Garp-deficient Tregs.

This thesis provides indications that GARP-bound TGFβ1 functions as a TGFβ1 source for autocrine signalling in Tregs. Based on previous studies, it has been concluded that GARP-associated TGFβ1 acts in a paracrine manner mediating Th17 and iTreg generation rather than being utilised by Tregs themselves (Cuende et al., 2015; Stockis et al., 2009). This conclusion

was supported by the observation that Garp-deficient mice have normal Treg frequencies and demonstrate normal Treg-mediated T cell suppression *in vitro* (Edwards et al., 2013).

However, the data showed a reduced Foxp3 expression stability of Garp-deficient Tregs in cell culture and diminished Foxp3 protein half-life in Garp-deficient Tregs and Tregs from PID patients with mutations in *LRRC32* compared to control Tregs. Furthermore, patients had reduced frequency of Tregs in CD4 T cell populations. In contrast, human Treg in GVHD experiments were not depleted in the presence of anti-hGARP antibody (Cuende et al., 2015). But *in vivo* experiments in mice demonstrated decreased Treg frequencies when anti-GARP antibodies were used (Metelli et al., 2016).

Furthermore, Tgfβ1-deficient Tregs displayed a regular suppressive capacity in *in vitro* experiments (Edwards et al., 2013; Piccirillo et al., 2002). In contrast, however, assessing the suppressive capacity of Tgfb1- and of Garp-deficient Tregs *in vivo* demonstrated their incapability to inhibit the development of colitis in a transfer model of inflammatory bowel disease (Li et al., 2007; Salem et al., 2019). This result is consistent with our observation that Garp-deficient Tregs show an apparently normal suppressive capacity *in vitro* but are unable to control the expansion of effector T cell after adaptive transfer *in vivo*. Further, we demonstrated that Garp-deficient Tregs were also unable to inhibit induced disease development in murine autoimmune models. This indicates that *in vitro* analysis of Treg suppressive capacity can have its limitations.

4.3 Altered gene transcription in GARP-deficient Tregs

The observed alterations in the gene expression of GARP-deficient Tregs can be an indicator for the importance of GARP for Tregs. Among the identified genes with altered expression levels, Hdac9 was particularly notable. Hdac9 is specifically expressed in Tregs and described as a negative Foxp3 regulator by promoting its deacetylation resulting in unstable Foxp3 protein (Li et al., 2015; Tao et al., 2007). Microarray analysis showed an increase in Hdac9 expression in Garp-deficient Tregs. This was confirmed by real-time PCR experiments. Patients with GARP mutations also displayed elevated mRNA levels of *HDAC9* compared to healthy controls.

Acetylation of Foxp3 is defined by the activity of histone deacetylases and histone acetyltransferases. When Foxp3 is acetylated it prevents its polyubiquitination and protects it from proteasomal degradation and promotes thereby Foxp3 protein stability (van Loosdregt et

al., 2010). In addition, acetylation is also necessary for exerting Foxp3-mediated transcriptional repression and has been shown to correlate with increased chromatin binding (Li et al., 2007; Samanta et al., 2008). Sirt1, HDAC7 and HDAC6 have also been reported to be involved in Foxp3 deacetylation (Beier et al., 2011; de Zoeten et al., 2011; Li et al., 2007; van Loosdregt et al., 2011). However, Hdac9 was the only differently expressed histone deacetylase in Garp-deficient Tregs with a two-fold higher expression than control Tregs. HDAC9 is also the only Treg specific HDAC with considerably higher expression in Tregs than non-regulatory $CD4^+$ T cells (Tao 2007). Histone acetyltransferases p300 and TIP60 have been shown to interact with Foxp3 promoting its acetylation and stability (Li et al., 2007). The mRNA levels of p300 and Tip60 displayed no significant differences in our studies in control and Garp-deficient Tregs. The deregulation of HDAC9 results in an imbalance in the equilibrium of HATs and HDACs promoting Foxp3 deacetylation. The hypothesis is thus that Foxp3 is less acetylated and thereby more unstable in Garp-deficient Tregs as a result of the abundance of HDAC9.

This expectation was confirmed by Foxp3 acetylation analysis with flow cytometry experiments that utilize a FRET antibody pair for Foxp3 and acetylated lysine (AcK). The detection of the FRET signal required that an anti-Foxp3 antibody and an anti-AcK antibody bind to their targets in close proximity. The FRET analysis demonstrated significantly reduced Foxp3 acetylation levels in Garp-deficient Tregs compared to control Tregs.

4.4 Acetylation-mediated Foxp3 protein stability

The lysine acetylation of Foxp3 is a reversible post-translational modification which defines Foxp3 protein stability by preventing polyubiquitination and thereby proteasome-mediated Foxp3 degradation (van Loosdregt et al., 2010). Protein acetylation is the attachment of an acetyl group to the ε-amino group of lysine residues or to the N-terminus of proteins. Poly-ubiquitination initiates also at lysine residues. When these are obstructed by an acetyl group, ubiquitination processes are unable to initiate and proteasomal degradation is prohibited (Drazic et al., 2016). Deacetylation of lysine residues result in an increased susceptibility to poly-ubiquitination and protein degradation by the proteasome.

Loosdregt et al. confirmed this concept with Foxp3 transfected HEK293 cells. Foxp3 acetylation was increased when cells were co-transfected with p300 and in the presence of HDAC inhibitors TSA and NAM. It was shown that the acetylation state of Foxp3 is able to modulate Foxp3 protein levels. Further the use of proteasome inhibitor MG132 as well as the mutation of all

lysine residues to arginine in Foxp3 demonstrated similar stabilization of Foxp3 in HEK293 cells as the promotion of acetylation (van Loosdregt et al., 2010).

Our data showed that the reduced Foxp3 acetylation in Garp-deficient Tregs correlates with reduced Foxp3 protein stability as it was hypothesised. Basal Foxp3 protein levels and expression stability of Foxp3 were significantly diminished in Garp-deficient Tregs compared to control Tregs. Most importantly, protein stability experiments with CHX, which abolishes all protein biosynthesis and excludes the influence of potential differences in gene transcription during the incubation, demonstrated a diminished half-life of Foxp3 protein in Garp-deficient Tregs. Corresponding to results in mice, the half-life of human Foxp3 protein was also impaired in PID patients compared to healthy controls. Although the basal protein levels of Foxp3 were reduced, frequency of Foxp3 positive Tregs was not affected by the lack of acetylation-mediated protein stability in mice. In PID patients with GARP mutations, however, the frequency of Foxp3 positive Tregs was significantly diminished.

Despite the fact that HDAC inhibition can induce lymphocyte cell-cyle arrest and apoptosis (Choi et al., 2005; Moreira et al., 2003) Tao et al. demonstrated in *in vivo* experiments that Tregs from mice treated with TSA had increased Foxp3 acetylation and protein levels (Tao et al., 2007). For this study different HDAC inhibitors were tested *in vitro* with murine $CD4^+$ T cells to increase Foxp3 acetylation and to improve Foxp3 protein stability. However, beneficial effects on Foxp3 stability could not be observed in cell culture experiments. HDAC inhibition increased overall lysine acetylation effectively in higher doses, but Foxp3 expression was diminished. The loss of Foxp3 expression was most likely caused by induction of apoptosis. Positive effects on Foxp3 stability were also not observed when HDAC inhibitors were used in lower doses or short term.

4.5 Analysis of TGFβ1 effect on Garp-deficient Tregs

This study showed that defects and deregulations identified in Garp-deficient Tregs are directly connected to TGFβ1 deprivation. In the absence of GARP, TGFβ1 maturation is limited and pSMAD2/3 signalling reduced. When Garp-deficient and control Tregs were treated with exogenous TGFβ1, we observed a restored Treg phenotype in the form of direct and indirect molecular effects of TGFβ1 signalling. HDAC9 expression in Tregs was reduced up to 50% in the presence of TGFβ1. Garp-deficient Tregs treated with TGFβ1 reached Hdac9 mRNA levels similar to control Tregs without TGFβ1 stimulation. Real-time PCR experiments revealed that

TGFβ1 has a specific inhibitory effect on HDAC9 expression while the expression of other HDACs was unaltered in presence of TGFβ1 in control and Garp-deficient Tregs. In consequence to reduced Hdac9 mRNA levels Tregs displayed a significantly higher degree of Foxp3 acetylation upon TGFβ1 stimulation. This effect was seen in control and Garp-deficient Tregs. In both cases similar Foxp3 acetylation was observed in response to TGFβ1 stimulation.

The responsiveness of Hdac9 mRNA levels to TGFβ1 signalling can be explained by TGFβ-mediated transcriptional repression. SMAD binding elements (SBE) were identified within the promoter region of HDAC9 with a predicted binding site for SMAD3 and SMAD4 respectively. The N-terminal Mad homology domain 1 (MH1) of SMAD3 can bind to distinct promoters that harbour the SBEs sequence GTCT or its palindrome AGAC (Shi et al., 1998). SMAD2 and SMAD3 are direct mediators of TGFβ1 signalling. Upon TGFβ receptor activation SMAD2/3 are phosphorylated and translocated to the nucleus by SMAD4 (Horbelt et al., 2012). In a similar manner Frederick et al. showed that TGFβ-mediated repression of c-myc requires direct binding of Smad3 to a repressive Smad binding element (RSBE) which Smad4 can also bind to (Frederick et al., 2004).

By reducing HDAC9 levels in Tregs that enable increased Foxp3 acetylation, exogenous TGFβ1 managed to restore the diminished Foxp3 acetylation and the reduced protein half-life of Foxp3 in Garp-deficient Tregs. Half-life of Foxp3 was equal in control and Garp-deficient Tregs after they were incubated with TGFβ1 before adding CHX to the cell culture. Significant differences in Foxp3 half-life were, however, still observed when Tregs were pre-incubated without TGFβ1. Without pre-incubation, the presence of TGFβ1 showed no effect on the stabilization of Foxp3 neither for control or Garp-deficient Tregs. When protein biosynthesis and thereby protein turnover is inhibited, TGFβ1 does not alter the HDAC9 to HAT equilibrium by effecting mRNA levels of Hdac9. It is therefore expected that TGFβ1 is not modulating translation independent pathways to benefit Foxp3 stability but rather takes indirect influence on Foxp3 acetylation by reducing HDAC9 expression. TGFβ1 also showed a stabilizing effect on Foxp3 frequency in cell culture experiments without CHX.

To summarise, exogenous TGFβ1 resulted in a considerable reduction of Hdac9 mRNA expression in both Garp-deficient and control Tregs. Thereby, exogenous TGFβ1 was able to restore the decreased Foxp3 acetylation level as well as the diminished half-life of Foxp3 that was observed in Garp-deficient Tregs.

4.6 Phenotype of TGFβ1 deprivation

The destabilization of Garp-deficient Tregs resulting from increased Foxp3 deacetylation was likely the central mechanism defining the unstable phenotype of Garp-deficient Tregs. Stable Foxp3 is essential for Tregs as it is the key regulator of Treg function and development (Fontenot et al., 2003). Multiple studies have shown that Tregs lose their regulatory phenotype and acquire the phenotype of an effector T cell when Foxp3 expression is downregulated or lost (Komatsu et al., 2009; Miyara et al., 2009; Tsuji et al., 2009). In this study Garp-deficient Tregs displayed an increased expression of several cytokines regardless of the types (Th1, Th2 or Th17). This might be associated with a reduced Foxp3-dependent transcriptional repression that results in an overall deregulated expression of cytokines in Tregs. It is further compelling that Garp-deficient Tregs demonstrate a phenotype that is similar to that of Tregs from mice were Foxp3 expression was attenuated by genetical engineering (Wan and Flavell, 2007). In consequence of the reduced Foxp3 expression, Tregs from those animals displayed a decreased regulatory capacity and expressed effector cytokines. The results of our study are therefore consistent with the hypothesis that a certain level of Foxp3 is essential to promote Treg maturation and the formation of a stable phenotype. Depis et al. showed that mice prone to develop lupus nephritis were associated with unstable Tregs due to a reduced expression of Foxp3 (Depis et al., 2016). Moreover, it was reported that reduced Foxp3 expression associates with the occurrence of immune disorders in humans (Balandina et al., 2005; Huan et al., 2005). Thus, taken together, this study demonstrates that Tregs display signs of TGFβ1 deprivation when GARP is absent or diminished on their surface. The reduced TGFβ signalling results in increased Hdac9 expression and subsequently in Foxp3 protein destabilization, as a consequence of reduced acetylation. Therefore, GARP plays an important role in stabilizing the immune system.

Bibliography

Acosta-Rodriguez, E.V., Napolitani, G., Lanzavecchia, A. & Sallusto, F. Interleukins 1beta and 6 but not transforming growth factor-beta are essential for the differentiation of interleukin 17-producing human T helper cells. *Nature immunology* **8**, 942-949 (2007).

Alberts, B., Johnson, A., Lewis, J., Raff, M., Roberts, K. & Walter, P. Molecular Biology of the Cell. Lymphocytes and the Cellular Basis of Adaptive Immunity. Vol. 4 (Garland Science, New York, 2002).

Allfrey, V.G., Faulkner, R. & Mirsky, A.E. Acetylation and Methylation of Histones and Their Possible Role in the Regulation of Rna Synthesis. *Proc Natl Acad Sci U S A* **51**, 786-794 (1964).

Amaya-Uribe, L., Rojas, M., Azizi, G., Anaya, J.M. & Gershwin, M.E. Primary immunodeficiency and autoimmunity: A comprehensive review. *J Autoimmun* **99**, 52-72 (2019).

Annunziato, F. & Romagnani, S. Heterogeneity of human effector CD4+ T cells. *Arthritis research & therapy* **11**, 257 (2009).

Arpaia, N., Campbell, C., Fan, X., Dikiy, S., van der Veeken, J., deRoos, P., Liu, H., Cross, J.R., Pfeffer, K., Coffer, P.J. & Rudensky, A.Y. Metabolites produced by commensal bacteria promote peripheral regulatory T-cell generation. *Nature* **504**, 451-455 (2013).

Asseman, C., Mauze, S., Leach, M.W., Coffman, R.L. & Powrie, F. An essential role for interleukin 10 in the function of regulatory T cells that inhibit intestinal inflammation. *The Journal of experimental medicine* **190**, 995-1004 (1999).

Avrameas, S. Natural autoantibodies: from 'horror autotoxicus' to 'gnothi seauton'. *Immunol Today* **12**, 154-159 (1991).

Balandina, A., Lecart, S., Dartevelle, P., Saoudi, A. & Berrih-Aknin, S. Functional defect of regulatory CD4(+)CD25+ T cells in the thymus of patients with autoimmune myasthenia gravis. *Blood* **105**, 735-741 (2005).

Bansal, K., Yoshida, H., Benoist, C. & Mathis, D. The transcriptional regulator Aire binds to and activates super-enhancers. *Nat Immunol* **18**, 263-273 (2017).

Barber, G.N. STING-dependent cytosolic DNA sensing pathways. *Trends Immunol* **35**, 88-93 (2014).

Baron, U., Floess, S., Wieczorek, G., Baumann, K., Grutzkau, A., Dong, J., Thiel, A., Boeld, T.J., Hoffmann, P., Edinger, M.*, et al.* DNA demethylation in the human FOXP3 locus discriminates regulatory T cells from activated FOXP3(+) conventional T cells. *Eur J Immunol* **37**, 2378-2389 (2007).

Battke, F., Symons, S. & Nieselt, K. Mayday--integrative analytics for expression data. *BMC bioinformatics* **11**, 121 (2010).

Beier, U.H., Wang, L., Bhatti, T.R., Liu, Y., Han, R., Ge, G. & Hancock, W.W. Sirtuin-1 targeting promotes Foxp3+ T-regulatory cell function and prolongs allograft survival. *Mol Cell Biol* **31**, 1022-1029 (2011).

Beier, U.H., Wang, L., Han, R., Akimova, T., Liu, Y. & Hancock, W.W. Histone deacetylases 6 and 9 and sirtuin-1 control Foxp3+ regulatory T cell function through shared and isoform-specific mechanisms. *Sci Signal* **5**, ra45 (2012).

Belkaid, Y. Role of Foxp3-positive regulatory T cells during infection. *European journal of immunology* **38**, 918-921 (2008).

Belkaid, Y. & Hand, T.W. Role of the microbiota in immunity and inflammation. *Cell* **157**, 121-141 (2014).

Bennett, C.L., Christie, J., Ramsdell, F., Brunkow, M.E., Ferguson, P.J., Whitesell, L., Kelly, T.E., Saulsbury, F.T., Chance, P.F. & Ochs, H.D. The immune dysregulation, polyendocrinopathy, enteropathy, X-linked syndrome (IPEX) is caused by mutations of FOXP3. *Nature genetics* **27**, 20-21 (2001).

Bettelli, E., Dastrange, M. & Oukka, M. Foxp3 interacts with nuclear factor of activated T cells and NF-kappa B to repress cytokine gene expression and effector functions of T helper cells. *Proceedings of the National Academy of Sciences of the United States of America* **102**, 5138-5143 (2005).

Bettelli, E., Carrier, Y., Gao, W., Korn, T., Strom, T.B., Oukka, M., Weiner, H.L. & Kuchroo, V.K. Reciprocal developmental pathways for the generation of pathogenic effector TH17 and regulatory T cells. *Nature* **441**, 235-238 (2006).

Blasius, A.L. & Beutler, B. Intracellular toll-like receptors. *Immunity* **32**, 305-315 (2010).

Bleich, A., Mahler, M., Most, C., Leiter, E.H., Liebler-Tenorio, E., Elson, C.O., Hedrich, H.J., Schlegelberger, B. & Sundberg, J.P. Refined histopathologic scoring system improves power to detect colitis QTL in mice. *Mamm Genome* **15**, 865-871 (2004).

Bonilla, F.A., Bernstein, I.L., Khan, D.A., Ballas, Z.K., Chinen, J., Frank, M.M., Kobrynski, L.J., Levinson, A.I., Mazer, B., Nelson, R.P., Jr*., et al.* Practice parameter for the diagnosis and management of primary immunodeficiency. *Ann Allergy Asthma Immunol* **94**, S1-63 (2005).

Bonilla, F.A., Khan, D.A., Ballas, Z.K., Chinen, J., Frank, M.M., Hsu, J.T., Keller, M., Kobrynski, L.J., Komarow, H.D., Mazer, B*., et al.* Practice parameter for the diagnosis and management of primary immunodeficiency. *J Allergy Clin Immunol* **136**, 1186-1205 e1181-1178 (2015).

Bonilla, F.A., Barlan, I., Chapel, H., Costa-Carvalho, B.T., Cunningham-Rundles, C., de la Morena, M.T., Espinosa-Rosales, F.J., Hammarstrom, L., Nonoyama, S., Quinti, I*., et al.* International Consensus Document (ICON): Common Variable Immunodeficiency Disorders. *J Allergy Clin Immunol Pract* **4**, 38-59 (2016).

Bousfiha, A., Jeddane, L., Picard, C., Ailal, F., Bobby Gaspar, H., Al-Herz, W., Chatila, T., Crow, Y.J., Cunningham-Rundles, C., Etzioni, A*., et al.* The 2017 IUIS Phenotypic Classification for Primary Immunodeficiencies. *J Clin Immunol* **38**, 129-143 (2018).

Bovenschen, H.J., van de Kerkhof, P.C., van Erp, P.E., Woestenenk, R., Joosten, I. & Koenen, H.J. Foxp3+ regulatory T cells of psoriasis patients easily differentiate into IL-17A-producing cells and are found in lesional skin. *J Invest Dermatol* **131**, 1853-1860 (2011).

Boyle, J.M. & Buckley, R.H. Population prevalence of diagnosed primary immunodeficiency diseases in the United States. *J Clin Immunol* **27**, 497-502 (2007).

Brown, N.F. & Marshall, J.F. Integrin-Mediated TGFbeta Activation Modulates the Tumour Microenvironment. *Cancers* **11**(2019).

Brunkow, M.E., Jeffery, E.W., Hjerrild, K.A., Paeper, B., Clark, L.B., Yasayko, S.A., Wilkinson, J.E., Galas, D., Ziegler, S.F. & Ramsdell, F. Disruption of a new forkhead/winged-helix protein, scurfin, results in the fatal lymphoproliferative disorder of the scurfy mouse. *Nat Genet* **27**, 68-73 (2001).

Bruton, O.C. Agammaglobulinemia. *Pediatrics* **9**, 722-728 (1952).

Bucciol, G., Moens, L., Bosch, B., Bossuyt, X., Casanova, J.L., Puel, A. & Meyts, I. Lessons learned from the study of human inborn errors of innate immunity. *J Allergy Clin Immunol* **143**, 507-527 (2019).

Cani, P.D., Bibiloni, R., Knauf, C., Waget, A., Neyrinck, A.M., Delzenne, N.M. & Burcelin, R. Changes in gut microbiota control metabolic endotoxemia-induced inflammation in high-fat diet-induced obesity and diabetes in mice. *Diabetes* **57**, 1470-1481 (2008).

Carrozza, M.J., Utley, R.T., Workman, J.L. & Cote, J. The diverse functions of histone acetyltransferase complexes. *Trends Genet* **19**, 321-329 (2003).

Ceeraz, S., Sergent, P.A., Plummer, S.F., Schned, A.R., Pechenick, D., Burns, C.M. & Noelle, R.J. VISTA Deficiency Accelerates the Development of Fatal Murine Lupus Nephritis. *Arthritis Rheumatol* **69**, 814-825 (2017).

Chan, D.V., Somani, A.K., Young, A.B., Massari, J.V., Ohtola, J., Sugiyama, H., Garaczi, E., Babineau, D., Cooper, K.D. & McCormick, T.S. Signal peptide cleavage is essential for surface expression of a regulatory T cell surface protein, leucine rich repeat containing 32 (LRRC32). *BMC Biochem* **12**, 27 (2011).

Chassaing, B. & Gewirtz, A.T. Gut microbiota, low-grade inflammation, and metabolic syndrome. *Toxicol Pathol* **42**, 49-53 (2014).

Chen, C., Rowell, E.A., Thomas, R.M., Hancock, W.W. & Wells, A.D. Transcriptional regulation by Foxp3 is associated with direct promoter occupancy and modulation of histone acetylation. *J Biol Chem* **281**, 36828-36834 (2006).

Chen, Q., Sun, L. & Chen, Z.J. Regulation and function of the cGAS-STING pathway of cytosolic DNA sensing. *Nat Immunol* **17**, 1142-1149 (2016).

Choi, J.H., Oh, S.W., Kang, M.S., Kwon, H.J., Oh, G.T. & Kim, D.Y. Trichostatin A attenuates airway inflammation in mouse asthma model. *Clin Exp Allergy* **35**, 89-96 (2005).

Collison, L.W., Workman, C.J., Kuo, T.T., Boyd, K., Wang, Y., Vignali, K.M., Cross, R., Sehy, D., Blumberg, R.S. & Vignali, D.A. The inhibitory cytokine IL-35 contributes to regulatory T-cell function. *Nature* **450**, 566-569 (2007).

Conley, M.E., Dobbs, A.K., Farmer, D.M., Kilic, S., Paris, K., Grigoriadou, S., Coustan-Smith, E., Howard, V. & Campana, D. Primary B cell immunodeficiencies: comparisons and contrasts. *Annu Rev Immunol* **27**, 199-227 (2009).

Coutinho, A. & Carneiro-Sampaio, M. Primary immunodeficiencies unravel critical aspects of the pathophysiology of autoimmunity and of the genetics of autoimmune disease. *J Clin Immunol* **28 Suppl 1**, S4-10 (2008).

Crow, M.K. Type I interferon in the pathogenesis of lupus. *J Immunol* **192**, 5459-5468 (2014).

Cuende, J., Lienart, S., Dedobbeleer, O., van der Woning, B., De Boeck, G., Stockis, J., Huygens, C., Colau, D., Somja, J., Delvenne, P.*, et al.* Monoclonal antibodies against GARP/TGF-beta1 complexes inhibit the immunosuppressive activity of human regulatory T cells in vivo. *Sci Transl Med* **7**, 284ra256 (2015).

Curotto de Lafaille, M.A. & Lafaille, J.J. Natural and adaptive foxp3+ regulatory T cells: more of the same or a division of labor? *Immunity* **30**, 626-635 (2009).

de Zoeten, E.F., Wang, L., Sai, H., Dillmann, W.H. & Hancock, W.W. Inhibition of HDAC9 increases T regulatory cell function and prevents colitis in mice. *Gastroenterology* **138**, 583-594 (2010).

de Zoeten, E.F., Wang, L., Butler, K., Beier, U.H., Akimova, T., Sai, H., Bradner, J.E., Mazitschek, R., Kozikowski, A.P., Matthias, P. & Hancock, W.W. Histone deacetylase 6 and heat shock protein 90 control the functions of Foxp3(+) T-regulatory cells. *Mol Cell Biol* **31**, 2066-2078 (2011).

Depis, F., Kwon, H.K., Mathis, D. & Benoist, C. Unstable FoxP3+ T regulatory cells in NZW mice. *Proc Natl Acad Sci U S A* **113**, 1345-1350 (2016).

DePristo, M.A., Banks, E., Poplin, R., Garimella, K.V., Maguire, J.R., Hartl, C., Philippakis, A.A., del Angel, G., Rivas, M.A., Hanna, M.*, et al.* A framework for variation discovery and genotyping using next-generation DNA sequencing data. *Nat Genet* **43**, 491-498 (2011).

Dokmanovic, M., Clarke, C. & Marks, P.A. Histone deacetylase inhibitors: overview and perspectives. *Mol Cancer Res* **5**, 981-989 (2007).

Drazic, A., Myklebust, L.M., Ree, R. & Arnesen, T. The world of protein acetylation. *Biochim Biophys Acta* **1864**, 1372-1401 (2016).

Duraisingham, S.S., Buckland, M., Dempster, J., Lorenzo, L., Grigoriadou, S. & Longhurst, H.J. Primary vs. secondary antibody deficiency: clinical features and infection outcomes of immunoglobulin replacement. *PLoS One* **9**, e100324 (2014).

Duraisingham, S.S., Buckland, M.S., Grigoriadou, S. & Longhurst, H.J. Secondary antibody deficiency. *Expert Rev Clin Immunol* **10**, 583-591 (2014).

Eberharter, A. & Becker, P.B. Histone acetylation: a switch between repressive and permissive chromatin. Second in review series on chromatin dynamics. *EMBO Rep* **3**, 224-229 (2002).

Edwards, J.P., Fujii, H., Zhou, A.X., Creemers, J., Unutmaz, D. & Shevach, E.M. Regulation of the expression of GARP/latent TGF-beta1 complexes on mouse T cells and their role in regulatory T cell and Th17 differentiation. *J Immunol* **190**, 5506-5515 (2013).

Edwards, J.P., Thornton, A.M. & Shevach, E.M. Release of active TGF-beta1 from the latent TGF-beta1/GARP complex on T regulatory cells is mediated by integrin beta8. *J Immunol* **193**, 2843-2849 (2014).

Elangovan, B. & Chinnadurai, G. Functional dissection of the pro-apoptotic protein Bik. Heterodimerization with anti-apoptosis proteins is insufficient for induction of cell death. *J Biol Chem* **272**, 24494-24498 (1997).

Ennis, H.L. & Lubin, M. Cycloheximide: Aspects of Inhibition of Protein Synthesis in Mammalian Cells. *Science* **146**, 1474-1476 (1964).

Fathman, C.G. & Lineberry, N.B. Molecular mechanisms of CD4+ T-cell anergy. *Nat Rev Immunol* **7**, 599-609 (2007).

Fischer, A. & Rausell, A. Primary immunodeficiencies suggest redundancy within the human immune system. *Sci Immunol* **1**(2016).

Fischer, A., Provot, J., Jais, J.P., Alcais, A., Mahlaoui, N. & members of the, C.F.P.I.D.s.g. Autoimmune and inflammatory manifestations occur frequently in patients with primary immunodeficiencies. *J Allergy Clin Immunol* **140**, 1388-1393 e1388 (2017).

Fleming, J. & Fabry, Z. The hygiene hypothesis and multiple sclerosis. *Ann Neurol* **61**, 85-89 (2007).

Fontenot, J.D., Gavin, M.A. & Rudensky, A.Y. Foxp3 programs the development and function of CD4+CD25+ regulatory T cells. *Nat Immunol* **4**, 330-336 (2003).

Frederick, J.P., Liberati, N.T., Waddell, D.S., Shi, Y. & Wang, X.F. Transforming growth factor beta-mediated transcriptional repression of c-myc is dependent on direct binding of Smad3 to a novel repressive Smad binding element. *Molecular and cellular biology* **24**, 2546-2559 (2004).

Freeman, A.F. & Holland, S.M. Clinical manifestations of hyper IgE syndromes. *Dis Markers* **29**, 123-130 (2010).

Furusawa, Y., Obata, Y., Fukuda, S., Endo, T.A., Nakato, G., Takahashi, D., Nakanishi, Y., Uetake, C., Kato, K., Kato, T.*, et al.* Commensal microbe-derived butyrate induces the differentiation of colonic regulatory T cells. *Nature* **504**, 446-450 (2013).

Gambineri, E., Torgerson, T.R. & Ochs, H.D. Immune dysregulation, polyendocrinopathy, enteropathy, and X-linked inheritance (IPEX), a syndrome of systemic autoimmunity caused by mutations of FOXP3, a critical regulator of T-cell homeostasis. *Curr Opin Rheumatol* **15**, 430-435 (2003).

Getahun, A., Beavers, N.A., Larson, S.R., Shlomchik, M.J. & Cambier, J.C. Continuous inhibitory signaling by both SHP-1 and SHIP-1 pathways is required to maintain unresponsiveness of anergic B cells. *J Exp Med* **213**, 751-769 (2016).

Godfrey, V.L., Wilkinson, J.E. & Russell, L.B. X-linked lymphoreticular disease in the scurfy (sf) mutant mouse. *The American journal of pathology* **138**, 1379-1387 (1991).

Green, E.A., Gorelik, L., McGregor, C.M., Tran, E.H. & Flavell, R.A. CD4+CD25+ T regulatory cells control anti-islet CD8+ T cells through TGF-beta-TGF-beta receptor interactions in type 1 diabetes. *Proceedings of the National Academy of Sciences of the United States of America* **100**, 10878-10883 (2003).

Grimaldi, C.M., Jeganathan, V. & Diamond, B. Hormonal regulation of B cell development: 17 beta-estradiol impairs negative selection of high-affinity DNA-reactive B cells at more than one developmental checkpoint. *J Immunol* **176**, 2703-2710 (2006).

Grossman, W.J., Verbsky, J.W., Barchet, W., Colonna, M., Atkinson, J.P. & Ley, T.J. Human T regulatory cells can use the perforin pathway to cause autologous target cell death. *Immunity* **21**, 589-601 (2004).

Gutierrez-Arcelus, M., Rich, S.S. & Raychaudhuri, S. Autoimmune diseases - connecting risk alleles with molecular traits of the immune system. *Nat Rev Genet* **17**, 160-174 (2016).

Hahn, S.A., Stahl, H.F., Becker, C., Correll, A., Schneider, F.J., Tuettenberg, A. & Jonuleit, H. Soluble GARP has potent antiinflammatory and immunomodulatory impact on human CD4(+) T cells. *Blood* **122**, 1182-1191 (2013).

Hancock, W.W. & Ozkaynak, E. Three distinct domains contribute to nuclear transport of murine Foxp3. *PLoS One* **4**, e7890 (2009).

Haupt, S., Sontgerath, V.S., Leipe, J., Schulze-Koops, H. & Skapenko, A. Methylation of an intragenic alternative promoter regulates transcription of GARP. *Biochim Biophys Acta* **1859**, 223-234 (2016).

Horbelt, D., Denkis, A. & Knaus, P. A portrait of Transforming Growth Factor beta superfamily signalling: Background matters. *The international journal of biochemistry & cell biology* **44**, 469-474 (2012).

Hori, S., Nomura, T. & Sakaguchi, S. Control of regulatory T cell development by the transcription factor Foxp3. *Science* **299**, 1057-1061 (2003).

Huan, J., Culbertson, N., Spencer, L., Bartholomew, R., Burrows, G.G., Chou, Y.K., Bourdette, D., Ziegler, S.F., Offner, H. & Vandenbark, A.A. Decreased FOXP3 levels in multiple sclerosis patients. *J Neurosci Res* **81**, 45-52 (2005).

Huang, L.T. & Gromiha, M.M. First insight into the prediction of protein folding rate change upon point mutation. *Bioinformatics* **26**, 2121-2127 (2010).

Hunt, K.A., Mistry, V., Bockett, N.A., Ahmad, T., Ban, M., Barker, J.N., Barrett, J.C., Blackburn, H., Brand, O., Burren, O.*, et al.* Negligible impact of rare autoimmune-locus coding-region variants on missing heritability. *Nature* **498**, 232-235 (2013).

Iwasaki, A. & Medzhitov, R. Control of adaptive immunity by the innate immune system. *Nat Immunol* **16**, 343-353 (2015).

Janeway, C.A., Travers, P., Walport, M. & Shlomchik, M.J. *Immunobiology: The Immune Systemin Health and Disease. Principles of innate and adaptive immunity*, (Garland Science, New York, 2001).

Janeway, C.A., Travers, P., Walport, M. & Shlomchik, M.J. Immunobiology: The Immune System in Health and Disease. Principles of innate and adaptive immunity. Vol. 1 (Garland Science, New York, 2001).

Kalekar, L.A., Schmiel, S.E., Nandiwada, S.L., Lam, W.Y., Barsness, L.O., Zhang, N., Stritesky, G.L., Malhotra, D., Pauken, K.E., Linehan, J.L*., et al.* CD4(+) T cell anergy prevents autoimmunity and generates regulatory T cell precursors. *Nat Immunol* **17**, 304-314 (2016).

Kamada, N., Chen, G.Y., Inohara, N. & Nunez, G. Control of pathogens and pathobionts by the gut microbiota. *Nat Immunol* **14**, 685-690 (2013).

Kehrl, J.H., Wakefield, L.M., Roberts, A.B., Jakowlew, S., Alvarez-Mon, M., Derynck, R., Sporn, M.B. & Fauci, A.S. Production of transforming growth factor beta by human T lymphocytes and its potential role in the regulation of T cell growth. *J Exp Med* **163**, 1037-1050 (1986).

Khattri, R., Cox, T., Yasayko, S.A. & Ramsdell, F. An essential role for Scurfin in CD4+CD25+ T regulatory cells. *Nat Immunol* **4**, 337-342 (2003).

Knutson, K.L., Disis, M.L. & Salazar, L.G. CD4 regulatory T cells in human cancer pathogenesis. *Cancer immunology, immunotherapy : CII* **56**, 271-285 (2007).

Kobie, J.J., Shah, P.R., Yang, L., Rebhahn, J.A., Fowell, D.J. & Mosmann, T.R. T regulatory and primed uncommitted CD4 T cells express CD73, which suppresses effector CD4 T cells by converting 5'-adenosine monophosphate to adenosine. *Journal of immunology* **177**, 6780-6786 (2006).

Komatsu, N., Mariotti-Ferrandiz, M.E., Wang, Y., Malissen, B., Waldmann, H. & Hori, S. Heterogeneity of natural Foxp3+ T cells: a committed regulatory T-cell lineage and an uncommitted minor population retaining plasticity. *Proc Natl Acad Sci U S A* **106**, 1903-1908 (2009).

Konig, M.F., Abusleme, L., Reinholdt, J., Palmer, R.J., Teles, R.P., Sampson, K., Rosen, A., Nigrovic, P.A., Sokolove, J., Giles, J.T*., et al.* Aggregatibacter actinomycetemcomitans-induced hypercitrullination links periodontal infection to autoimmunity in rheumatoid arthritis. *Sci Transl Med* **8**, 369ra176 (2016).

Kono, D. & Theofilopoulos, A. Kelley and Firestein's Textbook of Rheumatology. Vol. 10 301-317 (Elsevier, Philadelphia, 2017).

Korn, T., Bettelli, E., Oukka, M. & Kuchroo, V.K. IL-17 and Th17 Cells. *Annual review of immunology* **27**, 485-517 (2009).

Kuehn, H.S., Ouyang, W., Lo, B., Deenick, E.K., Niemela, J.E., Avery, D.T., Schickel, J.N., Tran, D.Q., Stoddard, J., Zhang, Y*., et al.* Immune dysregulation in human subjects with heterozygous germline mutations in CTLA4. *Science* **345**, 1623-1627 (2014).

Kuhn, A., Wenzel, J. & Weyd, H. Photosensitivity, apoptosis, and cytokines in the pathogenesis of lupus erythematosus: a critical review. *Clin Rev Allergy Immunol* **47**, 148-162 (2014).

Kuhn, K.A. & Stappenbeck, T.S. Peripheral education of the immune system by the colonic microbiota. *Semin Immunol* **25**, 364-369 (2013).

Lamagna, C., Hu, Y., DeFranco, A.L. & Lowell, C.A. B cell-specific loss of Lyn kinase leads to autoimmunity. *J Immunol* **192**, 919-928 (2014).

Lauffer, B.E., Mintzer, R., Fong, R., Mukund, S., Tam, C., Zilberleyb, I., Flicke, B., Ritscher, A., Fedorowicz, G., Vallero, R.*, et al.* Histone deacetylase (HDAC) inhibitor kinetic rate constants correlate with cellular histone acetylation but not transcription and cell viability. *J Biol Chem* **288**, 26926-26943 (2013).

Legoux, F.P., Lim, J.B., Cauley, A.W., Dikiy, S., Ertelt, J., Mariani, T.J., Sparwasser, T., Way, S.S. & Moon, J.J. CD4+ T Cell Tolerance to Tissue-Restricted Self Antigens Is Mediated by Antigen-Specific Regulatory T Cells Rather Than Deletion. *Immunity* **43**, 896-908 (2015).

Lehman, H.K. Autoimmunity and Immune Dysregulation in Primary Immune Deficiency Disorders. *Curr Allergy Asthma Rep* **15**, 53 (2015).

Lehmkuhl, P., Gentz, M., Garcia de Otezya, A.C., Grimbacher, B., Schulze-Koops, H. & Skapenko, A. Dysregulated immunity in PID patients with low GARP expression on Tregs due to mutations in LRRC32. *Cell Mol Immunol* (2021).

Li, B., Samanta, A., Song, X., Iacono, K.T., Bembas, K., Tao, R., Basu, S., Riley, J.L., Hancock, W.W., Shen, Y.*, et al.* FOXP3 interactions with histone acetyltransferase and class II histone deacetylases are required for repression. *Proc Natl Acad Sci U S A* **104**, 4571-4576 (2007).

Li, M.O., Sanjabi, S. & Flavell, R.A. Transforming growth factor-beta controls development, homeostasis, and tolerance of T cells by regulatory T cell-dependent and -independent mechanisms. *Immunity* **25**, 455-471 (2006).

Li, M.O., Wan, Y.Y. & Flavell, R.A. T cell-produced transforming growth factor-beta1 controls T cell tolerance and regulates Th1- and Th17-cell differentiation. *Immunity* **26**, 579-591 (2007).

Li, M.O. & Rudensky, A.Y. T cell receptor signalling in the control of regulatory T cell differentiation and function. *Nat Rev Immunol* **16**, 220-233 (2016).

Li, X., Liang, Y., LeBlanc, M., Benner, C. & Zheng, Y. Function of a Foxp3 cis-element in protecting regulatory T cell identity. *Cell* **158**, 734-748 (2014).

Li, Z., Li, D., Tsun, A. & Li, B. FOXP3+ regulatory T cells and their functional regulation. *Cell Mol Immunol* **12**, 558-565 (2015).

Lienart, S., Merceron, R., Vanderaa, C., Lambert, F., Colau, D., Stockis, J., van der Woning, B., De Haard, H., Saunders, M., Coulie, P.G.*, et al.* Structural basis of latent TGF-beta1 presentation and activation by GARP on human regulatory T cells. *Science* **362**, 952-956 (2018).

Liu, Y., Wang, L., Predina, J., Han, R., Beier, U.H., Wang, L.C., Kapoor, V., Bhatti, T.R., Akimova, T., Singhal, S.*, et al.* Inhibition of p300 impairs Foxp3(+) T regulatory cell function and promotes antitumor immunity. *Nat Med* **19**, 1173-1177 (2013).

Liu, Y., Wang, L., Han, R., Beier, U.H., Akimova, T., Bhatti, T., Xiao, H., Cole, P.A., Brindle, P.K. & Hancock, W.W. Two histone/protein acetyltransferases, CBP and p300, are indispensable for Foxp3+ T-regulatory cell development and function. *Mol Cell Biol* **34**, 3993-4007 (2014).

Liu, Z., Gerner, M.Y., Van Panhuys, N., Levine, A.G., Rudensky, A.Y. & Germain, R.N. Immune homeostasis enforced by co-localized effector and regulatory T cells. *Nature* **528**, 225-230 (2015).

Louis, P. & O'Byrne, C.P. Life in the gut: microbial responses to stress in the gastrointestinal tract. *Sci Prog* **93**, 7-36 (2010).

Macaulay, I.C., Tijssen, M.R., Thijssen-Timmer, D.C., Gusnanto, A., Steward, M., Burns, P., Langford, C.F., Ellis, P.D., Dudbridge, F., Zwaginga, J.J.*, et al.* Comparative gene expression profiling of in vitro differentiated megakaryocytes and erythroblasts identifies novel activatory and inhibitory platelet membrane proteins. *Blood* **109**, 3260-3269 (2007).

Macauley, M.S., Crocker, P.R. & Paulson, J.C. Siglec-mediated regulation of immune cell function in disease. *Nat Rev Immunol* **14**, 653-666 (2014).

MacPherson, G. & Austyn, J. *Exploring Immunology—Concepts and Evidence*, (Wiley - Blackwell, 2012).

Malhotra, D., Linehan, J.L., Dileepan, T., Lee, Y.J., Purtha, W.E., Lu, J.V., Nelson, R.W., Fife, B.T., Orr, H.T., Anderson, M.S.*, et al.* Tolerance is established in polyclonal CD4(+) T cells by distinct mechanisms, according to self-peptide expression patterns. *Nat Immunol* **17**, 187-195 (2016).

Manz, J., Rodriguez, E., ElSharawy, A., Oesau, E.M., Petersen, B.S., Baurecht, H., Mayr, G., Weber, S., Harder, J., Reischl, E.*, et al.* Targeted Resequencing and Functional Testing Identifies Low-Frequency Missense Variants in the Gene Encoding GARP as Significant Contributors to Atopic Dermatitis Risk. *J Invest Dermatol* **136**, 2380-2386 (2016).

Markle, J.G., Frank, D.N., Mortin-Toth, S., Robertson, C.E., Feazel, L.M., Rolle-Kampczyk, U., von Bergen, M., McCoy, K.D., Macpherson, A.J. & Danska, J.S. Sex differences in the gut microbiome drive hormone-dependent regulation of autoimmunity. *Science* **339**, 1084-1088 (2013).

Markle, J.G. & Fish, E.N. SeXX matters in immunity. *Trends Immunol* **35**, 97-104 (2014).

Marks, P., Rifkind, R.A., Richon, V.M., Breslow, R., Miller, T. & Kelly, W.K. Histone deacetylases and cancer: causes and therapies. *Nat Rev Cancer* **1**, 194-202 (2001).

Marrie, R.A. Environmental risk factors in multiple sclerosis aetiology. *Lancet Neurol* **3**, 709-718 (2004).

Marsden, V.S., O'Connor, L., O'Reilly, L.A., Silke, J., Metcalf, D., Ekert, P.G., Huang, D.C., Cecconi, F., Kuida, K., Tomaselli, K.J., *et al.* Apoptosis initiated by Bcl-2-regulated caspase activation independently of the cytochrome c/Apaf-1/caspase-9 apoptosome. *Nature* **419**, 634-637 (2002).

Mazmanian, S.K., Round, J.L. & Kasper, D.L. A microbial symbiosis factor prevents intestinal inflammatory disease. *Nature* **453**, 620-625 (2008).

McCusker, C. & Warrington, R. Primary immunodeficiency. *Allergy Asthma Clin Immunol* **7 Suppl 1**, S11 (2011).

McCusker, C., Upton, J. & Warrington, R. Primary immunodeficiency. *Allergy Asthma Clin Immunol* **14**, 61 (2018).

McKenna, A., Hanna, M., Banks, E., Sivachenko, A., Cibulskis, K., Kernytsky, A., Garimella, K., Altshuler, D., Gabriel, S., Daly, M. & DePristo, M.A. The Genome Analysis Toolkit: a MapReduce framework for analyzing next-generation DNA sequencing data. *Genome Res* **20**, 1297-1303 (2010).

Meffre, E. The establishment of early B cell tolerance in humans: lessons from primary immunodeficiency diseases. *Ann N Y Acad Sci* **1246**, 1-10 (2011).

Metelli, A., Wu, B.X., Fugle, C.W., Rachidi, S., Sun, S., Zhang, Y., Wu, J., Tomlinson, S., Howe, P.H., Yang, Y., *et al.* Surface Expression of TGFbeta Docking Receptor GARP Promotes Oncogenesis and Immune Tolerance in Breast Cancer. *Cancer Res* **76**, 7106-7117 (2016).

Metelli, A., Salem, M., Wallace, C.H., Wu, B.X., Li, A., Li, X. & Li, Z. Immunoregulatory functions and the therapeutic implications of GARP-TGF-beta in inflammation and cancer. *J Hematol Oncol* **11**, 24 (2018).

Meyer-Martin, H., Hahn, S.A., Beckert, H., Belz, C., Heinz, A., Jonuleit, H., Becker, C., Taube, C., Korn, S., Buhl, R., *et al.* GARP inhibits allergic airway inflammation in a humanized mouse model. *Allergy* **71**, 1274-1283 (2016).

Meyts, I., Bosch, B., Bolze, A., Boisson, B., Itan, Y., Belkadi, A., Pedergnana, V., Moens, L., Picard, C., Cobat, A., *et al.* Exome and genome sequencing for inborn errors of immunity. *J Allergy Clin Immunol* **138**, 957-969 (2016).

Mills, K.H. TLR-dependent T cell activation in autoimmunity. *Nat Rev Immunol* **11**, 807-822 (2011).

Miyara, M., Yoshioka, Y., Kitoh, A., Shima, T., Wing, K., Niwa, A., Parizot, C., Taflin, C., Heike, T., Valeyre, D., *et al.* Functional delineation and differentiation dynamics of human CD4+ T cells expressing the FoxP3 transcription factor. *Immunity* **30**, 899-911 (2009).

Miyazono, K., Olofsson, A., Colosetti, P. & Heldin, C.H. A role of the latent TGF-beta 1-binding protein in the assembly and secretion of TGF-beta 1. *EMBO J* **10**, 1091-1101 (1991).

Modell, V., Gee, B., Lewis, D.B., Orange, J.S., Roifman, C.M., Routes, J.M., Sorensen, R.U., Notarangelo, L.D. & Modell, F. Global study of primary immunodeficiency diseases (PI)--diagnosis, treatment, and economic impact: an updated report from the Jeffrey Modell Foundation. *Immunol Res* **51**, 61-70 (2011).

Moreira, J.M., Scheipers, P. & Sorensen, P. The histone deacetylase inhibitor Trichostatin A modulates CD4+ T cell responses. *BMC Cancer* **3**, 30 (2003).

Morikawa, H. & Sakaguchi, S. Genetic and epigenetic basis of Treg cell development and function: from a FoxP3-centered view to an epigenome-defined view of natural Treg cells. *Immunol Rev* **259**, 192-205 (2014).

Mosmann, T.R., Cherwinski, H., Bond, M.W., Giedlin, M.A. & Coffman, R.L. Two types of murine helper T cell clone. I. Definition according to profiles of lymphokine activities and secreted proteins. *Journal of immunology* **136**, 2348-2357 (1986).

Munger, J.S., Huang, X., Kawakatsu, H., Griffiths, M.J., Dalton, S.L., Wu, J., Pittet, J.F., Kaminski, N., Garat, C., Matthay, M.A.*, et al.* The integrin alpha v beta 6 binds and activates latent TGF beta 1: a mechanism for regulating pulmonary inflammation and fibrosis. *Cell* **96**, 319-328 (1999).

Murphy, K.P., Janeway, C.A. & Travers, P. Janeway's Immunobiology. The adaptive immune response. Vol. 8 (Garland Science, London, 2012).

Murphy, K.P., Janeway, C.A., Travers, P., Walport, M., Mowat, A. & Weaver, C.T. *Janeway's Immunobiology*, (Garland Science, London, 2012).

Nagano, N., Ota, M. & Nishikawa, K. Strong hydrophobic nature of cysteine residues in proteins. *FEBS Lett* **458**, 69-71 (1999).

Neff, C.P., Rhodes, M.E., Arnolds, K.L., Collins, C.B., Donnelly, J., Nusbacher, N., Jedlicka, P., Schneider, J.M., McCarter, M.D., Shaffer, M.*, et al.* Diverse Intestinal Bacteria Contain Putative Zwitterionic Capsular Polysaccharides with Anti-inflammatory Properties. *Cell Host Microbe* **20**, 535-547 (2016).

Neish, A.S. Microbes in gastrointestinal health and disease. *Gastroenterology* **136**, 65-80 (2009).

Nemazee, D. Mechanisms of central tolerance for B cells. *Nat Rev Immunol* **17**, 281-294 (2017).

Notarangelo, L.D., Gambineri, E. & Badolato, R. Immunodeficiencies with autoimmune consequences. *Adv Immunol* **89**, 321-370 (2006).

Notarangelo, L.D. Primary immunodeficiencies. *J Allergy Clin Immunol* **125**, S182-194 (2010).

Nunez, G., Benedict, M.A., Hu, Y. & Inohara, N. Caspases: the proteases of the apoptotic pathway. *Oncogene* **17**, 3237-3245 (1998).

Ochoa-Reparaz, J., Mielcarz, D.W., Ditrio, L.E., Burroughs, A.R., Begum-Haque, S., Dasgupta, S., Kasper, D.L. & Kasper, L.H. Central nervous system demyelinating disease protection by the human commensal Bacteroides fragilis depends on polysaccharide A expression. *J Immunol* **185**, 4101-4108 (2010).

Odegaard, A.O., Koh, W.P., Yuan, J.M., Gross, M.D. & Pereira, M.A. Western-style fast food intake and cardiometabolic risk in an Eastern country. *Circulation* **126**, 182-188 (2012).

Ohkura, N., Kitagawa, Y. & Sakaguchi, S. Development and maintenance of regulatory T cells. *Immunity* **38**, 414-423 (2013).

Okazaki, T., Chikuma, S., Iwai, Y., Fagarasan, S. & Honjo, T. A rheostat for immune responses: the unique properties of PD-1 and their advantages for clinical application. *Nat Immunol* **14**, 1212-1218 (2013).

Oliveira, J.B. & Fleisher, T.A. Laboratory evaluation of primary immunodeficiencies. *J Allergy Clin Immunol* **125**, S297-305 (2010).

Ollendorff, V., Noguchi, T., deLapeyriere, O. & Birnbaum, D. The GARP gene encodes a new member of the family of leucine-rich repeat-containing proteins. *Cell Growth Differ* **5**, 213-219 (1994).

Pandiyan, P., Zheng, L., Ishihara, S., Reed, J. & Lenardo, M.J. CD4+CD25+Foxp3+ regulatory T cells induce cytokine deprivation-mediated apoptosis of effector CD4+ T cells. *Nature immunology* **8**, 1353-1362 (2007).

Parish, C.R. Fluorescent dyes for lymphocyte migration and proliferation studies. *Immunol Cell Biol* **77**, 499-508 (1999).

Park, H., Bourla, A.B., Kastner, D.L., Colbert, R.A. & Siegel, R.M. Lighting the fires within: the cell biology of autoinflammatory diseases. *Nat Rev Immunol* **12**, 570-580 (2012).

Paterson, A.M. & Sharpe, A.H. Taming tissue-specific T cells: CTLA-4 reins in self-reactive T cells. *Nat Immunol* **11**, 109-111 (2010).

Pesce, B., Soto, L., Sabugo, F., Wurmann, P., Cuchacovich, M., Lopez, M.N., Sotelo, P.H., Molina, M.C., Aguillon, J.C. & Catalan, D. Effect of interleukin-6 receptor blockade on the balance between regulatory T cells and T helper type 17 cells in rheumatoid arthritis patients. *Clin Exp Immunol* **171**, 237-242 (2013).

Phillips, D.M. The presence of acetyl groups of histones. *Biochem J* **87**, 258-263 (1963).

Picard, C., Bobby Gaspar, H., Al-Herz, W., Bousfiha, A., Casanova, J.L., Chatila, T., Crow, Y.J., Cunningham-Rundles, C., Etzioni, A., Franco, J.L.*, et al.* International Union of Immunological Societies: 2017 Primary Immunodeficiency Diseases Committee Report on Inborn Errors of Immunity. *J Clin Immunol* **38**, 96-128 (2018).

Piccirillo, C.A., Letterio, J.J., Thornton, A.M., McHugh, R.S., Mamura, M., Mizuhara, H. & Shevach, E.M. CD4(+)CD25(+) regulatory T cells can mediate suppressor function in the absence of transforming growth factor beta1 production and responsiveness. *J Exp Med* **196**, 237-246 (2002).

Pincetic, A., Bournazos, S., DiLillo, D.J., Maamary, J., Wang, T.T., Dahan, R., Fiebiger, B.M. & Ravetch, J.V. Type I and type II Fc receptors regulate innate and adaptive immunity. *Nat Immunol* **15**, 707-716 (2014).

Polansky, J.K., Kretschmer, K., Freyer, J., Floess, S., Garbe, A., Baron, U., Olek, S., Hamann, A., von Boehmer, H. & Huehn, J. DNA methylation controls Foxp3 gene expression. *Eur J Immunol* **38**, 1654-1663 (2008).

Prasad, S., Starck, S.R. & Shastri, N. Presentation of Cryptic Peptides by MHC Class I Is Enhanced by Inflammatory Stimuli. *J Immunol* **197**, 2981-2991 (2016).

Probst-Kepper, M., Geffers, R., Kroger, A., Viegas, N., Erck, C., Hecht, H.J., Lunsdorf, H., Roubin, R., Moharregh-Khiabani, D., Wagner, K.*, et al.* GARP: a key receptor controlling FOXP3 in human regulatory T cells. *J Cell Mol Med* **13**, 3343-3357 (2009).

Probst-Kepper, M., Kroger, A., Garritsen, H.S. & Buer, J. Perspectives on Regulatory T Cell Therapies. *Transfus Med Hemother* **36**, 302-308 (2009).

Probst-Kepper, M., Balling, R. & Buer, J. FOXP3: required but not sufficient. the role of GARP (LRRC32) as a safeguard of the regulatory phenotype. *Curr Mol Med* **10**, 533-539 (2010).

Procaccini, C., Carbone, F., Di Silvestre, D., Brambilla, F., De Rosa, V., Galgani, M., Faicchia, D., Marone, G., Tramontano, D., Corona, M.*, et al.* The Proteomic Landscape of Human Ex Vivo Regulatory and Conventional T Cells Reveals Specific Metabolic Requirements. *Immunity* **44**, 406-421 (2016).

Quan, L., Lv, Q. & Zhang, Y. STRUM: structure-based prediction of protein stability changes upon single-point mutation. *Bioinformatics* **32**, 2936-2946 (2016).

Rifkin, D.B. Latent transforming growth factor-beta (TGF-beta) binding proteins: orchestrators of TGF-beta availability. *J Biol Chem* **280**, 7409-7412 (2005).

Robertson, I.B. & Rifkin, D.B. Unchaining the beast; insights from structural and evolutionary studies on TGFbeta secretion, sequestration, and activation. *Cytokine Growth Factor Rev* **24**, 355-372 (2013).

Romagnani, S. Regulation of the T cell response. *Clinical and experimental allergy : journal of the British Society for Allergy and Clinical Immunology* **36**, 1357-1366 (2006).

Root-Bernstein, R. & Fairweather, D. Complexities in the relationship between infection and autoimmunity. *Curr Allergy Asthma Rep* **14**, 407 (2014).

Roth, S.Y., Denu, J.M. & Allis, C.D. Histone acetyltransferases. *Annu Rev Biochem* **70**, 81-120 (2001).

Rubtsova, K., Marrack, P. & Rubtsov, A.V. Sexual dimorphism in autoimmunity. *J Clin Invest* **125**, 2187-2193 (2015).

Safinia, N., Scotta, C., Vaikunthanathan, T., Lechler, R.I. & Lombardi, G. Regulatory T Cells: Serious Contenders in the Promise for Immunological Tolerance in Transplantation. *Frontiers in immunology* **6**, 438 (2015).

Sakaguchi, S., Sakaguchi, N., Shimizu, J., Yamazaki, S., Sakihama, T., Itoh, M., Kuniyasu, Y., Nomura, T., Toda, M. & Takahashi, T. Immunologic tolerance maintained by CD25+ CD4+ regulatory T cells: their common role in controlling autoimmunity, tumor immunity, and transplantation tolerance. *Immunol Rev* **182**, 18-32 (2001).

Sakaguchi, S., Miyara, M., Costantino, C.M. & Hafler, D.A. FOXP3+ regulatory T cells in the human immune system. *Nat Rev Immunol* **10**, 490-500 (2010).

Salem, M., Wallace, C., Velegraki, M., Li, A., Ansa-Addo, E., Metelli, A., Kwon, H., Riesenberg, B., Wu, B., Zhang, Y.*, et al.* GARP Dampens Cancer Immunity by Sustaining Function and Accumulation of Regulatory T Cells in the Colon. *Cancer Res* **79**, 1178-1190 (2019).

Samanta, A., Li, B., Song, X., Bembas, K., Zhang, G., Katsumata, M., Saouaf, S.J., Wang, Q., Hancock, W.W., Shen, Y. & Greene, M.I. TGF-beta and IL-6 signals modulate chromatin binding and promoter occupancy by acetylated FOXP3. *Proc Natl Acad Sci U S A* **105**, 14023-14027 (2008).

Scher, J.U., Littman, D.R. & Abramson, S.B. Microbiome in Inflammatory Arthritis and Human Rheumatic Diseases. *Arthritis Rheumatol* **68**, 35-45 (2016).

Schmidt, A., Oberle, N. & Krammer, P.H. Molecular mechanisms of treg-mediated T cell suppression. *Front Immunol* **3**, 51 (2012).

Schmierer, B. & Hill, C.S. TGFbeta-SMAD signal transduction: molecular specificity and functional flexibility. *Nat Rev Mol Cell Biol* **8**, 970-982 (2007).

Schmitt, H., Sell, S., Koch, J., Seefried, M., Sonnewald, S., Daniel, C., Winkler, T.H. & Nitschke, L. Siglec-H protects from virus-triggered severe systemic autoimmunity. *J Exp Med* **213**, 1627-1644 (2016).

Schubert, D., Bode, C., Kenefeck, R., Hou, T.Z., Wing, J.B., Kennedy, A., Bulashevska, A., Petersen, B.S., Schaffer, A.A., Gruning, B.A.*, et al.* Autosomal dominant immune dysregulation syndrome in humans with CTLA4 mutations. *Nature medicine* **20**, 1410-1416 (2014).

Schwartz, R.H. A cell culture model for T lymphocyte clonal anergy. *Science* **248**, 1349-1356 (1990).

Schwartz, R.H. Costimulation of T lymphocytes: the role of CD28, CTLA-4, and B7/BB1 in interleukin-2 production and immunotherapy. *Cell* **71**, 1065-1068 (1992).

Seidel, M.G. Autoimmune and other cytopenias in primary immunodeficiencies: pathomechanisms, novel differential diagnoses, and treatment. *Blood* **124**, 2337-2344 (2014).

Shehata, N., Palda, V., Bowen, T., Haddad, E., Issekutz, T.B., Mazer, B., Schellenberg, R., Warrington, R., Easton, D., Anderson, D. & Hume, H. The use of immunoglobulin therapy for patients with primary immune deficiency: an evidence-based practice guideline. *Transfus Med Rev* **24 Suppl 1**, S28-50 (2010).

Shevach, E.M. CD4+ CD25+ suppressor T cells: more questions than answers. *Nat Rev Immunol* **2**, 389-400 (2002).

Shi, M., Zhu, J., Wang, R., Chen, X., Mi, L., Walz, T. & Springer, T.A. Latent TGF-beta structure and activation. *Nature* **474**, 343-349 (2011).

Shi, Y., Wang, Y.F., Jayaraman, L., Yang, H., Massague, J. & Pavletich, N.P. Crystal structure of a Smad MH1 domain bound to DNA: insights on DNA binding in TGF-beta signaling. *Cell* **94**, 585-594 (1998).

Smith, P.M., Howitt, M.R., Panikov, N., Michaud, M., Gallini, C.A., Bohlooly, Y.M., Glickman, J.N. & Garrett, W.S. The microbial metabolites, short-chain fatty acids, regulate colonic Treg cell homeostasis. *Science* **341**, 569-573 (2013).

Smith, S.H., Brown, M.H., Rowe, D., Callard, R.E. & Beverley, P.C. Functional subsets of human helper-inducer cells defined by a new monoclonal antibody, UCHL1. *Immunology* **58**, 63-70 (1986).

Srivastava, S. & Wood, P. Secondary antibody deficiency - causes and approach to diagnosis. *Clin Med (Lond)* **16**, 571-576 (2016).

Stockis, J., Colau, D., Coulie, P.G. & Lucas, S. Membrane protein GARP is a receptor for latent TGF-beta on the surface of activated human Treg. *Eur J Immunol* **39**, 3315-3322 (2009).

Stockis, J., Dedobbeleer, O. & Lucas, S. Role of GARP in the activation of latent TGF-beta1. *Mol Biosyst* **13**, 1925-1935 (2017).

Stockis, J., Lienart, S., Colau, D., Collignon, A., Nishimura, S.L., Sheppard, D., Coulie, P.G. & Lucas, S. Blocking immunosuppression by human Tregs in vivo with antibodies targeting integrin alphaVbeta8. *Proc Natl Acad Sci U S A* **114**, E10161-E10168 (2017).

Strauss, L., Bergmann, C., Szczepanski, M., Gooding, W., Johnson, J.T. & Whiteside, T.L. A unique subset of CD4+CD25highFoxp3+ T cells secreting interleukin-10 and transforming growth factor-beta1 mediates suppression in the tumor microenvironment. *Clinical cancer research : an official journal of the American Association for Cancer Research* **13**, 4345-4354 (2007).

Takahashi, T., Tagami, T., Yamazaki, S., Uede, T., Shimizu, J., Sakaguchi, N., Mak, T.W. & Sakaguchi, S. Immunologic self-tolerance maintained by CD25(+)CD4(+) regulatory T cells constitutively expressing cytotoxic T lymphocyte-associated antigen 4. *The Journal of experimental medicine* **192**, 303-310 (2000).

Takeuchi, O. & Akira, S. Pattern recognition receptors and inflammation. *Cell* **140**, 805-820 (2010).

Tangye, S.G., Al-Herz, W., Bousfiha, A., Chatila, T., Cunningham-Rundles, C., Etzioni, A., Franco, J.L., Holland, S.M., Klein, C., Morio, T.*, et al.* Human Inborn Errors of Immunity: 2019 Update on the Classification from the International Union of Immunological Societies Expert Committee. *J Clin Immunol* **40**, 24-64 (2020).

Tao, R., de Zoeten, E.F., Ozkaynak, E., Chen, C., Wang, L., Porrett, P.M., Li, B., Turka, L.A., Olson, E.N., Greene, M.I.*, et al.* Deacetylase inhibition promotes the generation and function of regulatory T cells. *Nat Med* **13**, 1299-1307 (2007).

Taylor, A.W. Review of the activation of TGF-beta in immunity. *J Leukoc Biol* **85**, 29-33 (2009).

Ter Horst, R., Jaeger, M., Smeekens, S.P., Oosting, M., Swertz, M.A., Li, Y., Kumar, V., Diavatopoulos, D.A., Jansen, A.F.M., Lemmers, H.*, et al.* Host and Environmental Factors Influencing Individual Human Cytokine Responses. *Cell* **167**, 1111-1124 e1113 (2016).

Theofilopoulos, A.N., Kono, D.H., Beutler, B. & Baccala, R. Intracellular nucleic acid sensors and autoimmunity. *J Interferon Cytokine Res* **31**, 867-886 (2011).

Theofilopoulos, A.N., Kono, D.H. & Baccala, R. The multiple pathways to autoimmunity. *Nat Immunol* **18**, 716-724 (2017).

Thorburn, A.N., Macia, L. & Mackay, C.R. Diet, metabolites, and "western-lifestyle" inflammatory diseases. *Immunity* **40**, 833-842 (2014).

Thorburn, A.N., McKenzie, C.I., Shen, S., Stanley, D., Macia, L., Mason, L.J., Roberts, L.K., Wong, C.H., Shim, R., Robert, R.*, et al.* Evidence that asthma is a developmental origin disease influenced by maternal diet and bacterial metabolites. *Nat Commun* **6**, 7320 (2015).

Thornton, A.M. & Shevach, E.M. CD4+CD25+ immunoregulatory T cells suppress polyclonal T cell activation in vitro by inhibiting interleukin 2 production. *The Journal of experimental medicine* **188**, 287-296 (1998).

Tone, Y., Furuuchi, K., Kojima, Y., Tykocinski, M.L., Greene, M.I. & Tone, M. Smad3 and NFAT cooperate to induce Foxp3 expression through its enhancer. *Nat Immunol* **9**, 194-202 (2008).

Tran, D.Q., Andersson, J., Wang, R., Ramsey, H., Unutmaz, D. & Shevach, E.M. GARP (LRRC32) is essential for the surface expression of latent TGF-beta on platelets and activated FOXP3+ regulatory T cells. *Proc Natl Acad Sci U S A* **106**, 13445-13450 (2009).

Trompette, A., Gollwitzer, E.S., Yadava, K., Sichelstiel, A.K., Sprenger, N., Ngom-Bru, C., Blanchard, C., Junt, T., Nicod, L.P., Harris, N.L. & Marsland, B.J. Gut microbiota metabolism of dietary fiber influences allergic airway disease and hematopoiesis. *Nat Med* **20**, 159-166 (2014).

Tsuji, M., Komatsu, N., Kawamoto, S., Suzuki, K., Kanagawa, O., Honjo, T., Hori, S. & Fagarasan, S. Preferential generation of follicular B helper T cells from Foxp3+ T cells in gut Peyer's patches. *Science* **323**, 1488-1492 (2009).

Van der Auwera, G.A., Carneiro, M.O., Hartl, C., Poplin, R., Del Angel, G., Levy-Moonshine, A., Jordan, T., Shakir, K., Roazen, D., Thibault, J.*, et al.* From FastQ data to high confidence variant calls: the Genome Analysis Toolkit best practices pipeline. *Curr Protoc Bioinformatics* **43**, 11 10 11-33 (2013).

van Loosdregt, J., Vercoulen, Y., Guichelaar, T., Gent, Y.Y., Beekman, J.M., van Beekum, O., Brenkman, A.B., Hijnen, D.J., Mutis, T., Kalkhoven, E.*, et al.* Regulation of Treg functionality by acetylation-mediated Foxp3 protein stabilization. *Blood* **115**, 965-974 (2010).

van Loosdregt, J., Brunen, D., Fleskens, V., Pals, C.E., Lam, E.W. & Coffer, P.J. Rapid temporal control of Foxp3 protein degradation by sirtuin-1. *PLoS One* **6**, e19047 (2011).

Veldhoen, M., Hirota, K., Westendorf, A.M., Buer, J., Dumoutier, L., Renauld, J.C. & Stockinger, B. The aryl hydrocarbon receptor links TH17-cell-mediated autoimmunity to environmental toxins. *Nature* **453**, 106-109 (2008).

Vignali, D.A., Collison, L.W. & Workman, C.J. How regulatory T cells work. *Nat Rev Immunol* **8**, 523-532 (2008).

Volpe, E., Touzot, M., Servant, N., Marloie-Provost, M.A., Hupe, P., Barillot, E. & Soumelis, V. Multiparametric analysis of cytokine-driven human Th17 differentiation reveals a differential regulation of IL-17 and IL-22 production. *Blood* **114**, 3610-3614 (2009).

Wan, Y.Y. & Flavell, R.A. Regulatory T-cell functions are subverted and converted owing to attenuated Foxp3 expression. *Nature* **445**, 766-770 (2007).

Wang, R., Wan, Q., Kozhaya, L., Fujii, H. & Unutmaz, D. Identification of a regulatory T cell specific cell surface molecule that mediates suppressive signals and induces Foxp3 expression. *PLoS One* **3**, e2705 (2008).

Wang, R., Kozhaya, L., Mercer, F., Khaitan, A., Fujii, H. & Unutmaz, D. Expression of GARP selectively identifies activated human FOXP3+ regulatory T cells. *Proc Natl Acad Sci U S A* **106**, 13439-13444 (2009).

Wang, R., Zhu, J., Dong, X., Shi, M., Lu, C. & Springer, T.A. GARP regulates the bioavailability and activation of TGFbeta. *Mol Biol Cell* **23**, 1129-1139 (2012).

Wang, W., Jovel, J., Halloran, B., Wine, E., Patterson, J., Ford, G., O'Keefe, S., Meng, B., Song, D., Zhang, Y.*, et al.* Metagenomic analysis of microbiome in colon tissue from subjects with inflammatory bowel diseases reveals interplay of viruses and bacteria. *Inflamm Bowel Dis* **21**, 1419-1427 (2015).

Wardemann, H., Yurasov, S., Schaefer, A., Young, J.W., Meffre, E. & Nussenzweig, M.C. Predominant autoantibody production by early human B cell precursors. *Science* **301**, 1374-1377 (2003).

Wegner, N., Wait, R., Sroka, A., Eick, S., Nguyen, K.A., Lundberg, K., Kinloch, A., Culshaw, S., Potempa, J. & Venables, P.J. Peptidylarginine deiminase from Porphyromonas gingivalis citrullinates human fibrinogen and alpha-enolase: implications for autoimmunity in rheumatoid arthritis. *Arthritis Rheum* **62**, 2662-2672 (2010).

Weidinger, S. & Novak, N. Atopic dermatitis. *Lancet* **387**, 1109-1122 (2016).

Wildin, R.S., Ramsdell, F., Peake, J., Faravelli, F., Casanova, J.L., Buist, N., Levy-Lahad, E., Mazzella, M., Goulet, O., Perroni, L.*, et al.* X-linked neonatal diabetes mellitus, enteropathy and endocrinopathy syndrome is the human equivalent of mouse scurfy. *Nat Genet* **27**, 18-20 (2001).

Wilson, N.J., Boniface, K., Chan, J.R., McKenzie, B.S., Blumenschein, W.M., Mattson, J.D., Basham, B., Smith, K., Chen, T., Morel, F.*, et al.* Development, cytokine profile and function of human interleukin 17-producing helper T cells. *Nature immunology* **8**, 950-957 (2007).

Wu, Y., Borde, M., Heissmeyer, V., Feuerer, M., Lapan, A.D., Stroud, J.C., Bates, D.L., Guo, L., Han, A., Ziegler, S.F., *et al.* FOXP3 controls regulatory T cell function through cooperation with NFAT. *Cell* **126**, 375-387 (2006).

Xiao, Y., Li, B., Zhou, Z., Hancock, W.W., Zhang, H. & Greene, M.I. Histone acetyltransferase mediated regulation of FOXP3 acetylation and Treg function. *Curr Opin Immunol* **22**, 583-591 (2010).

Xu, W., Ngo, L., Perez, G., Dokmanovic, M. & Marks, P.A. Intrinsic apoptotic and thioredoxin pathways in human prostate cancer cell response to histone deacetylase inhibitor. *Proc Natl Acad Sci U S A* **103**, 15540-15545 (2006).

Yang, L., Anderson, D.E., Baecher-Allan, C., Hastings, W.D., Bettelli, E., Oukka, M., Kuchroo, V.K. & Hafler, D.A. IL-21 and TGF-beta are required for differentiation of human T(H)17 cells. *Nature* **454**, 350-352 (2008).

Yang, Z., Mu, Z., Dabovic, B., Jurukovski, V., Yu, D., Sung, J., Xiong, X. & Munger, J.S. Absence of integrin-mediated TGFbeta1 activation in vivo recapitulates the phenotype of TGFbeta1-null mice. *J Cell Biol* **176**, 787-793 (2007).

Yu, W., Jiang, N., Ebert, P.J., Kidd, B.A., Muller, S., Lund, P.J., Juang, J., Adachi, K., Tse, T., Birnbaum, M.E., *et al.* Clonal Deletion Prunes but Does Not Eliminate Self-Specific alphabeta CD8(+) T Lymphocytes. *Immunity* **42**, 929-941 (2015).

Yurkovetskiy, L., Burrows, M., Khan, A.A., Graham, L., Volchkov, P., Becker, L., Antonopoulos, D., Umesaki, Y. & Chervonsky, A.V. Gender bias in autoimmunity is influenced by microbiota. *Immunity* **39**, 400-412 (2013).

Zhang, H., Xiao, Y., Zhu, Z., Li, B. & Greene, M.I. Immune regulation by histone deacetylases: a focus on the alteration of FOXP3 activity. *Immunol Cell Biol* **90**, 95-100 (2012).

Zheng, Y., Josefowicz, S., Chaudhry, A., Peng, X.P., Forbush, K. & Rudensky, A.Y. Role of conserved non-coding DNA elements in the Foxp3 gene in regulatory T-cell fate. *Nature* **463**, 808-812 (2010).

Zhou, A.X., Kozhaya, L., Fujii, H. & Unutmaz, D. GARP-TGF-beta complexes negatively regulate regulatory T cell development and maintenance of peripheral CD4+ T cells in vivo. *J Immunol* **190**, 5057-5064 (2013).

Zhou, X., Bailey-Bucktrout, S., Jeker, L.T. & Bluestone, J.A. Plasticity of CD4(+) FoxP3(+) T cells. *Curr Opin Immunol* **21**, 281-285 (2009).

Zikherman, J., Parameswaran, R. & Weiss, A. Endogenous antigen tunes the responsiveness of naive B cells but not T cells. *Nature* **489**, 160-164 (2012).

Acknowledgements

I would like to thank Prof. Dr. Hendrik Schulze-Koops for the opportunity to perform my experiments for my PhD thesis in his group, for his support and guidance throughout the project and the chance to participate in national and international scientific conferences.

I am grateful to Prof. Dr. Alla Skapenko for supervising me and her technical and scientific guidance and her help with the manuscript.

I would like to thank Prof. Dr. Ludger Klein very much for taking over the supervision of my PhD thesis in the final stage and his revisons and help with the manuscript.

I would like to acknowledge all blood donors that provided me with the necessary research material and to the staff at the Max von Pettenkofer-Institute that took good care of the mice which were used as our research models.

I would like to thank all my colleagues for helpful discussions, creating a nice working environment and help with data generation. I would also like to thank former colleagues for providing preliminary data which was helpful in my publication and thesis.

I am grateful to the group of Prof. Dr. Bodo Grimbacher for their cooperation and discovery of PID patients with rare GARP mutations.

Lots of thanks go to my parents that have always supported me throughout my academic career.

My special thanks go to my wife Paulina for her love, support and encouragement.

Affidavit

LMU LUDWIG-MAXIMILIANS-UNIVERSITÄT MÜNCHEN | Promotionsbüro Medizinische Fakultät | MMRS

Eidesstattliche Versicherung

Lehmkuhl, Peter

Name, Vorname

Ich erkläre hiermit an Eides statt, dass ich die vorliegende Dissertation mit dem Titel:

GARP derived TGFβ promotes acetylation-mediated Foxp3 protein stabilization and Treg functionality

selbständig verfasst, mich außer der angegebenen keiner weiteren Hilfsmittel bedient und alle Erkenntnisse, die aus dem Schrifttum ganz oder annähernd übernommen sind, als solche kenntlich gemacht und nach ihrer Herkunft unter Bezeichnung der Fundstelle einzeln nachgewiesen habe.

Ich erkläre des Weiteren, dass die hier vorgelegte Dissertation nicht in gleicher oder in ähnlicher Form bei einer anderen Stelle zur Erlangung eines akademischen Grades eingereicht wurde.

Teilergebnisse der vorliegenden Arbeit wurden veröffentlicht in (Lehmkuhl et al., 2021). Es handelt sich hier um einen Open-Access-Artikel, es gelten die Nutzungsbedingungen der Creative Commons CC BY Lizenz. Figuren sowie Teile von Figuren die bereits in (Lehmkuhl et al., 2021) veröffentlicht wurden dürfen daher in dieser Dissertation ebenfalls genutzt werden ohne dass zusätzlich eine Erlaubnis vom Journal eingeholt werden muss. Die genutzten Figuren werden ordnungsgemäß zitiert.

Wuppertal, 20.10.22 — Ort, Datum

Peter Lehmkuhl — Unterschrift Doktorand